minerals

MDPI

Review

Applications of Mössbauer Spectroscopy in Meteoritical and Planetary Science, Part II: Differentiated Meteorites, Moon, and Mars

Alevtina A. Maksimova [1,2], Michael V. Goryunov [1] and Michael I. Oshtrakh [1,*]

[1] Department of Experimental Physics, Institute of Physics and Technology, Ural Federal University, 620002 Ekaterinburg, Russian Federation; alia55@bk.ru (A.A.M.); goryunov_asd@mail.ru (M.V.G.)
[2] The Zavaritsky Institute of Geology and Geochemistry of the Ural Branch of the Russian Academy of Sciences, 620016 Ekaterinburg, Russian Federation
* Correspondence: oshtrakh@gmail.com; Tel.: +7-912-283-7337

Abstract: Mössbauer (nuclear γ-resonance) spectroscopy is a powerful technique which is actively used in various fields from physics and chemistry to biology and medicine. Rudolf L. Mössbauer, who observed nuclear γ-resonance and published his results in 1958, got a Nobel Prize in physics in 1961 for this discovery. ^{57}Fe is the most widely used nucleus in Mössbauer spectroscopy. Therefore, a large variety of compounds containing iron can be studied by Mössbauer spectroscopy. It is well known that planetary matter contains various iron-bearing phases and minerals. Therefore, the extraterrestrial material from different meteorites, asteroids, and planets can be studied using ^{57}Fe Mössbauer spectroscopy as an additional powerful technique. Two parts of this review consider the results of more than 50 years of experience of Mössbauer spectroscopy applied for the studies of various meteorites, soils and rocks from the Moon and a recent investigation of the Martian surface using two rovers equipped with miniaturized Mössbauer spectrometers. Part I considered the results of Mössbauer spectroscopy of undifferentiated meteorites. Part II discusses the results of Mössbauer spectroscopy of differentiated meteorites formed in asteroids and protoplanets due to matter differentiation, as well as Lunar and Martian matter.

Keywords: ^{57}Fe Mössbauer spectroscopy; differentiated meteorites; Moon; Mars; iron-bearing minerals; ^{57}Fe hyperfine interactions; iron-bearing phase composition; Fe^{2+} partitioning in silicate phases; temperature of cation equilibrium distribution in silicate phases; meteorite weathering; fusion crust

Citation: Maksimova, A.A.; Goryunov, M.V.; Oshtrakh, M.I. Applications of Mössbauer Spectroscopy in Meteoritical and Planetary Science, Part II: Differentiated Meteorites, Moon, and Mars. *Minerals* **2021**, *11*, 614. https://doi.org/10.3390/min11060614

Academic Editor: Nigel J. Cook

Received: 14 January 2021
Accepted: 25 May 2021
Published: 8 June 2021

1. Introduction

Part I of this review [1] briefly presented the main features and applications of ^{57}Fe Mössbauer spectroscopy, together with the various studies on undifferentiated meteorites. The main parameters which can be obtained from ^{57}Fe Mössbauer spectroscopy are the following: (**i**) isomer shift δ, which is determined by the electron density on the ^{57}Fe nucleus and, therefore, is related to the iron valence/spin state; (**ii**) quadrupole splitting ΔE_Q (quadrupole shift ε for magnetically split spectra, $2\varepsilon = \Delta E_Q$), which is related to the electric field gradient on the ^{57}Fe nucleus and reflects any tiny variations in the ^{57}Fe local microenvironment (both δ and ΔE_Q determine the iron electron structure); (**iii**) magnetic hyperfine field H_{eff} on the ^{57}Fe nucleus; (**iv**) the line width at a half maximum Γ; (**v**) the relative spectrum/component area A, which is proportional to the product of the Mössbauer effect probability (*f*-factor) and the number of ^{57}Fe nuclei in the corresponding compound.

Modern classification divides meteorites into differentiated and undifferentiated [2]. This section (Part II) presents the investigations conducted on differentiated meteorites, which consist of two main types: the primitive achondrites, which are supposed to be a result of low-degree partial melting of chondritic material, and achondrites, resulting from a high degree of chondrite melting in asteroids and protoplanets. The primitive achondrite

division consists of several groups of stony and iron meteorites, while achondrites are divided into several clans of stony achondrites, stony-iron meteorites, and iron meteorites. Thus, differentiated meteorites were formed in their parent bodies (asteroids and protoplanets) resulting from the thermal metamorphism of the matter with further differentiation. As a result, various groups of stony meteorites (achondrites including the clan of howardites–eucrites–diogenites or HED, whose parent body is considered asteroid (4) Vesta [3], as well as Martian and Lunar meteorites), stony-iron meteorites (mesosiderites and three groups of pallasites), and iron meteorites (structural groups octahedrites, hexahedrites, ataxites) were formed.

The main iron-bearing phases and minerals in meteorites are as follows: Fe-Ni-Co alloy with α-Fe(Ni, Co), α_2-Fe(Ni, Co), γ-Fe(Ni, Co), and γ-FeNi phases (kamacite, martensite, taenite, and tetrataenite, respectively), olivine (Fe, Mg)$_2$SiO$_4$, orthopyroxene (Fe, Mg)SiO$_3$, clinopyroxene (Fe, Ca, Mg)SiO$_3$ with different Ca content, troilite FeS, chromite FeCr$_2$O$_4$, hercynite FeAl$_2$O$_4$, ilmenite FeTiO$_3$, and schreibersite (Fe, Ni)$_3$P and its microcrystals named rhabdites, daubréelite FeCr$_2$S$_4$, etc. (see [4,5]). Ferric compounds such as magnetite Fe$_3$O$_4$, magnesioferrite MgFe$_2$O$_4$, maghemite γ-Fe$_2$O$_3$, hematite α-Fe$_2$O$_3$, goethite α-FeOOH, and akaganéite β-FeOOH can appear with the fusion crust formation, when meteorites pass through the Earth atmosphere with a very high velocity and during terrestrial weathering. Information about registered meteorites can be found in the *Meteoritical Bulletin Database* (MBD) (https://www.lpi.usra.edu/meteor/, accessed on 6 June 2021), which is used further for the description of meteorites.

Successful Lunar return space missions allowed the study of various iron-bearing Lunar soils and rocks by Mössbauer spectroscopy in laboratories on Earth. The unique Mars space missions with two rovers equipped with miniaturized Mössbauer spectrometers made it possible to investigate the Martian surface in situ. As these planetary materials were also differentiated, the obtained data were combined with differentiated meteorites in Part II.

2. Differentiated Stony Meteorites

2.1. Primitive Achondrites

The first study of ureilites, ultramafic achondrites, the majority of which consist of olivine and uninverted pigeonite, i.e., a clinopyroxene subgroup with 5–25% of Ca^{2+} fraction (see MBD), by Mössbauer spectroscopy was done in [6]. The authors studied two falls: Novo Urei (this meteorite gave the name "ureilites" for the group of primitive achondrites) and Haverö, and seven finds in Antarctica: ALHA84136 (not mentioned in MBD), ALHA81101, Pecora Escarpment (PCA) 82506, Elephant Moraine (EET) 87517, EET 87511, Meteorite Hills (MET) A78008, and ALHA77257. The room temperature Mössbauer spectra of Novo Urei, Haverö, ALHA84136, and ALHA81101 meteorites are shown in Figure 1. All Mössbauer spectra consist of one or two magnetic sextets assigned to Fe-Ni-Co alloys and Fe^{3+} compounds (hematite or maghemite and goethite, ferrihydrite, akaganéite, or nanophase goethite as the authors supposed), two quadrupole doublets related to olivine and pyroxene, and one quadrupole doublet associated with the paramagnetic Fe^{3+} compound. The δ and ΔE_Q values of olivine are in the ranges ~1.14–1.21 mm/s and ~2.89–2.95 mm/s, respectively, while those for pyroxene (pigeonite) are in the ranges ~1.12–1.18 mm/s and ~1.88–2.35 mm/s, respectively. The δ and ΔE_Q values for the paramagnetic ferric compounds are in the ranges ~0.36–0.43 mm/s and ~0.59–0.71 mm/s, respectively. The relative fractions of Fe were found (**i**) in metallic alloy in the range ~0–47%, (**ii**) in olivine in the range ~31–90%, (**iii**) in pyroxene in the range ~10–69%, and (**iv**) in ferric compounds in the range ~3–69%.

Furthermore, the representative of this group of primitive achondrites, the Almahata Sitta anomalous ureilite, was studied by Mössbauer spectroscopy in [7]. The room temperature Mössbauer spectrum of Almahata Sitta is shown in Figure 2. The authors revealed from the spectrum fit four magnetic sextets and three quadrupole doublets. On the basis of the ^{57}Fe hyperfine parameters, these magnetic sextets were assigned to (**i**) α-Fe(Ni)

phase, kamacite (δ = −0.002 mm/s, H_{eff} = 332.2 kOe, A = 35%), (**ii**) γ-Fe(Ni) phase, taenite (δ = −0.04 mm/s, H_{eff} = 306 kOe, A = 3%), (**iii**) troilite (δ = 0.76 mm/s, H_{eff} = 302 kOe, A = 2%), and (**iv**) cohenite $(Fe, Ni, Co)_3C$ (δ = 0.11 mm/s, H_{eff} = 199 kOe, A = 2%). Three quadrupole doublets were associated with (**i**) olivine (δ = 1.151 mm/s, ΔE_Q = 2.983 mm/s, A = 32%), (**ii**) pyroxene, which was assigned to unresolved contributions from orthopyroxene and pigeonite (δ = 1.147 mm/s, ΔE_Q = 2.139 mm/s, A = 24%), and (**iii**) an unknown Fe^{3+} compound or pyrite (δ = 0.52 mm/s, ΔE_Q = 0.67 mm/s, A = 2%).

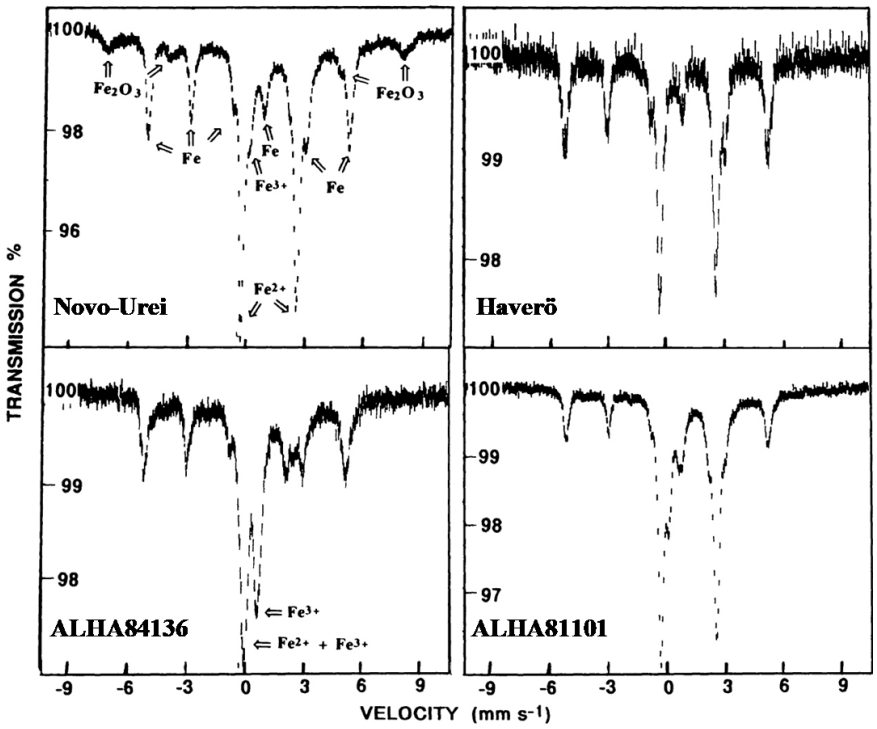

Figure 1. Room temperature Mössbauer spectra of ureilites Novo Urei, Haverö, ALHA84136, and ALHA81101. Adapted from [6].

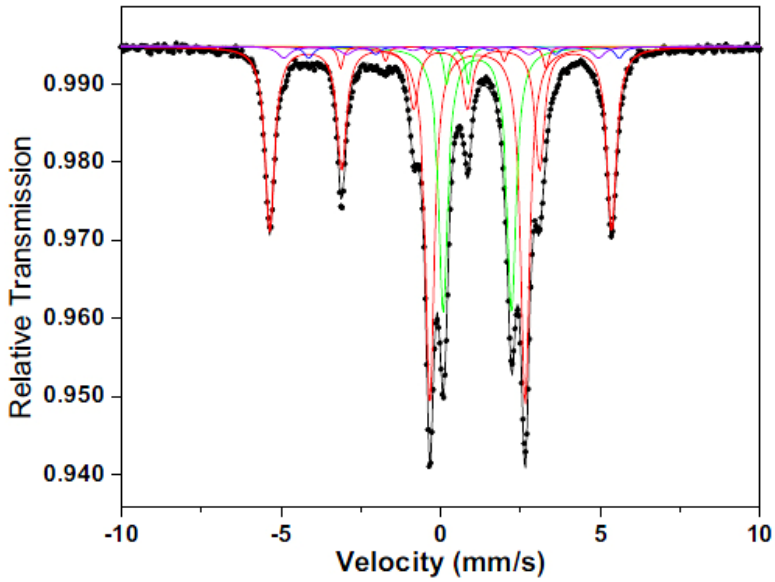

Figure 2. Room temperature Mössbauer spectra of the Almahata Sitta anomalous ureilite. Indicated spectral components are the result of the fit. Adapted from [7].

2.2. Achondrites (Stony Meteorites Except HED and Martian Meteorites)

The Zakłodzie meteorite, an ungrouped enstatite-rich achondrite, was studied by Mössbauer spectroscopy in [8]. The room temperature Mössbauer spectrum of this meteorite is shown in Figure 3. The authors used three fits with different components and compared their results with those obtained for the Abee EH4 enstatite chondrite in [9] (see Figure 8 in Part I [1]). The second and the third fits revealed the same components **1**–**6**, while components **7** and **8** were different (the second fit is shown in Figure 3). The first six components, which are common for the two fits, were assigned by the authors to (**1**) kamacite, α-Fe(Ni) phase (δ = 0.02 mm/s, H_{eff} = 330 kOe, A = 13%), (**2**) taenite, γ-Fe(Ni) phase (δ = 0.46 mm/s, H_{eff} = 310 kOe, A = 6%), (**3**) pyrrhotite (δ = 0.39 mm/s, H_{eff} = 170 kOe, A = 7%), (**4**) pyrrhotite (δ = 0.01 mm/s, H_{eff} = 260 kOe, A = 21%), (**5**) troilite (δ = 0.79 mm/s, H_{eff} = 310 kOe, A = 2%), and (**6**) plagioclase $NaAlSi_3O_8$–$CaAl_2Si_2O_8$ (δ = 1.31 mm/s, ΔE_Q = 3.07 mm/s, A = 6%). The remaining **7** and **8** components were associated in the second fit to (**7**) pentlandite $(Fe, Ni)_9S_8$ (δ = 1.02 mm/s, ΔE_Q = 0.19 mm/s, A = 2%) and (**8**) violarite ($Fe^{2+}Ni_2^{3+}S_4$) (δ = 0.36 mm/s, ΔE_Q = 0.67 mm/s, A = 42%), while those in the third fit were related to (**7**) γ-FeNi phase (δ = 0.02 mm/s, A = 20%) and (**8**) niningerite (Fe, Mg)S (δ = 0.72 mm/s, A = 24%).

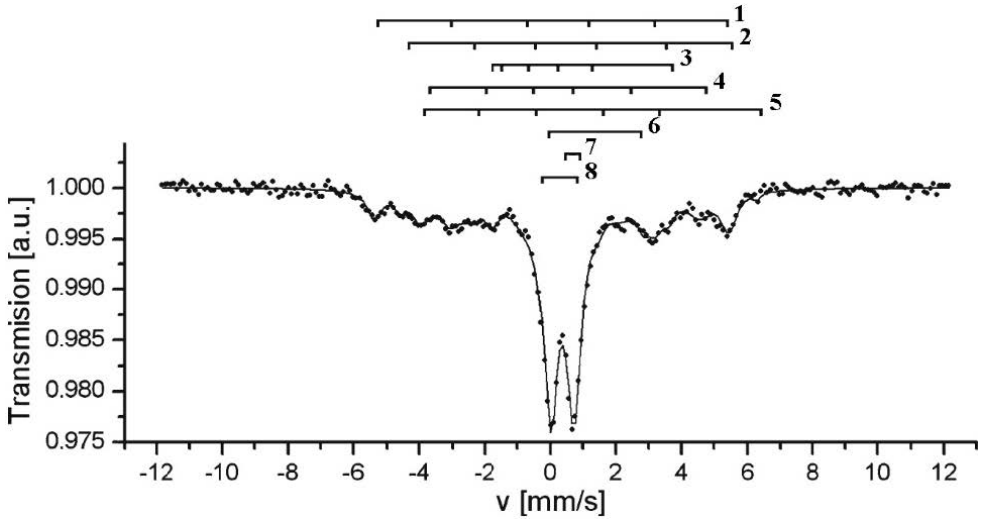

Figure 3. Room temperature Mössbauer spectra of the Zakłodzie ungrouped enstatite-rich achondrite. Indicated components are the result of the authors' second fit (see [8] and the text above). Adapted from [8].

However, the results of these fits lead to many questions for the following reasons: the δ value for the γ-Fe(Ni) phase (**2**) is unusually large; the parameters of two components associated with pyrrhotite are very different and also differ from Mössbauer parameters for pyrrhotite obtained in [10]; plagioclase (**6**) is a mineral that does not contain iron and cannot give the Mössbauer spectrum, while the ^{57}Fe hyperfine parameters for component **6** are close to olivine; if singlets **7** and **8** in the third fit are considered as a quadrupole doublet, they can correspond to the paramagnetic ferric compound. Therefore, the Mössbauer parameters obtained in [8] should be carefully verified.

Mössbauer spectroscopy was applied to the study of D'Orbigny angrite, a relatively rare type of basaltic achondrite, in [11,12]. The authors extracted and analyzed first the bulk and glass material [11] and then the druse clinopyroxene [12]. Glasses may be formed as a result of impact processes in the parent body or other factors. A comparison of the room temperature Mössbauer spectra of the bulk and glass materials from D'Orbigny angrite is shown in Figure 4.

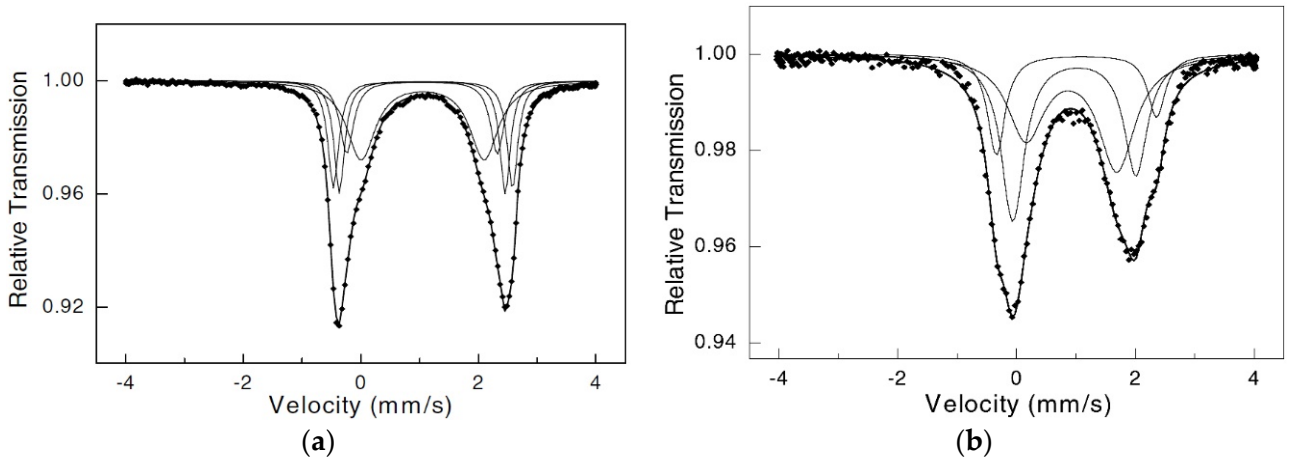

Figure 4. Comparison of the room temperature Mössbauer spectra of the bulk (**a**) and glass (**b**) materials from D'Orbigny angrite. Indicated spectral components are the results of the fits. Adapted from [11].

The Mössbauer spectrum of the bulk material from D'Orbigny angrite was fitted by the authors of [11] using four quadrupole doublets, two outer doublets of which were related to olivine while the two inner doublets were assigned to pyroxene. These four quadrupole doublets were associated with the M1 and M2 sites in both olivine and pyroxene. In contrast, the spectrum of glass material was decomposed with three quadrupole doublets only. Two doublets with the larger ΔE_Q values were assigned to the M1 and M2 sites in pyroxene. The ^{57}Fe hyperfine parameters for these sites in pyroxene from the bulk and glass materials were close: (**i**) δ = 1.15 mm/s, ΔE_Q = 2.56 mm/s (M1) and δ = 1.16 mm/s, ΔE_Q = 2.09 mm/s (M2) for the bulk material and (**ii**) δ = 1.12 mm/s, ΔE_Q = 2.70 mm/s, A = 17% (M1) and δ = 1.08 mm/s, ΔE_Q = 2.07 mm/s, A = 40% (M2) for the glass material. The parameters for the third quadrupole doublet in the glass spectrum were determined as δ = 1.03 mm/s, ΔE_Q = 1.53 mm/s, A = 43%. The latter component was not identified. However, there is a question concerning the fit of the glass spectrum because the third quadrupole doublet has a broad line width Γ = 0.74 mm/s which is twice larger than that for the M1 component (Γ = 0.36 mm/s).

The room temperature Mössbauer spectra of the druse clinopyroxene extracted from the D'Orbigny angrite represent an asymmetrical quadrupole doublet with a small admixture of the paramagnetic ferric component in both single crystal and powder forms [12]. The authors fitted their spectra using the quadrupole splitting distribution with a Voigt line shape instead of individual quadrupole doublets with a Lorentzian line shape. Therefore, the obtained Mössbauer parameters seem questionable and require new decomposition with individual quadrupole doublets which can be better related to the M1 and M2 sites in clinopyroxene.

2.3. Achondrites (HED)

HED meteorites, whose parent body is considered the asteroid (4) Vesta [3], consist of the main iron bearing phases such as Fe-rich pyroxene in eucrites, orthopyroxene in diogenite, and pyroxene (mainly orthopyroxene) in howardites which are a polymict-breccia, i.e., a mixture of eucrites and diogenites (see MBD). The first Mössbauer studies of HED meteorites were performed in [13–18]. The Mössbauer spectra of ALHA77256 diogenite and Stannern eucrite measured in [13] were different. One quadrupole doublet corresponding to pyroxene was observed in the spectra of the former meteorite samples and assigned to the M2 sites occupied by Fe^{2+}. Four quadrupole doublets were revealed in the spectrum of the latter sample. These quadrupole doublets were related to the M1 and M2 sites and to the M1 sites in orthopyroxenes (probably pigeonite), as well as to ilmenite. Similar results were obtained for the paramagnetic components observed in the Stannern eucrite Mössbauer spectrum in [14]; however, in addition, the authors revealed the magnetic sextet

with parameters corresponding to troilite. The room temperature Mössbauer spectrum of Ibitira eucrite consisted of three quadrupole doublets that were assigned to the M1 and M2 sites in pigeonite and to ilmenite [15]. Furthermore, the authors estimated the ratio of Fe^{2+} populations in the M1 and M2 sites in pigeonite from Ibitira as A^{M2}/A^{M1} = 1.92 (in the 55 K Ibitira spectrum, the authors of [15,17] revealed two quadrupole doublets only related to the M1 and M2 sites in pigeonite with A^{M2}/A^{M1} = 2.11). Similar results were obtained in [16] for the Mössbauer spectra of Juvinas, ALHA80102, and EET 83232 eucrites with two quadrupole doublets related to the M1 and M2 sites in pyroxene and one quadrupole doublet assigned to ilmenite, as well as an additional quadrupole doublet associated with ferric compound. The Mössbauer spectra of Tatahouine, ALHA77256, and EETA79002 diogenites measured in [16] consisted of one quadrupole doublet related to the M2 sites in pyroxene and an additional quadrupole doublet assigned to ferric compounds. However, the room temperature Mössbauer spectrum of Kapoeta howardite was fitted using two quadrupole doublets related to the M1 and M2 sites in pyroxene [18].

The Mössbauer spectra of Cachari and Piplia Kalan eucrites (monomict breccias) measured in [11,19] are shown in Figure 5. In the spectrum of Cachari, the authors of [11] revealed three quadrupole doublets related to the M1 and M2 sites in pyroxenes and paramagnetic ferric compound. The ^{57}Fe hyperfine parameters for pyroxene were δ = 1.16 mm/s, ΔE_Q = 2.46 mm/s (M1 sites) and δ = 1.13 mm/s, ΔE_Q = 2.00 mm/s (M2 sites). However, the authors did not consider the meaning of a small peak at around +3 mm/s. Similar results were obtained for the Piplia Kalan spectra measured for two different lithologies A and B in [19]. The Mössbauer parameters for both lithologies were in fact the same and are as follows for the lithology A: δ = 1.13 mm/s, ΔE_Q = 2.40 mm/s, A = 22% (M1 sites), δ = 1.08 mm/s, ΔE_Q = 1.94 mm/s, A = 73% (M2 sites) and δ = 0.26 mm/s, ΔE_Q = 0.93 mm/s, A = 5% (ferric compound).

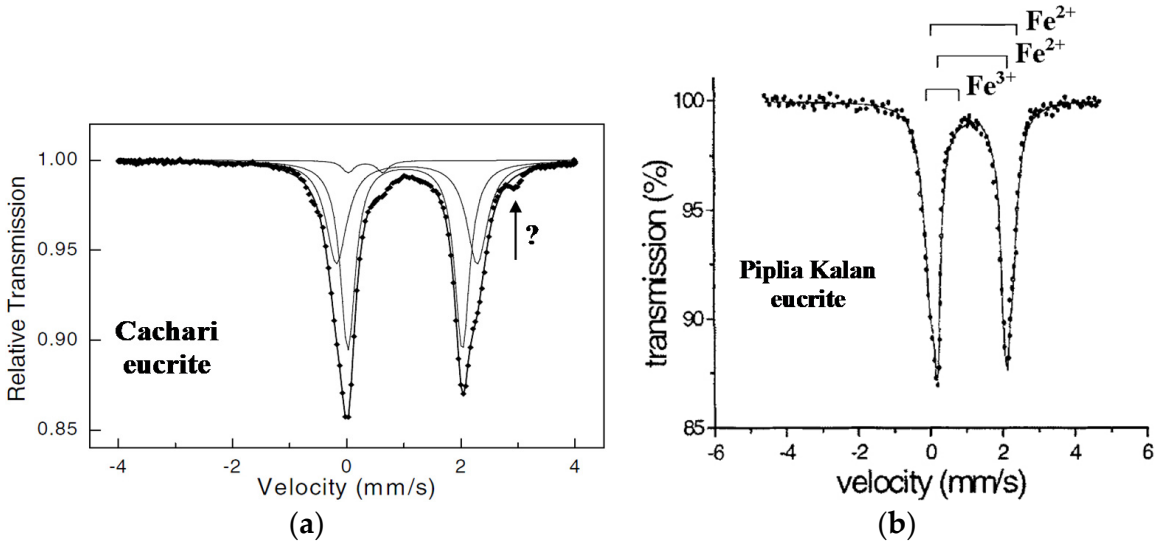

Figure 5. Comparison of the room temperature Mössbauer spectra of Cachari (**a**) and Piplia Kalan, lithology A (**b**) monomict eucrites. Indicated spectral components are the results of the fits. Adapted from [11,19].

A comparison of five cumulative and basaltic eucrites and one diogenite was done by Mössbauer spectroscopy in [20]. Cumulate eucrites and diogenites seem to have formed at depth in the asteroid (4) Vesta and crystallized quite slowly, while basaltic eucrites apparently formed at or near Vesta's surface and cooled relatively fast. The authors of [20] decomposed their Mössbauer spectra with different numbers of components: (**i**) one quadrupole doublet for cumulate eucrites and diogenite and (**ii**) two quadrupole doublets for basaltic eucrites as shown in Figure 6.

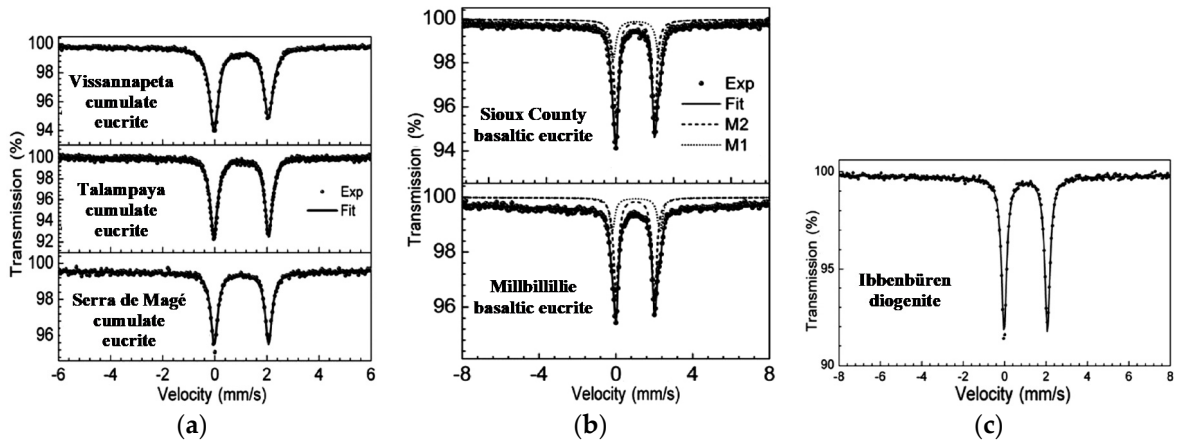

Figure 6. Comparison of the room temperature Mössbauer spectra of cumulative eucrites (**a**), basaltic eucrites (**b**), and diogenite (**c**). Adapted from [20].

The Mössbauer parameters for two quadrupole doublets in the spectra of basaltic eucrites were related to the M1 and M2 sites in pyroxene: δ = 1.15 mm/s, ΔE_Q = 2.42 mm/s, A = 35% (M1 sites), δ = 1.10 mm/s, ΔE_Q = 2.01 mm/s, A = 65% (M2 sites) for Sioux County and δ = 1.14 mm/s, ΔE_Q = 2.49 mm/s, A = 27% (M1 sites), δ = 1.10 mm/s, ΔE_Q = 2.01 mm/s, A = 73% (M2 sites) for Millbillillie. The ^{57}Fe hyperfine parameters for the M2 sites in pyroxene in cumulate eucrites and diogenite were almost the same (δ = 1.10–1.11 mm/s, ΔE_Q = 2.09–2.12 mm/s). The authors of [19] focused on the asymmetry of peak intensities in the Mössbauer spectra of cumulate eucrites which were fitted using one quadrupole doublet, while similar asymmetry in the spectra of basaltic eucrites was fitted using a superposition of two quadrupole doublets. The authors suggested that this asymmetry may be related to the pyroxene crystal orientation in the former group of meteorites. However, this should be verified by new studies, because the Mössbauer spectrum of Ibbenbüren diogenite demonstrated symmetrical peaks in one quadrupole doublet.

Earlier, one quadrupole doublet was applied to fit the Mössbauer spectra of three diogenites: ALHA77256, Tatahouine, and Bilanga [21]. These spectra are shown in Figure 7. The ^{57}Fe hyperfine parameters assigned to the M2 sites in pyroxene were almost the same: δ = 1.10–1.11 mm/s, ΔE_Q = 2.10–2.12 mm/s.

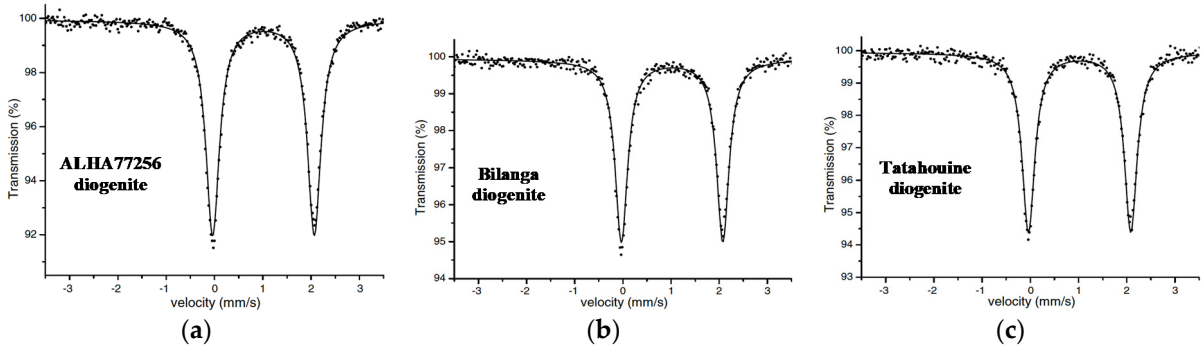

Figure 7. Comparison of the room temperature Mössbauer spectra of diogenites: ALHA77256 (**a**), Bilanga (**b**), and Tatahouine (**c**). Adapted from [21].

The effect of high pressure on Lohawat howardite and Piplia Kalan eucrite was studied by Mössbauer spectroscopy in [22,23]. The authors observed a decrease in the δ and ΔE_Q values for the M2 sites in pyroxene in both meteorites with increasing pressure as shown in Figure 8. These results may be useful for the study of meteorites and their parent body collisions.

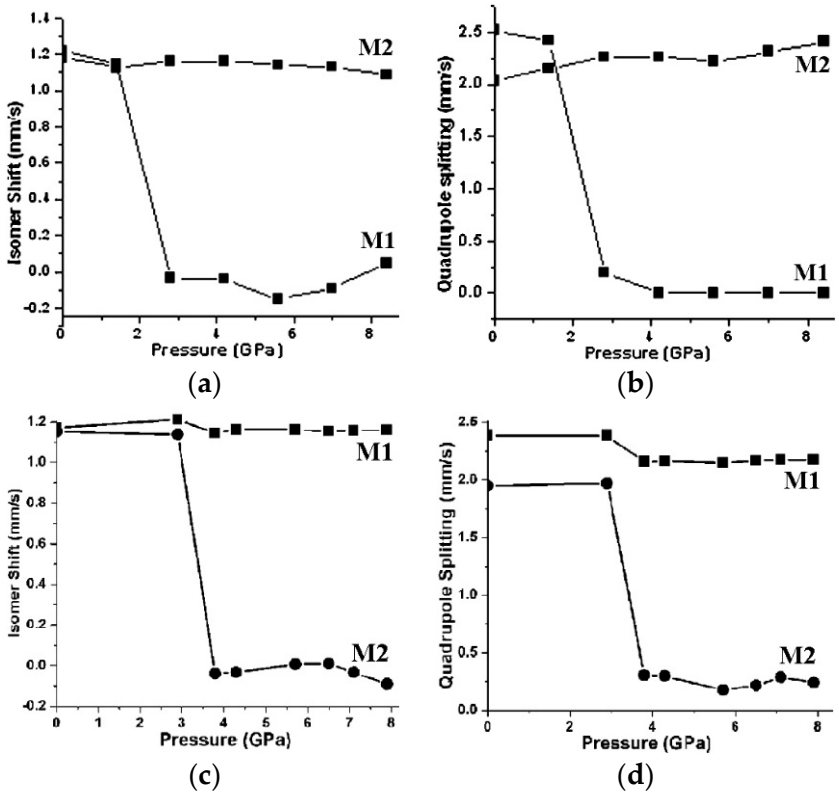

Figure 8. Different variations in the values of isomer shift (**a**,**c**) and quadrupole splitting (**b**,**d**) for the M1 and M2 sites in pyroxene vs. pressure in Lohawat howardite (**a**,**b**) and Piplia Kalan eucrite (**c**,**d**). Adapted from [22,23].

The Kapoeta howardite was studied by both XRD and Mössbauer spectroscopy in order to analyze its thermal history in [24]. The calculated values of the cation distribution coefficient K_D and closure temperature T_{Cl} (see Part I, Section 6.7 [1]) for orthopyroxene in Kapoeta were different for XRD and Mössbauer data, e.g., T_{Cl} = 684 K and 630 K from XRD and T_{Cl} = 1017 K from Mössbauer data. The obtained values of A^{M1} and A^{M2} for the M1 and M2 sites in orthopyroxene were ~20% and ~80%. However, these values disagreed with data A^{M1} = ~41% and A^{M2} = ~59% known from a previous Mössbauer study of Kapoeta in [18], which may be not correct.

Mössbauer spectroscopy with a high velocity resolution was used to study the bulk interior and the fusion crust of the Sariçiçek howardite in [25]. These Mössbauer spectra are shown in Figure 9. Two magnetic sextets, nine quadrupole doublets, and one paramagnetic singlet were revealed in the spectrum of the bulk interior. On the base of the ^{57}Fe hyperfine parameters, these spectral components were assigned to the following phases: (**i**) α-Fe(Ni, Co), δ = −0.002 mm/s, H_{eff} = 333.8 kOe, A = ~2.5%; (**ii**) troilite, δ = 0.763 mm/s, H_{eff} = 310.1 kOe, A = ~2.4%; (**iii**) M1 sites in orthopyroxene, δ = 1.053 mm/s, ΔE_Q = 2.708 mm/s, A = ~7.4%; (**iv**) M2 sites in orthopyroxene, δ = 1.124 mm/s, ΔE_Q = 2.070 mm/s, A = ~36.6%; (**v**) M1 sites in Ca-poor clinopyroxene, δ = 1.183 mm/s, ΔE_Q = 2.650 mm/s, A = ~10.3%; (**vi**) M2 sites in Ca-poor clinopyroxene, δ = 1.104 mm/s, ΔE_Q = 1.942 mm/s, A = ~15.6%; (**vii**) M1 sites in Ca-rich clinopyroxene, δ = 1.129 mm/s, ΔE_Q = 2.311 mm/s, A = ~12.8%; (**viii**) M2 sites in Ca-rich clinopyroxene, δ = 1.086 mm/s, ΔE_Q = 1.729 mm/s, A = ~5.3%; (**ix**) hercynite, δ = 1.012 mm/s, ΔE_Q = 1.363 mm/s, A = ~2.0%; (**x**) ferrous ilmenite, δ = 1.072 mm/s, ΔE_Q = 0.701 mm/s, A = ~1.8%; (**xi**) ferric ilmenite, δ = 0.210 mm/s, ΔE_Q = 0.689 mm/s, A = ~1.3%; (**xii**) chromite, δ = 0.953 mm/s, A = ~2.1%. These phases are in agreement with the results of chemical analysis by scanning electron microscopy with energy dispersive spectroscopy and phase analysis by XRD. The ratio of A^{M1} and A^{M2} for orthopyroxene in Sariçiçek is

close to that obtained for Kapoeta in [24]. Using approaches considered in Part 1, Sections 6.6 and 6.7 [1], the ratios of Fe^{2+} occupancies among the M1 and M2 sites in silicate crystals, as well as the values of K_D and T_{eq}, were calculated using both XRD and Mössbauer data. These ratios were the following: $A^{M1}/A^{M2} \approx 0.20$ and $X_{Fe}{}^{M1}/X_{Fe}{}^{M2} \approx 0.18$ for orthopyroxene, $A^{M1}/A^{M2} \approx 0.66$ and $X_{Fe}{}^{M1}/X_{Fe}{}^{M2} \approx 0.66$ for Ca-poor clinopyroxene, and $A^{M1}/A^{M2} \approx 2.40$ and $X_{Fe}{}^{M1}/X_{Fe}{}^{M2} \approx 1.84$ for Ca-rich clinopyroxene. These ratios agreed for the two independent techniques. The Fe^{2+} and Mg^{2+} cation equilibrium distributions among the M1 and M2 sites in orthopyroxene in Sariçiçek howardite related to its thermal history were $K_D = 0.12$ and $T_{eq} = 886$ K (XRD) and $K_D = 0.12$ and $T_{eq} = 878$ K (Mössbauer spectroscopy). The value of Fs was 28% (from MBD). The K_D and T_{eq} values also agreed for the two independent techniques.

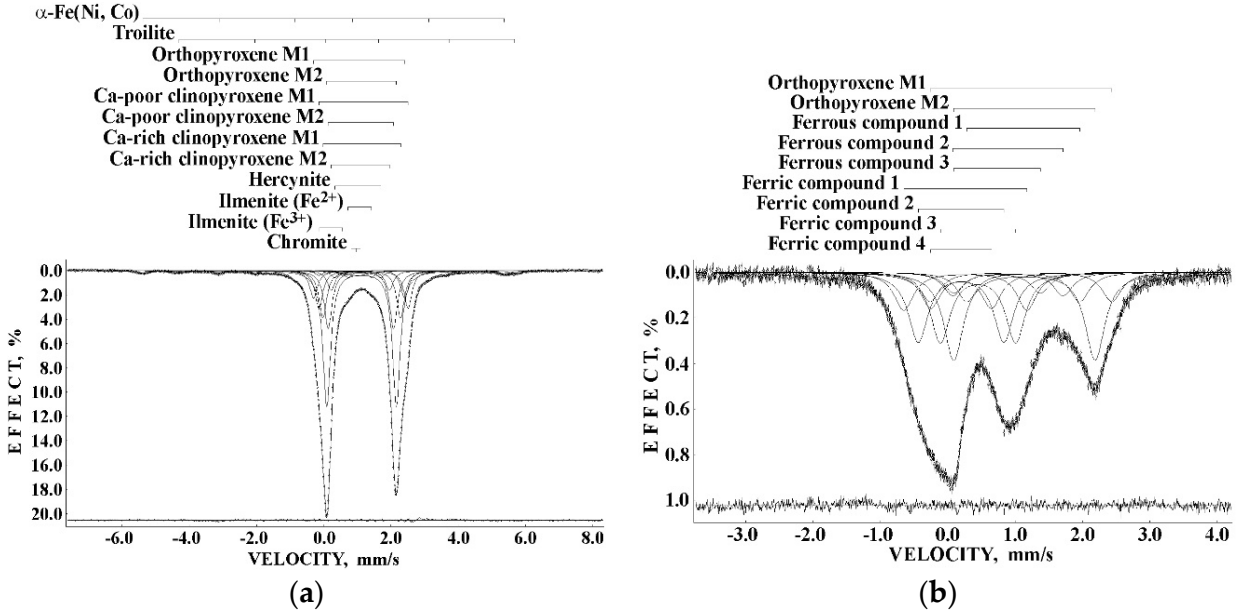

Figure 9. Room temperature Mössbauer spectra of Sariçiçek howardite measured with a high-velocity resolution: the bulk interior (**a**) and the fusion crust (**b**). Indicated components are the results of the best fits. The differential spectra are shown on the bottom. Adapted from [25].

The first study of the fusion crust by Mössbauer spectroscopy was carried out for Stannern eucrite in [14]. The authors used a 1:1 mixture of the bulk interior and the fusion crust and observed in the Mössbauer spectrum two quadrupole doublets related to the M1 and M2 sites in pyroxene, two quadrupole doublets assigned to ilmenite and ferric compound, and two magnetic sextets associated with troilite and Fe-Ni-Co alloy. In the study of Sariçiçek fusion crust [25], the sample contained only the fusion crust material. It was a glass-like matter as demonstrated by XRD. The Mössbauer spectrum of Sariçiçek fusion crust (see Figure 9b) did not contain any magnetic sextets but consisted of nine quadrupole doublets revealed from the fit with known components of orthopyroxene and unknown ferrous and ferric compounds. Two quadrupole doublets with the largest quadrupole splitting were related to the M1 and M2 sites in orthopyroxene ($\delta = 1.088$ mm/s, $\Delta E_Q = 2.699$ mm/s, A = ~7.3% for the M1 sites; $\delta = 1.139$ mm/s, $\Delta E_Q = 2.099$ mm/s, A = ~21.7% for the M2 sites). The ratio of Fe^{2+} occupancies among the M1 and M2 sites in orthopyroxene was $A^{M1}/A^{M2} \approx 0.34$, which is larger than that obtained for the bulk interior. The values of K_D and T_{FC} calculated for Sariçiçek fusion crust were 0.23 and 1177 K. The latter indicates that the fast cooling and solidification of the molten fusion crust was started in the temperature range 1100–1200 K.

2.4. Achondrites (Lunar and Martian Meteorites)

Lunar and Martian stony achondrites are rocks which were ejected from the Moon and Mars by impacts and later fell to the Earth as meteorites (see MBD). Martian meteorites are divided into three main groups: shergottites (named after the Shergotty meteorite), nakhlites (named after the Nakhla meteorite), and chassignites (named after the Chassigny meteorite). These groups were named as SNC meteorites as an abbreviation using the first letters of the above-mentioned meteorite names. Until now, no studies on Lunar meteorites using Mössbauer spectroscopy have been carried out. On the contrary, Mössbauer investigations of Martian meteorites and their extracted iron-bearing phases have been carried out since mid-1980s (see, e.g., [6,16,26]). In the first study [26] of three SNC achondrites (Zagami and EETA79001 shergottites and Nakhla) the authors identified different iron-bearing phases in these meteorites. The spectrum of Zagami consisted of two quadrupole doublets related to the M1 and M2 sites in pyroxene (δ = 1.16 mm/s, ΔE_Q = 2.47 mm/s and δ = 1.14 mm/s, ΔE_Q = 2.01 mm/s, respectively). The Mössbauer spectrum of EETA79001 was decomposed into three quadrupole doublets, two of which were assigned to the M1 and M2 sites in pyroxene (δ = 1.16 mm/s, ΔE_Q = 2.40 mm/s and δ = 1.14 mm/s, ΔE_Q = 2.27 mm/s, respectively) while one was assigned to the M1 site in olivine (δ = 1.15 mm/s, ΔE_Q = 2.88 mm/s). The spectrum of Nakhla was much more complex and consisted of magnetic and paramagnetic components. Therefore, the authors also measured the paramagnetic and magnetic separation. The Mössbauer spectrum of the paramagnetic separate from Nakhla was decomposed into four quadrupole doublets: two different M1 sites and M2 sites in pyroxene (δ = 1.17 mm/s, ΔE_Q = 2.60 mm/s; δ = 1.16 mm/s, ΔE_Q = 2.03 mm/s and δ = 1.16 mm/s, ΔE_Q = 1.83 mm/s, respectively) and M1 sites in olivine (δ = 1.17 mm/s, ΔE_Q = 2.90 mm/s). The spectrum of magnetic separate from Nakhla was fitted using two magnetic sextets for the (A) and [B] sites in magnetite (δ = 0.27 mm/s, H_{eff} = 475 kOe and δ = 0.68 mm/s, H_{eff} = 463 kOe, respectively) and four quadrupole doublets assigned to ilmenite (δ = 1.06 mm/s, ΔE_Q = 0.68 mm/s), ulvöspinel Fe_2TiO_4 (δ = 1.16 mm/s, ΔE_Q = 1.52 mm/s), and residual pyroxene. Investigations of [6,16] were dedicated to the SNC meteorite weathering and detection of ferric compounds in order to consider the possible preterrestial oxidation, i.e., oxidation on Mars.

Two different samples of Zagami shergottite, marked as BM (from British Museum) and DN (from the firm David New, Anacortes, Washington), were studied by Mössbauer spectroscopy in [27]. The authors demonstrated inhomogeneity of the Zagami meteorite showing different Mössbauer spectra for these samples (see Figure 10). Both spectra were different from that measured for Zagami in [26] and consisted of two quadrupole doublets only (see above). The Mössbauer spectrum of Zagami BM was fitted with three quadrupole doublets related to two different M1 sites and M1 + M2 sites in pyroxene (δ = 1.16 mm/s, ΔE_Q = 2.66 mm/s, A = ~15%; δ = 1.14 mm/s, ΔE_Q = 2.35 mm/s, A = ~16% and δ = 1.13 mm/s, ΔE_Q = 1.97 mm/s, A = ~69%, respectively). In contrast, the spectrum of Zagami DN consisted of the same quadrupole doublets for two different M1 sites and M1 + M2 sites in pyroxene (δ = 1.14 mm/s, ΔE_Q = 2.69 mm/s, A = ~24%; δ = 1.17 mm/s, ΔE_Q = 2.38 mm/s, A = ~16% and δ = 1.14 mm/s, ΔE_Q = 1.95 mm/s, A = ~37%, respectively), an additional quadruple doublet for olivine (δ = 1.17 mm/s, ΔE_Q = 2.92 mm/s, A = ~23%), a quadrupole doublet assigned to ilmenite, and two magnetic sextets associated with pyrrhotite.

Ten various SNC meteorites with different lithologies and extracted olivine and pyroxene were studied by Mössbauer spectroscopy in [28] in order to analyze ferric compounds. The Mössbauer spectra of the bulk material from selected SNC meteorites are shown in Figure 11.

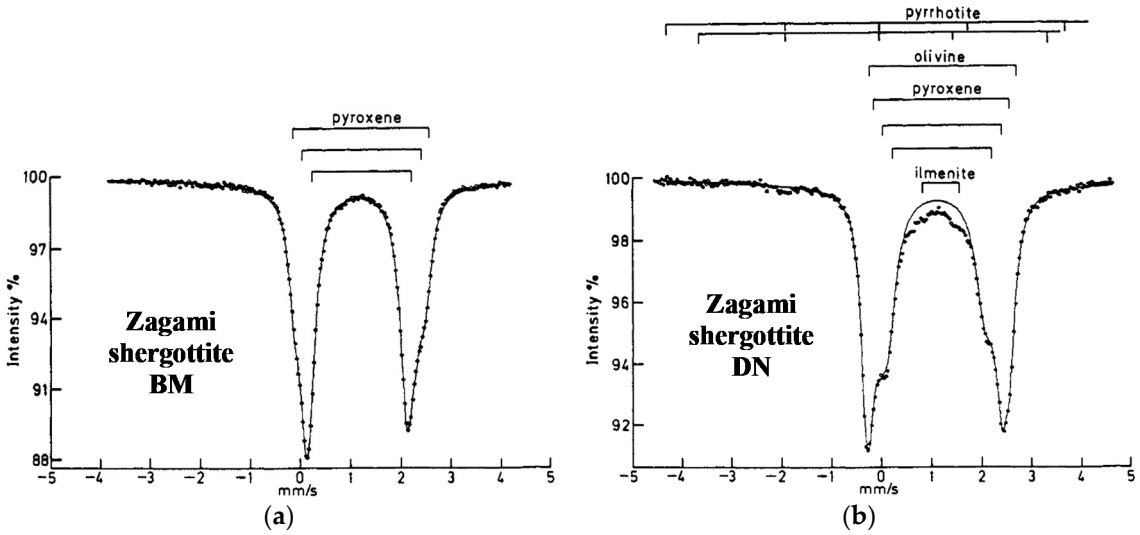

Figure 10. Room temperature Mössbauer spectra of Zagami shergottite: sample BM (**a**) and sample DN (**b**). Indicated components are the results of the fits. Adapted from [27].

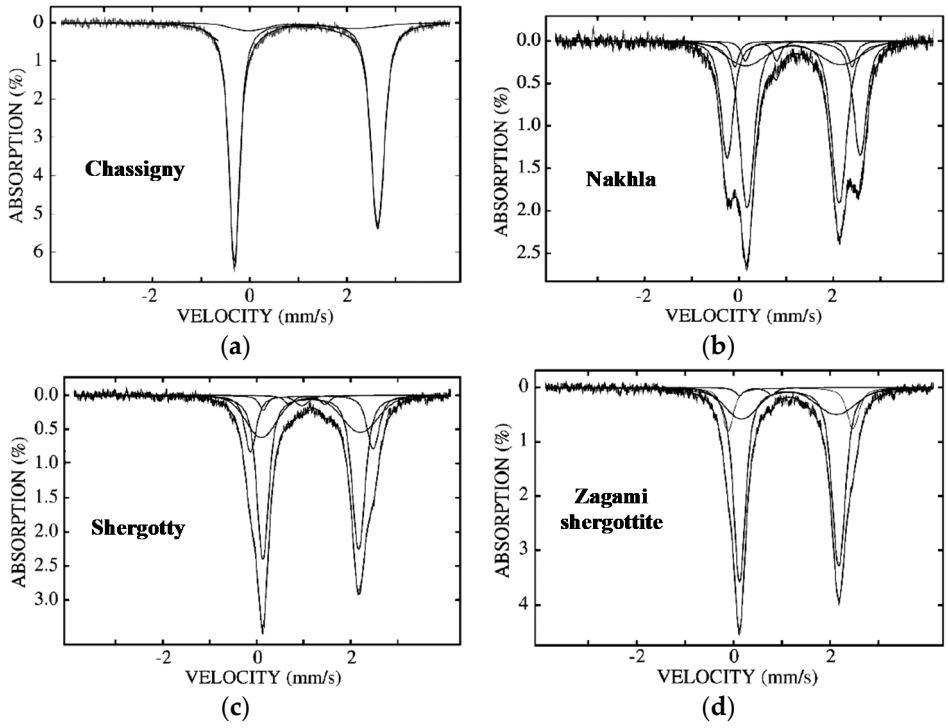

Figure 11. Room temperature Mössbauer spectra of selected SNC meteorites (bulk material): Chassigny (**a**), Nakhla (**b**), Shergotty (**c**), and Zagami shergottite (**d**). Indicated components are the results of the fits. Adapted from [28].

These spectra show different fractions of olivine and pyroxene in these meteorites and different spectral components in the spectra of the bulk materials and separated olivine and pyroxene. The presence of ferric compounds was observed in the Mössbauer spectra of some SNC meteorites. These spectra were fitted using the quadrupole splitting distribution that lead to some questions because, in the case of the thin absorber with well-defined crystal sites for the ^{57}Fe nuclei, the fit with individual quadrupole doublets directly related to these sites seems much more reasonable than the fit by the model-independent distribution function. It is noteworthy that the Mössbauer spectra of Zagami shergottite measured in [27,28] were different.

Investigations of MIL 03346 nakhlite with dominant clinopyroxene content and extracted clinopyroxene, as well as NWA 2737 chassignite, which is rich with olivine and extracted olivine, were studied by Mössbauer spectroscopy in [29–31], respectively. The Mössbauer spectra of the bulk materials and extracted silicates from the MIL 03346 and NWA 2737 meteorites are shown in Figure 12.

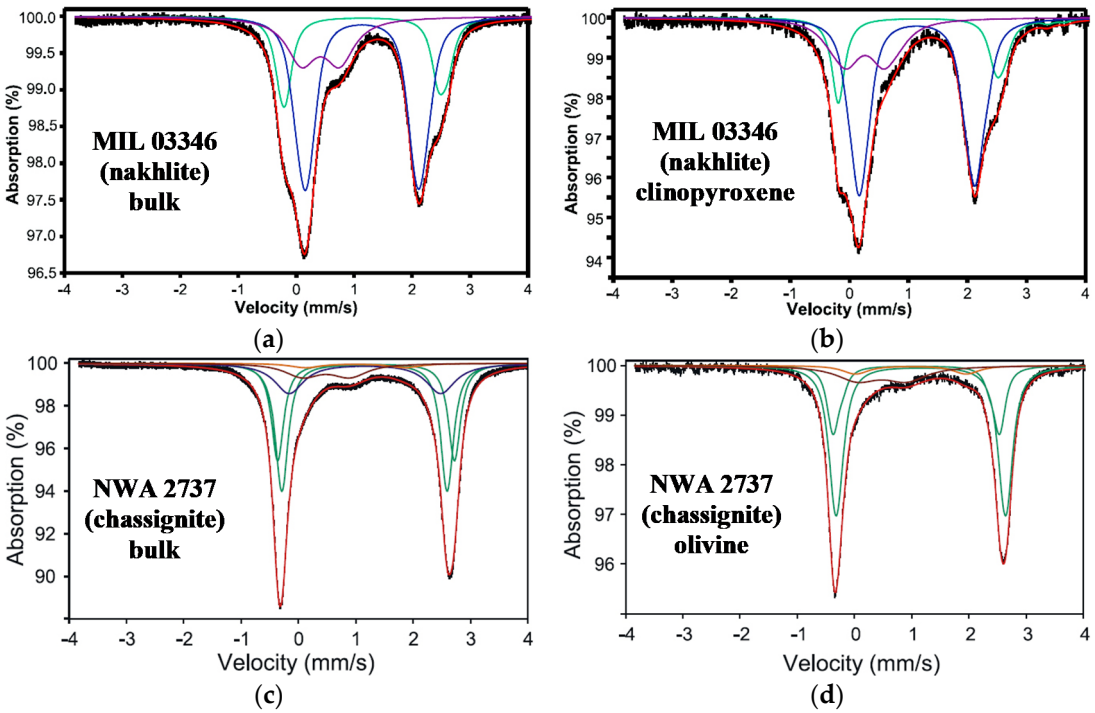

Figure 12. Room temperature Mössbauer spectra of the MIL 03346 and NWA 2737 SNC meteorites: bulk material (**a**,**c**), extracted MIL 03346 clinopyroxene (**b**), and extracted NWA 2737 olivine (**d**). Indicated components are the results of the fits. Adapted from [29,30].

The spectra of the bulk materials were similar to those of the extracted silicates, confirming the dominant content of clinopyroxene in MIL 03346 and olivine in NWA 2737. Measuring the low temperature Mössbauer spectra of NWA 2737 samples did not reveal any magnetically split components. The room temperature Mössbauer parameters obtained for MIL 03346 samples were as follows: (**i**) Fe^{2+} (δ = 1.14 mm/s, ΔE_Q = 2.60 mm/s, A = 23.1% for the bulk material and δ = 1.15 mm/s, ΔE_Q = 2.68 mm/s, A = 19.8% for the extracted clinopyroxene), (**ii**) Fe^{2+} (δ = 1.13 mm/s, ΔE_Q = 1.95 mm/s, A = 54.2% for the bulk material and δ = 1.15 mm/s, ΔE_Q = 1.97 mm/s, A = 56.1% for the extracted clinopyroxene), and (**iii**) Fe^{3+} compounds (δ = 0.42 mm/s, ΔE_Q = 0.66 mm/s, A = 22.8% for the bulk material and δ = 0.27 mm/s, ΔE_Q = 0.61 mm/s, A = 24.2% for the extracted clinopyroxene). The authors of [29] revealed a large content of Fe^{3+} compounds and assigned them to augite. The room temperature Mössbauer parameters which were obtained for NWA 2737 samples by the authors of [30] were the following: (**i**) Fe^{2+} in olivine (δ = 1.18 mm/s, ΔE_Q = 3.07 mm/s, A = 28% for the bulk material and δ = 1.08 mm/s, ΔE_Q = 2.91 mm/s, A = 23% for extracted olivine), (**ii**) Fe^{2+} in olivine (δ = 1.15 mm/s, ΔE_Q = 2.84 mm/s, A = 38% for the bulk material and δ = 1.16 mm/s, ΔE_Q = 2.98 mm/s, A = 55% for the extracted olivine), (**iii**) Fe^{2+} in pyroxene (δ = 1.16 mm/s, ΔE_Q = 2.64 mm/s, A = 21% for the bulk material only), (**iv**) Fe^{2+} in chromite (δ = 0.99 mm/s, ΔE_Q = 1.72 mm/s, A = 3% for the bulk material and δ = 0.99 mm/s, ΔE_Q = 1.97 mm/s, A = 6% for the extracted olivine), and (**v**) Fe^{3+} in olivine, chromite (δ = 0.48 mm/s, ΔE_Q = 0.82 mm/s, A = 10% for the bulk material and δ = 0.48 mm/s, ΔE_Q = 0.84 mm/s, A = 15% for the extracted olivine). It should be noted that these results for chromite are quite different from those for the chromite component observed in the room temperature Mössbauer spectra of some ordinary chondrites (see

Figures 29 and 34 in Part I [1]) and Sariçiçek howardite (see Figure 9a above), which is a paramagnetic singlet (see, e.g., [32] and references therein and [33]). However, the presence of Fe^{2+} and Fe^{3+} in the tetrahedral or octahedral sites, respectively, is possible in the synthetic spinels $Fe_{1+x}Cr_{2-x}O_4$ if $x \neq 0$ or in the natural Cr-bearing spinels, such as magnesiochromite containing Fe and Al, by the observation of several quadrupole doublets in the Mössbauer spectra (see [33,34]). In general, the term "chromite" is used for Cr-bearing spinels [34]. Therefore, this general term mixes with the term meaning the stoichiometric or close to stoichiometric chromite with small Cr substitutions by Al, Mg, Ti, and Mn atoms. The Mössbauer spectra of the latter chromites demonstrate a single peak with some variations in δ and Γ values. The authors of [29] determined the NWA 2737 chromite formula as $(Fe^{2+}_{0.70}Mg_{0.29}Mn_{0.01})$ $(Fe^{2+}_{0.05}Ti_{0.05}Fe^{3+}_{0.10}Al_{0.34}Cr_{1.46})O_4$. These results for Cr-bearing spinels can be compared with those for chromite separate from the ALH 84001 Martian meteorite which does not belong to the SNC group, and it is considered as an orthopyroxene-rich Martian meteorite (OPX). The Mössbauer spectrum of chromite extracted from ALH 84001 OPX and measured in [35] is shown in Figure 13. This spectrum shows two quadrupole doublets corresponding to the ferrous and ferric compounds. It is possible that the Cr-bearing spinel extracted from ALH 84001 OPX also has a complex formula containing Fe^{2+} in tetrahedral and Fe^{3+} in octahedral sites and some substitutions of Cr by Fe, Al, Ti, and other metals presented in this spinel.

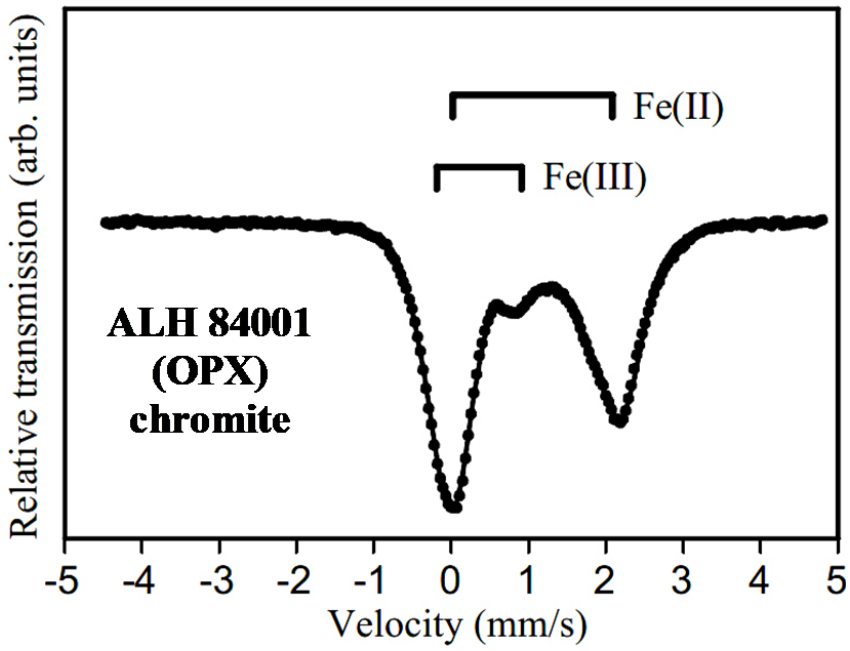

Figure 13. Room temperature Mössbauer spectrum of chromite separate from ALH 84001 OPX. Indicated spectral components are the result of the fit. Adapted from [35].

A detailed study of Yamato 984028 (Y-984028), a lherzolitic shergottite from Antarctica, was carried out with various techniques including Mössbauer spectroscopy in [36]. The authors used two fragments of Y-984028 from the bulk interior and exterior chips including the fusion crust. Moreover, they additionally extracted olivine and pyroxene from both chips. The room temperature Mössbauer spectra of the bulk material, as well as olivine and pyroxene extracts from the interior and exterior chips of Y-984028, are shown in Figure 14. These spectra were measured in 2048 channels before folding and, therefore, can be considered as measured with a high velocity resolution with discretization of the velocity reference signal on 2^{10} steps.

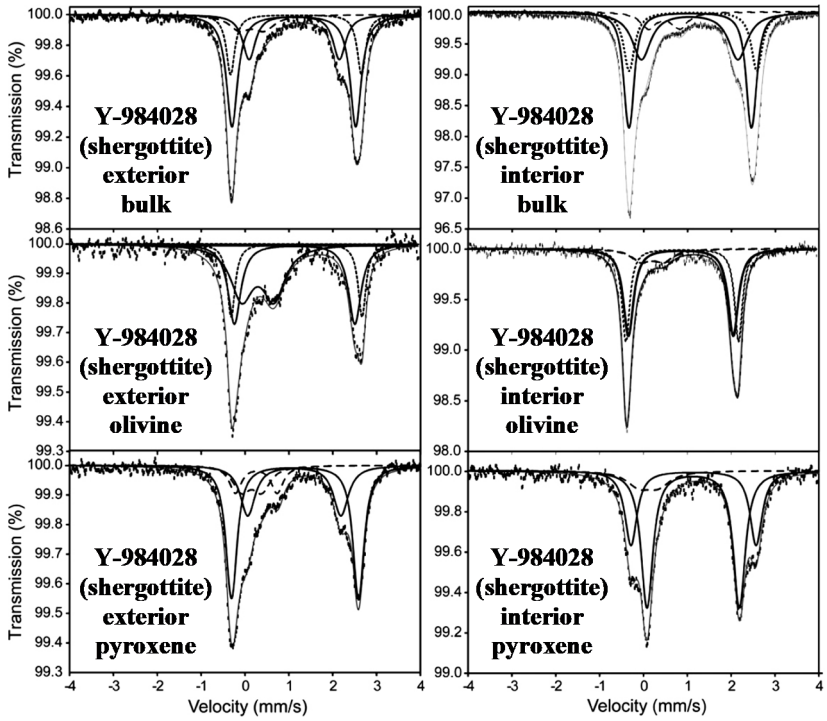

Figure 14. Room temperature Mössbauer spectra of the exterior and interior chips (bulk material) and olivine and pyroxene separates from the Y-984028 lherzolitic shergottite. Indicated spectral components are the results of the fits. Adapted from [36].

The ^{57}Fe hyperfine parameters for the same spectral components in the studied samples were very similar while the relative areas (the relative fractions) of these components in some cases were different. Mössbauer parameters for the bulk samples were as follows: (**i**) Fe^{2+} in pyroxene (δ = 1.12 mm/s, ΔE_Q = 2.04 mm/s, A = 22% for the exterior material and δ = 1.10 mm/s, ΔE_Q = 2.25 mm/s, A = 31% for the interior material), (**ii**) Fe^{2+} in olivine (δ = 1.16 mm/s, ΔE_Q = 2.99 mm/s, A = 19% for the exterior material and δ = 1.17 mm/s, ΔE_Q = 2.99 mm/s, A = 22% for the interior material), (**iii**) Fe^{2+} in olivine $\pm$ pyroxene (δ = 1.11 mm/s, ΔE_Q = 2.82 mm/s, A = 48% for the exterior material and δ = 1.11 mm/s, ΔE_Q = 2.78 mm/s, A = 39% for the interior material), and (**iv**) Fe^{3+} (δ = 0.17 mm/s, ΔE_Q = 0.55 mm/s, A = 11% for the exterior material and δ = 0.51 mm/s, ΔE_Q = 0.73 mm/s, A = 9% for the interior material). Mössbauer parameters for the olivine separates were as follows: (**i**) Fe^{2+} in olivine (δ = 1.18 mm/s, ΔE_Q = 2.98 mm/s, A = 24% for the exterior material and δ = 1.16 mm/s, ΔE_Q = 3.01 mm/s, A = 39% for the interior material), (**ii**) Fe^{2+} in olivine $\pm$ pyroxene (δ = 1.12 mm/s, ΔE_Q = 2.74 mm/s, A = 34% for the exterior material and δ = 1.12 mm/s, ΔE_Q = 2.82 mm/s, A = 48% for the interior material), and (**iii**) Fe^{3+} (δ = 0.29 mm/s, ΔE_Q = 0.71 mm/s, A = 42% for the exterior material and δ = 0.36 mm/s, ΔE_Q = 0.61 mm/s, A = 13% for the interior material). Mössbauer parameters for the pyroxene separates were as follows: (**i**) Fe^{2+} in pyroxene (δ = 1.13 mm/s, ΔE_Q = 2.17 mm/s, A = 25% for the exterior material and δ = 1.13 mm/s, ΔE_Q = 2.17 mm/s, A = 56% for the interior material), (**ii**) Fe^{2+} in olivine $\pm$ pyroxene (δ = 1.14 mm/s, ΔE_Q = 2.83 mm/s, A = 49% for the exterior material and δ = 1.14 mm/s, ΔE_Q = 2.83 mm/s, A = 32% for the interior material), (**iii**) Fe^{3+} (δ = 0.15 mm/s, ΔE_Q = 0.55 mm/s, A = 14% for the exterior material and δ = 0.11 mm/s, ΔE_Q = 0.42 mm/s, A = 12% for the interior material), and (**iv**) Fe^{3+} (δ = 0.28 mm/s, ΔE_Q = 0.96 mm/s, A = 12% for the exterior material). The spectral component marked by the authors as olivine $\pm$ pyroxene indicated a quadrupole doublet with probably unresolved contributions from both olivine and pyroxene. The exterior olivine separate contained more Fe^{3+} fraction than the interior olivine separate. This component was related to phyllosilicate.

Mössbauer spectroscopy was used for the determination of Fe^{3+} in the augite (clinopyroxene) core-crystal from MIL 03346 nakhlite in [37]. The room temperature Mössbauer spectra of the MIL 03346 augite single crystal with two different orientations are shown in Figure 15. The authors determined that the content of ferric compound was around 7%, which is significantly smaller than the ferric compound fraction obtained in [29] for clinopyroxene separate from MIL 03346.

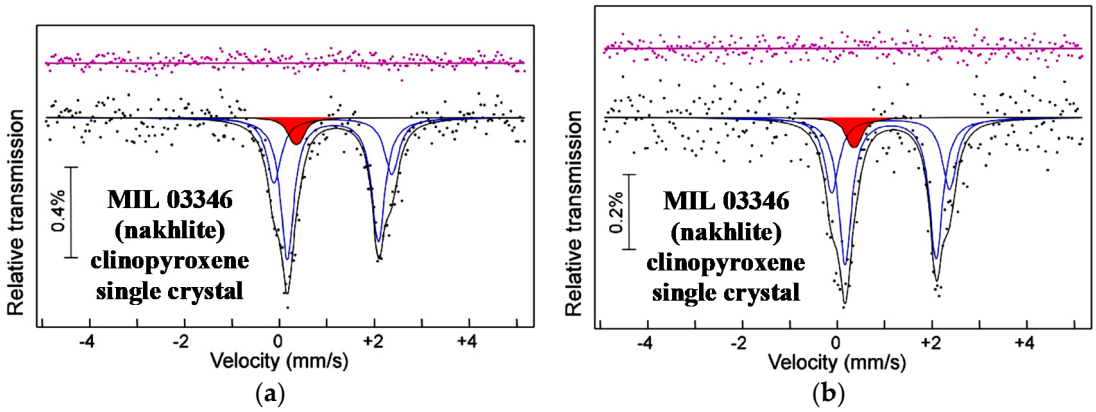

Figure 15. Room temperature Mössbauer spectra of MIL 03346 augite (clinopyroxene) single crystal at two different orientations (**a**,**b**). Indicated components are the results of the fits. The ferric component is shaded in red. The differential spectra are shown on the top. Adapted from [37].

3. Stony-Iron Meteorites

3.1. Pallasites

Pallasites are stony-iron meteorites that formed as a result of the solidification of the mixture of molten Fe-Ni-Co alloy and olivine-rich rock fragments. This process may take place in differentiated asteroids and protoplanets, which contain the molten metallic core and olivine-rich mantle or a molten metallic layer between the solid metallic core and the olivine-rich mantel. After destructive impact with another large body in space, this mixture can be formed and slowly cooled. Therefore, pallasites consist of Fe-Ni-Co alloy matrix with stony fragments. There are several groups of pallasites, the largest of which is named the main group pallasites (PMG).

The first study of olivine extracted from Omolon PMG and Seymchan PMG using Mössbauer spectroscopy with a high velocity resolution was performed in [38–40]. The Mössbauer spectra of olivine separates from both pallasites measured at 295 and 90 K are shown in Figure 16. These spectra demonstrate well-known peak asymmetry, which becomes inverse at low temperature. These spectra were decomposed with two main quadrupole doublets marked **1** and **2** in Figure 16 and related to the M1 and M2 sites in olivine. All spectra also contain the minor quadrupole doublet **3** assigned to unknown ferrous compound X, while the 295 K spectrum of Omolon only shows a very small quadrupole doublet **4** associated with ferric compound. The room temperature Mössbauer parameters for both olivines were the following: (**1**) δ = 1.156 mm/s, ΔE_Q = 3.020 mm/s, A = 51% for Omolon and δ = 1.158 mm/s, ΔE_Q = 3.058 mm/s, A = 50% for Seymchan; (**2**) δ = 1.117 mm/s, ΔE_Q = 2.849 mm/s, A = 43% for Omolon and δ = 1.137 mm/s, ΔE_Q = 2.876 mm/s, A = 45% for Seymchan; (**3**) δ = 1.007 mm/s, ΔE_Q = 3.108 mm/s, A = 5% for Omolon and δ = 0.952 mm/s, ΔE_Q = 3.032 mm/s, A = 5% for Seymchan; (**4**) δ = 0.389 mm/s, ΔE_Q = 0.570 mm/s, A = 1% for Omolon. Mössbauer parameters at 90 K were also similar for both olivines. It was observed that the δ values for the ^{57}Fe in the M1 and M2 sites in both meteorites showed different tendencies of decrease with the increase in temperature. The decrease in the isomer shift was related to the second-order Doppler shift (see details in, e.g., [41]), while the differences in the observed tendencies indicated the different Mössbauer temperatures for the ^{57}Fe in the M1 and M2 sites in olivines from Omolon and Seymchan, resulting from the different ^{57}Fe mean square velocities in these

sites. Using the approach described in Part I, Section 6.7, for the ordinary chondrites [1], the values of K_D and T_{eq} were estimated for olivine extracted from Omolon PMG on the basis of XRD and Mössbauer data. For the room temperature measurements, the values of K_D and T_{eq} were 1.39 and 795 K, respectively (XRD). In the case of the room temperature Mössbauer data, these values were unrealistic until the authors considered the value of $A^{M1} + A^{X}$ instead of A^{M1}, supposing the possibility of the presence of some distorted M1 sites associated with the X spectral component. In the latter case, the values of K_D and T_{eq} were 1.40 and 743 K, respectively, which agree with the values calculated from XRD data. For the room temperature Mössbauer data for olivine from Seymchan PMG, the values of K_D and T_{eq} were 1.25 and 1118 K, respectively. The same calculations for the 90 K olivine Mössbauer data demonstrated K_D = 1.29, T_{eq} = 997 K for Omolon and K_D = 1.31, T_{eq} = 938 K for Seymchan. The results calculated for the 90 K Mössbauer spectra were considered the most reliable [39]. It was noteworthy that the ΔE_Q values for the ^{57}Fe in both M1 and M2 sites were slightly different for olivines extracted from Omolon and Seymchan PMG meteorites at 295 K and at 90 K. This result indicates that the ^{57}Fe local microenvironments in the M1 sites and in the M2 sites in the two olivines were slightly different. Moreover, a comparison of these parameters for olivine in the studied pallasites and earlier studied ordinary chondrites Farmington L5 and Tsarev L5 showed some small differences, indicating possible variations in the ^{57}Fe local microenvironments in the M1 and M2 sites in olivine from different meteorites [40].

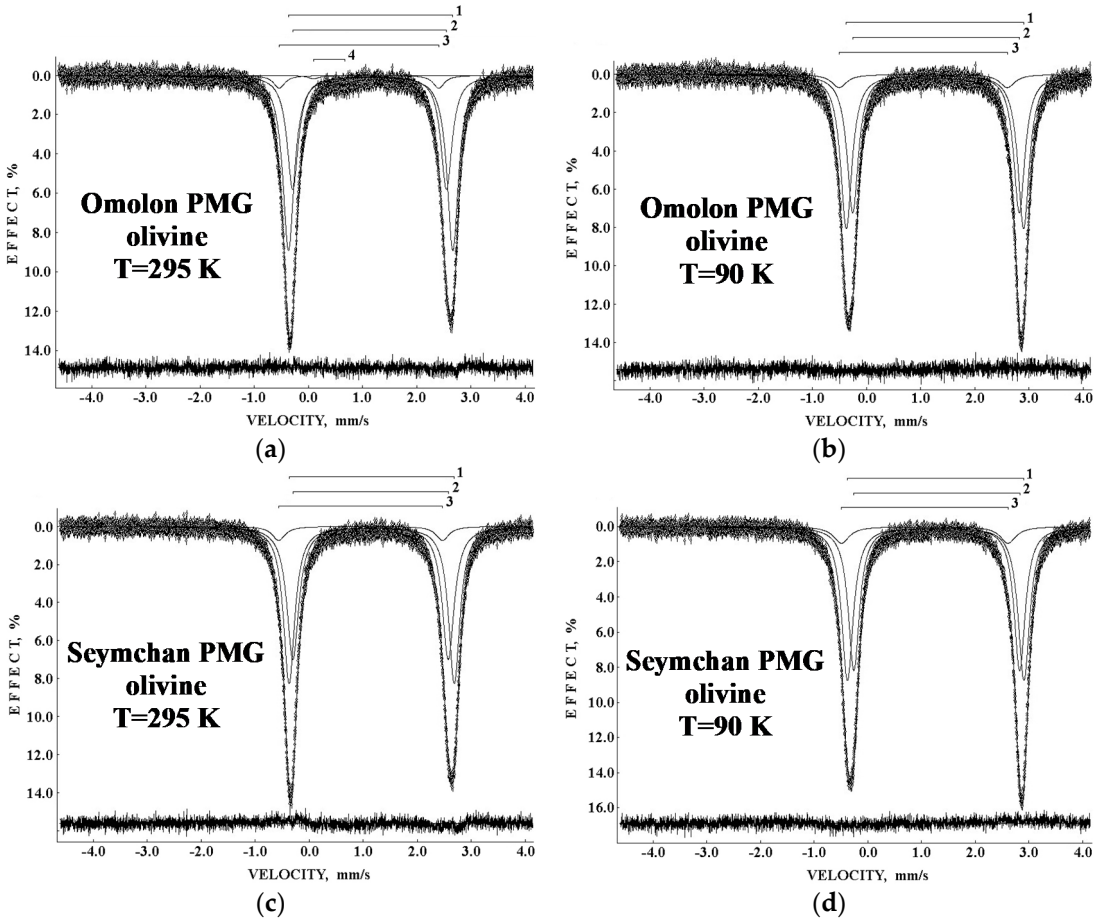

Figure 16. Mössbauer spectra of olivine extracted from the main group pallasites Omolon (**a**,**b**) and Seymchan (**c**,**d**) measured in 4096 channels at 295 K (**a**,**c**) and 90 K (**b**,**d**). Indicated components are the results of the fits. The differential spectra are shown on the bottom. Adapted from [39].

Investigations of the Fe-Ni-Co alloy in the slices with a thickness of ~100 μm prepared from Krasnojarsk PMG-an ("an" means with anomalous properties), Imilac PMG, and

Brenham PMG-an were done by Mössbauer spectroscopy in [42]. The room temperature Mössbauer spectrum of Imilac PMG is shown in Figure 17. This spectrum was fitted with two magnetic sextets and one paramagnetic singlet, which were assigned to the following metal phases: kamacite, the α-Fe(Ni, Co) phase (δ = 0.02 mm/s, H_{eff} = 337 kOe, A = 95%), tetrataenite, the γ-FeNi phase (δ = 0.04 mm/s, H_{eff} = 286 kOe, A = 4%), and "antitaenite" (the incorrect term used by the authors of [42]; see Part I, Figure 15c,d, and further explanation in the text [1]), which is in fact the paramagnetic γ-Fe(Ni, Co) phase (δ = 0.14 mm/s, A = 1%). The same spectral components were revealed for the Mössbauer spectra of Krasnojarsk PMG-an and Brenham PMG-an: the α-Fe(Ni, Co) phase (δ = 0.02 mm/s, H_{eff} = 337 kOe, A = 94% for Krasnojarsk and δ = 0.02 mm/s, H_{eff} = 337 kOe, A = 97% for Brenham), the γ-FeNi phase (δ = 0.04 mm/s, H_{eff} = 286 kOe, A = 4% for Krasnojarsk and δ = 0.02 mm/s, H_{eff} = 280 kOe, A = 1% for Brenham), and the paramagnetic γ-Fe(Ni, Co) phase (δ = −0.05 mm/s, A = 2% for Krasnojarsk and δ = −0.07 mm/s, A = 2% for Brenham).

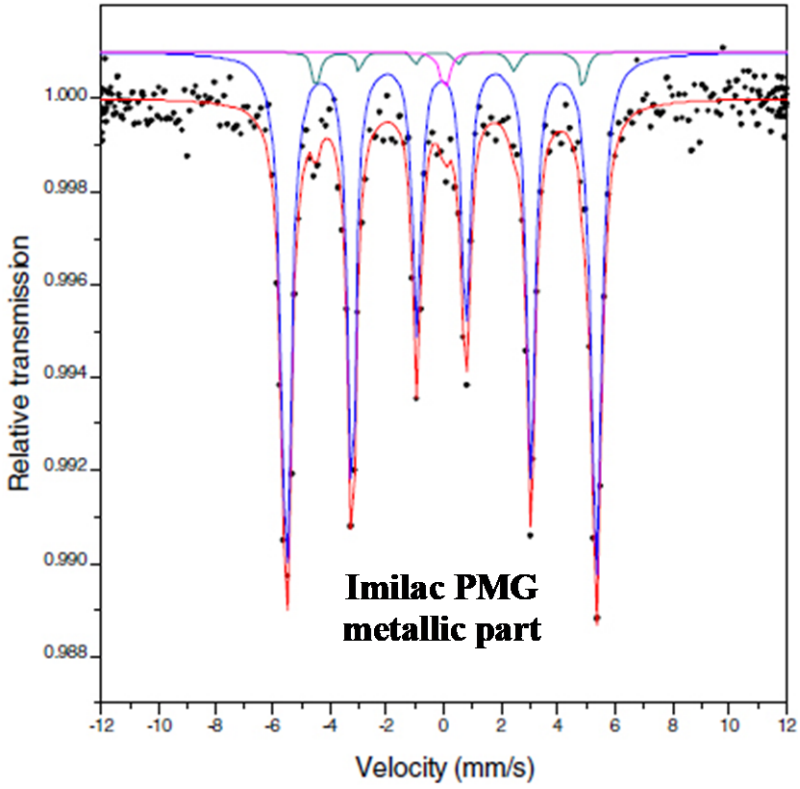

Figure 17. Room temperature Mössbauer spectrum of Imilac PMG metallic alloy. Indicated spectral components are the result of the fit. Adapted from [42].

It should be noted that the authors of [42] used a Mössbauer spectrometer with the sinusoidal velocity reference signal that increases the nonlinearity of the velocity scale. The sample thickness was substantially higher than the limit of thin absorber and the limit for the Lorentzian line shape. The values of Γ for sextets were in the ranges 0.33–0.37 mm/s for kamacite and 0.30–0.34 mm/s for tetrataenite, indicating that the lines were not narrow.

The unique studies of Esquel PMG were carried out using ^{57}Fe synchrotron Mössbauer spectroscopy with a spatial resolution of 10–20 μm [43,44]. The sample of Esquel meteorite was polished to obtain a thin section with a thickness of 20–40 μm. This permitted the authors to measure the Mössbauer spectra in the local areas of different metal phases, their mixtures (plessite structure α-Fe(Ni, Co)/$α_2$-Fe(Ni, Co) + γ-Fe(Ni, Co), and the cloudy zone as a transition region between kamacite and plessite), and inclusions such as schreibersite. The authors chose two line-profile transects, (**1**) the kamacite–cloudy zone–plessite transition (300 μm) and (**2**) the schreibersite grain close to kamacite/taenite

interface (140 μm), for measuring 18 and 15 spectra, respectively. Some of these Mössbauer spectra are shown in Figure 18. These spectra demonstrate the presence of two magnetic sextets related to kamacite and tetrataenite, a paramagnetic singlet (the authors assigned this singlet to questionable "antitaenite", while this component should be considered as the paramagnetic γ-Fe(Ni, Co) phase), and a quadrupole doublet for schreibersite. The values of H_{eff} for all sextets assigned to the α-Fe(Ni, Co) phase were the same within the error (~334–338 kOe), while those for all sextets related to the γ-FeNi phase were in the range ~281–288 kOe.

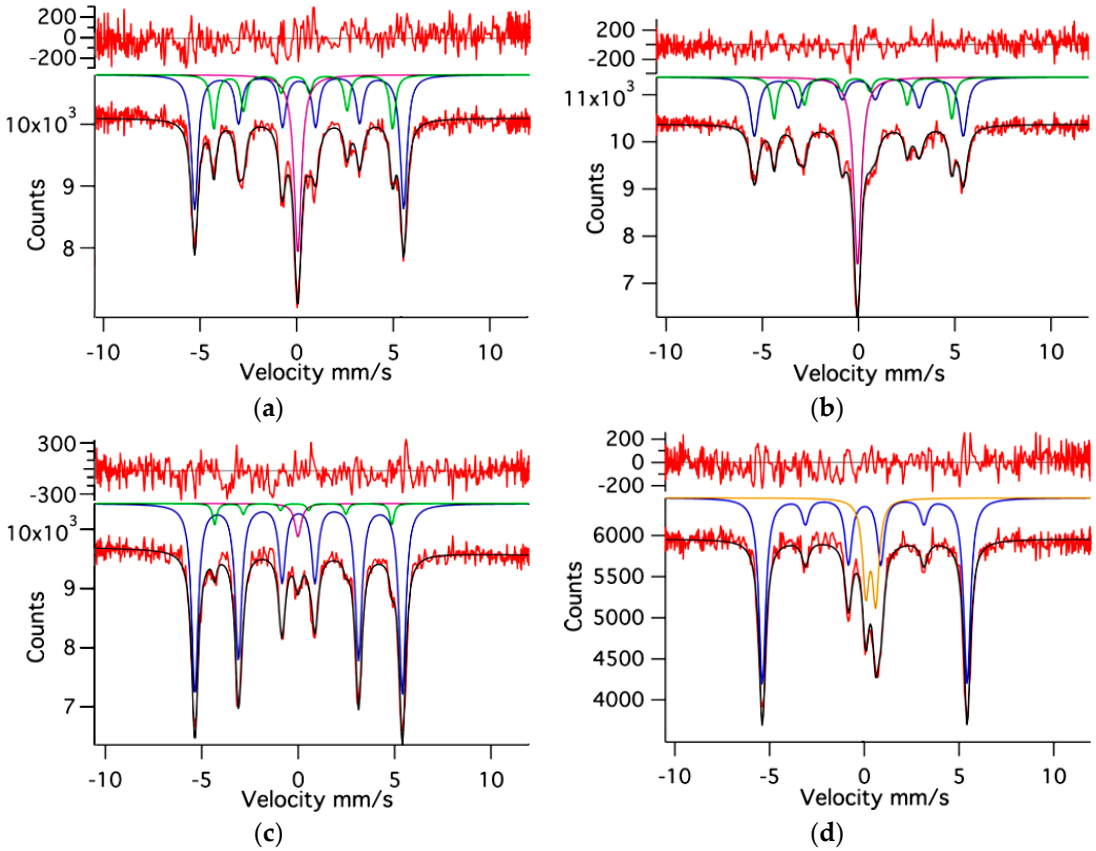

Figure 18. Selected room temperature synchrotron Mössbauer spectra measured for the Esquel PMG thin section: (**a**) the coarse cloudy zone, closer to the large kamacite lamella, (**b**) the fine cloudy zone, closer to plessite and (**c**) deep into plessite, and (**d**) the area containing schreibersite. Indicated components are the results of the fits. The differential spectra are shown on the top. Adapted from [43].

A new fragment of Seymchan PMG was studied by Mössbauer spectroscopy with a high velocity resolution in [45]. The authors extracted the metallic and the stony parts separately and investigated these separates. The room temperature Mössbauer spectra of Seymchan metallic part in comparison with the reference bcc α-Fe foil with a thickness of 7 μm are shown in Figure 19. The α-Fe foil spectrum is a symmetrical sextet with respect to the sextet center (the slightly higher intensity of the second and the fifth absorption lines than the ratio 3:2:1 for intensities of the first (sixth) to the second (fifth) and to the third (fourth) lines is the result of the texture effect after 7 μm foil preparation). In contrast, the spectrum of metallic part extracted from Seymchan PMG demonstrated an asymmetrical six-line pattern, which was more pronounced than that in the spectra of the Imilac metallic part (see Figure 17) and Esquel plessite (see Figure 18c). This six-line pattern was fitted using eight magnetic sextets and one quadrupole doublet.

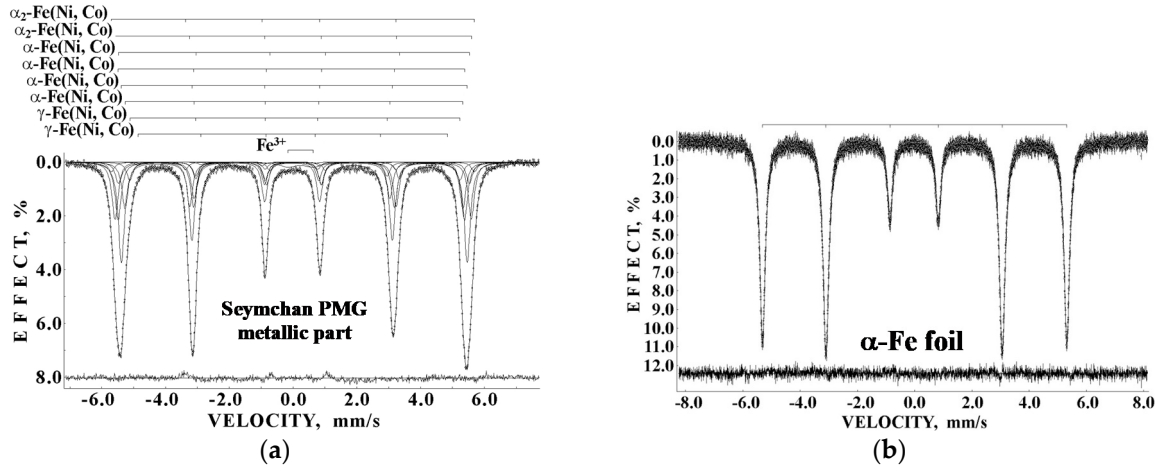

Figure 19. Room temperature Mössbauer spectra of Seymchan PMG metallic part measured in 4096 channels and presented in 1024 channels (**a**) and reference α-Fe foil measured in 4096 channels (**b**). Indicated components are the results of the best fits. The differential spectra are shown on the bottom. Adapted from [45].

The Seymchan PMG matrix alloy consisted of α-Fe(Ni, Co) phase, γ-Fe(Ni, Co) phase, and plessite structure as shown by metallography. Therefore, the following phases were assigned to revealed magnetic sextets: α_2-Fe(Ni, Co) phase (δ = −0.036 mm/s, H_{eff} = 353.3 kOe, A = ~3.8% and δ = 0.003 mm/s, H_{eff} = 346.9 kOe, A = ~17.4%), α-Fe(Ni, Co) phase (δ = 0.086 mm/s, H_{eff} = 341.9 kOe, A = ~6.9%; δ = −0.010 mm/s, H_{eff} = 337.2 kOe, A = ~18.0%; δ = 0.006 mm/s, H_{eff} = 336.8 kOe, A = ~30.6% and δ = −0.003 mm/s, H_{eff} = 328.8 kOe, A = ~15.1%), and γ-Fe(Ni, Co) phase (δ = 0.004 mm/s, H_{eff} = 321.0 kOe, A = ~5.1% and δ = −0.037 mm/s, H_{eff} = 301.3 kOe, A = ~1.1%). The quadrupole doublet was related to the ferric compound resulting from meteorite terrestrial weathering (δ = 0.270 mm/s, ΔE_Q = 0.825 mm/s, A = 1.9%). Assignment of the values of H_{eff} to the martensite, an α_2-Fe(Ni, Co) phase in [45], was different than that in [43]. It is possible that the increase in the number of spectral points in the complex Mössbauer spectra permits decomposing these spectra with a larger number of spectral components, which can be assigned to slightly different local ^{57}Fe microenvironments.

The Mössbauer spectra of the stony part of Seymchan PMG were measured in the large and small velocity ranges in order to verify the presence of the magnetically split components first and then to obtain the spectrum with a better resolution in the small velocity range (see Figure 20).

The stony part of Seymchan PMG did not contain Fe-Ni-Co alloy and orthopyroxene; the absence of these phases was confirmed by XRD and scanning electron microscopy with energy dispersive spectroscopy. These techniques and Mössbauer spectroscopy showed the presence of olivine as the expected main mineral (δ = 1.188 mm/s, ΔE_Q = 3.024 mm/s, A = ~51.5% for the M1 sites and δ = 1.106 mm/s, ΔE_Q = 2.955 mm/s, A = 34.2% for the M2 sites) and some other phases such as troilite (δ = 0.752 mm/s, H_{eff} = 312 kOe, A = ~3.3% in the spectrum measured in the large velocity range), Ca-rich clinopyroxene (δ = 1.278 mm/s, ΔE_Q = 2.620 mm/s, A = ~2.7% for the M1 sites and δ = 1.141 mm/s, ΔE_Q = 2.087 mm/s, A = 1.3% for the M2 sites), chromite (δ = 0.886 mm/s, A = ~3.4%), magnesiochromite $Fe_{1-x}Mg_xCr_2O_4$ (δ = 0.796 mm/s, A = ~0.2%), unknown ferrous compound (δ = 0.507 mm/s, ΔE_Q = 2.788 mm/s, A = ~1.6%), and unknown ferric compound (δ = 0.392 mm/s, ΔE_Q = 0.476 mm/s, A = ~4.0%). The authors of [45] demonstrated the presence of two types of chromites in the stony part of Seymchan PMG: the proper chromite $FeCr_2O_4$ and magnesiochromite $Fe_{1-x}Mg_xCr_2O_4$, which can be formed by partial substitution of Fe^{2+} by Mg^{2+} in chromite.

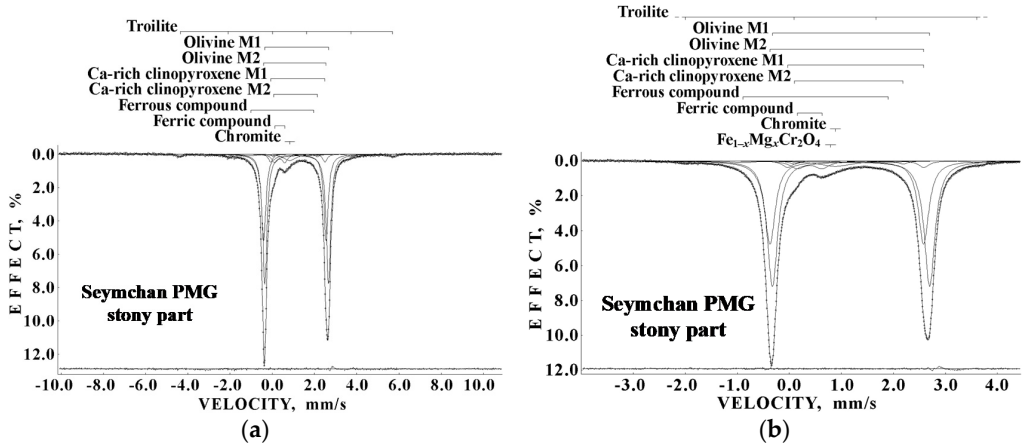

Figure 20. Room temperature Mössbauer spectra of Seymchan PMG stony part measured in 4096 channels and presented in 1024 channels in the large (**a**) and in the small velocity ranges (**b**). Indicated components are the results of the best fits. The differential spectra are shown on the bottom. Adapted from [45].

3.2. Mesosiderites

Mesosiderites are a rare type of stony-iron meteorite, which appear as brecciated rocks and contain subequal metal (Fe-Ni-Co alloy) and silicate components (olivine, pyroxenes); the silicates are dominantly igneous rock fragments. Mesosiderites are divided into different groups according to the petrologic class (A, B, C) and metamorphic grade (1, 2, 3, etc.) (see MBD). Only two articles have been published on investigations of mesosiderites using Mössbauer spectroscopy. The authors of [42] studied the following meteorites: Hainholz Mes-A4, Mincy Mes-B4, Crab Orchard Mes-A1, Estherville Mes-A3/4, Łowicz Mes-A3, Vaca Muerta Mes-A1, ALHA77219 Mes-B1, and Asuka 882023 (A-882023) that has not been assigned to a petrologic class or metamorphic grade. The samples of three mesosiderites, Estherville, Łowicz, and Vaca Muerta, were prepared from the metal-rich areas. The room temperature Mössbauer spectra of Hainholz and the metal-rich areas of Vaca Muerta are shown in Figure 21.

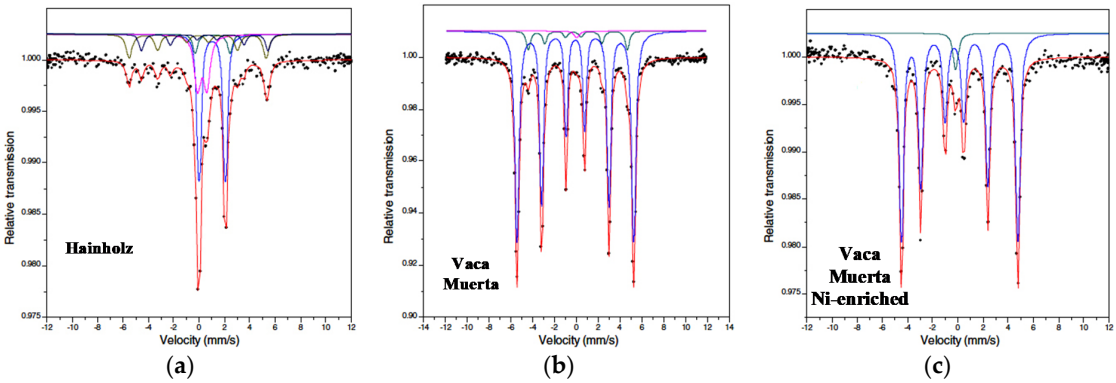

Figure 21. Room temperature Mössbauer spectra of mesosiderites: Hainholz Mes-A4 (**a**), metal-rich areas of Vaca Muerta Mes-A1 (**b**), and Ni-enriched metal-rich areas of Vaca Muerta (**c**). Indicated spectral components are the results of the fits. Adapted from [42].

The Mössbauer spectra of Hainholz, Mincy, Crab Orchard, ALHA77219, and A-882023 consisted of spectral components related to metallic and stony compounds. The revealed compounds and their Mössbauer parameters for these meteorites were the following: (**i**) olivine (δ = 1.17 mm/s, ΔE_Q = 2.72 mm/s, A = 6% for Hainholz; δ = 1.04 mm/s, ΔE_Q = 2.90 mm/s, A = 4% for Mincy; δ = 1.12 mm/s, ΔE_Q = 2.90 mm/s, A = 6% for Crab Orchard; δ = 1.16 mm/s, ΔE_Q = 2.89 mm/s, A = 4% for ALHA77219; and δ = 1.16 mm/s, ΔE_Q = 2.75 mm/s, A = 3% for A-882023), (**ii**) pyroxene (δ = 1.15 mm/s, ΔE_Q = 2.07 mm/s,

A = 41% for Hainholz; δ = 1.13 mm/s, ΔE_Q = 2.11 mm/s, A = 52% for Mincy; δ = 1.17 mm/s, ΔE_Q = 2.12 mm/s, A = 34% for Crab Orchard; δ = 1.15 mm/s, ΔE_Q = 2.08 mm/s, A = 42% for ALHA77219; and δ = 1.17 mm/s, ΔE_Q = 2.10 mm/s, A = 37% for A-882023), (**iii**) troilite (δ = 0.65 mm/s, H_{eff} = 309 kOe, A = 11% for Hainholz; δ = 0.57 mm/s, H_{eff} = 317 kOe, A = 5% for Crab Orchard; and δ = 0.75 mm/s, H_{eff} = 313 kOe, A = 4% for ALHA77219), (**iv**) kamacite (δ = 0.01 mm/s, H_{eff} = 335 kOe, A = 19% for Hainholz; δ = 0.01 mm/s, H_{eff} = 336 kOe, A = 30% for Mincy; δ = 0.01 mm/s, H_{eff} = 341 kOe, A = 29% for Crab Orchard; δ = 0.01 mm/s, H_{eff} = 335 kOe, A = 19% for ALHA77219; and δ = 0.01 mm/s, H_{eff} = 340.5 kOe, A = 46% for A-882023), and (**v**) ferric compounds (δ = 0.38 mm/s, ΔE_Q = 0.73 mm/s, A = 23% for Hainholz; δ = 0.52 mm/s, ΔE_Q = 0.55 mm/s, A = 14% for Mincy; δ = 0.38 mm/s, ΔE_Q = 0.68 mm/s, A = 21% for Crab Orchard; δ = 0.37 mm/s, ΔE_Q = 0.69 mm/s, A = 31% for ALHA77219; and δ = 0.40 mm/s, ΔE_Q = 0.69 mm/s, A = 14% for A-882023). The samples of Mincy and A-882023 did not contain troilite. The values of H_{eff} for kamacite varied in the range 335–341 kOe; some variations in the ^{57}Fe hyperfine parameters for ferric compounds could also be seen. Crab Orchard contained about 5% hematite (H_{eff} = ~500 kOe).

The metal-rich areas of Estherville, Łowicz, and Vaca Muerta demonstrated the presence of the following spectral components and their Mössbauer parameters: (**i**) kamacite (δ = 0.02 mm/s, H_{eff} = 338 kOe, A = 97% for Estherville; δ = 0.02 mm/s, H_{eff} = 337 kOe, A = 100% for Łowicz; δ = 0.02 mm/s, H_{eff} = 332 kOe, A = 92% for Vaca Muerta); (**ii**) tetrataenite (δ = 0.02 mm/s, H_{eff} = 283 kOe, A = 1% for Estherville; δ = 0.03 mm/s, H_{eff} = 281 kOe, A = 7% for Vaca Muerta; δ = 0.03 mm/s, H_{eff} = 288 kOe, A = 96% for Ni-rich metal from Vaca Muerta); (**iii**) "antitaenite", in fact, the paramagnetic γ-Fe(Ni, Co) phase (δ = 0.07 mm/s, A = 2% for Estherville; δ = 0.13 mm/s, A = 1% for Vaca Muerta; δ = −0.07 mm/s, A = 4% for Ni-rich metal from Vaca Muerta). The authors of [42] did not reveal components which could be assigned to the ferromagnetic γ-Fe(Ni, Co) phase (taenite).

The authors of [44] applied synchrotron Mössbauer spectroscopy to study individual metal grains in Estherville Mes-A3/4. They measured the room temperature spectra of two Fe-Ni-Co alloy grains with α-phase and with a mixture of α-phase and γ-phase (see Figure 22). The authors observed one magnetic sextet corresponding to kamacite (Figure 22a), two magnetic sextets assigned to kamacite and tetrataenite, and one paramagnetic singlet considered as "antitaenite" which is, in fact, the paramagnetic taenite (Figure 22b).

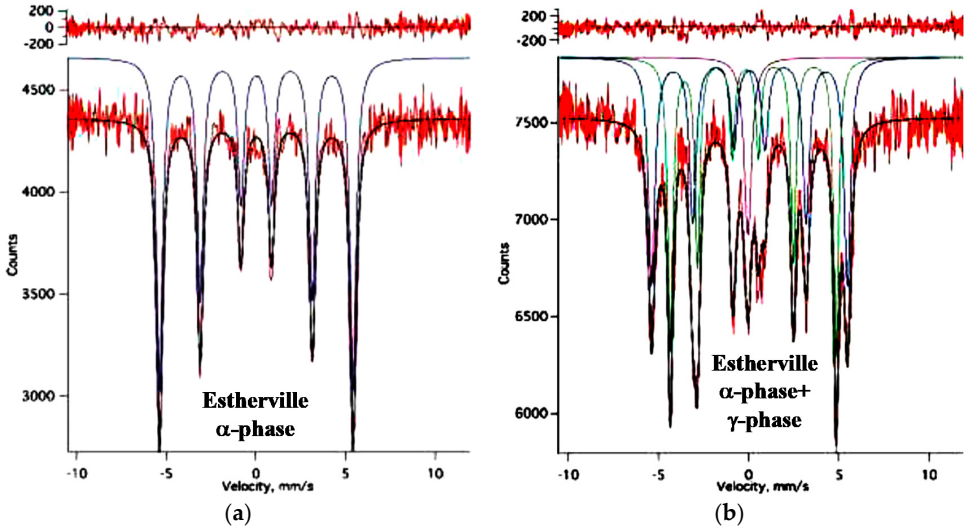

Figure 22. Room temperature synchrotron Mössbauer spectra of Estherville Mes-A3/4: α-phase area (**a**) and α-phase + γ-phase area (**b**). Indicated components are the results of the fits. Differential spectra are shown on the top. Adapted from the Supporting Information in [44].

4. Iron Meteorites

Iron meteorites consist of Fe-Ni-Co alloy with small inclusions of minerals such as troilite, schreibersite and rhabdites, daubréelite, and silicate phases. The main feature of iron meteorites is the Widmanstätten structures that can be seen on the polished slice. Iron meteorites are structurally divided in octahedrites O (fine Of, finest Off, medium Om, coarse Og, coarsest Ogg, and plessitic Opl), hexahedrites H, and ataxites D (see, e.g., [2]). Furthermore, chemical classification is used for iron meteorites, and they can be divided into 13 groups denoted using Roman numbers I–IV and one or two Latin letters A, B, C, D, E, F, and G: IAB complex iron, IC, IIAB, IIC, IID, IIE, IIF, IIG, IIIAB, IIIE, IIIF, IVA, and IVB (see MBD). Additionally, in the cases of anomalous or ungrouped iron meteorites, in the group name, the letters "-an" or "-ung", as well as "MG" for the main group, are added.

The first known study of iron meteorites by Mössbauer spectroscopy was carried out in [46]. The authors studied samples of Sikhote-Alin IIAB, Wabar IIIAB, Bartlett IIIAB, Odessa IAB-MG, and Canyon Diablo IAB-MG in comparison with metallic iron (α-Fe) foil using transmission and backscattering geometries of Mössbauer spectroscopy. Then, a number of studies were dedicated to investigations of tetrataenite, the γ-FeNi phase, (~50%Fe–~50%Ni), so-called disordered tetrataenite, paramagnetic taenite (γ-phase), and other phases in Santa Catharina IAB-ung, Cape York IIIAB, Odessa IAB-MG, Toluca IAB-sLL, Dayton IAB-sLH, Tlacotepec IVB, Cranbourne IAB-MG, Twin City IAB-ung, and Xiquipilco no. 2 [47–65]. Several studies were done using both transmission Mössbauer spectroscopy and conversion electron Mössbauer spectroscopy (CEMS) [58,60,61], as well as backscattering geometry [63] (CEMS and other backscattering methods are used for the surface studies). It was shown that the Ni concentration in the paramagnetic γ-Fe(Ni, Co) phase was around 28 at.% [64]. The Mössbauer spectra of kamacite, ferromagnetic and paramagnetic taenite, troilite and cohenite (Fe, Ni, Co)$_3$C, troilite, pyrite, and schreibersite extracted from Toluca IAB-sLL were measured in [66].

Further study of Fe-Ni alloys in the Antarctic Ni-rich ataxite Y-791694 IAB meteorite in comparison with non-Antarctic Ni-rich ataxites Santa Catharina IAB-ung, Twin City IAB-ung, and some other meteorites was done in [67]. The room temperature Mössbauer spectra of thin slices of Y-791694 and Twin City are shown in Figure 23. The spectrum of Y-791694 demonstrated two magnetic sextets indicating the presence of two Fe-Ni phases with the main component associated by the authors with fully disordered Fe-Ni alloy in spite of the Ni content being ~40 at.%. This may be a result of the fast cooling of Y-791694. In contrast, the spectra of Santa Catharina and Twin City (see Figure 23b) demonstrated the presence of a magnetic sextet and paramagnetic singlet. The magnetic sextet corresponded to the ordered γ-FeNi phases or tetrataenite (50 at.% Fe–50 at.% Ni) with $L1_0$ superstructure. This indicates that the decomposition of the phases in these meteorites was started at low temperature.

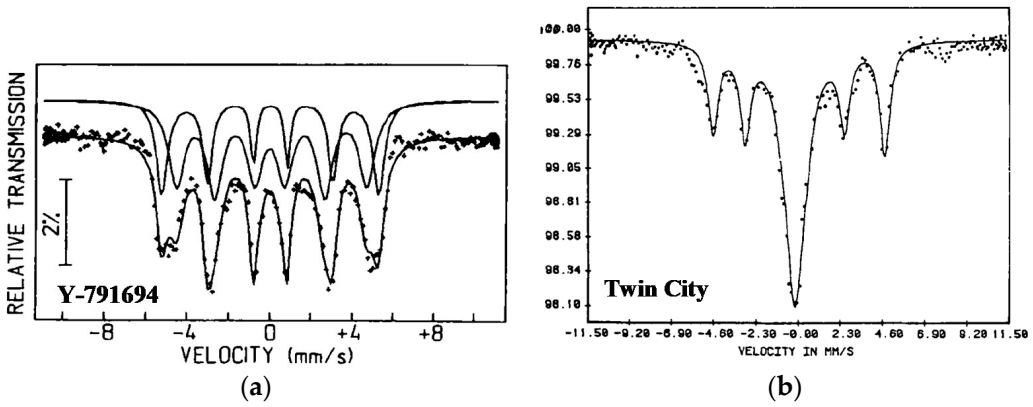

Figure 23. Room temperature Mössbauer spectra of iron meteorites: Y-791694 IAB complex (**a**) and Twin City IAB-ung (**b**). Indicated spectral components are the results of the fits. Adapted from [67].

A quite different Mössbauer spectrum was measured for Henbury IIIAB iron meteorite in [68] (see Figure 24a). This meteorite consisted of ~91.9 at.% Fe and ~7.5 at.% Ni. This alloy was a homogeneous bcc α-phase. Different fits of the measured spectrum showed the same ^{57}Fe hyperfine parameters: δ = ~0.02 mm/s, H_{eff} = 337.7 kOe. These values corresponded to the α-Fe(Ni, Co) phase (kamacite). In contrast, the Mössbauer spectrum of Santa Catharina IAB-ung measured in [69] was similar to the spectrum of Twin City (compare Figures 23b and 24b). Santa Catharina ataxite contained the highest known Ni content (35 wt.% Ni). The Mössbauer spectrum was fitted using two sextets: one symmetrical sextet with larger H_{eff} and broad lines, which was assigned to disordered tetrataenite (in fact this is taenite because tetrataenite is always ordered), and one asymmetrical sextet with smaller H_{eff} and narrow lines, which was associated with ordered tetrataenite, as well as one paramagnetic singlet, which the authors of [69] denoted as "antitaenite" similar to [70] and wrote about the experimental proof of their observation. A discussion about the questionable term "antitaenite" was already reported in Part I, Section 6.1 [1]. Moreover, the authors of [64], who also observed the paramagnetic singlet in the Mössbauer spectrum of Santa Catharina, determined the Ni content of 28 at.% for this component that corresponded to the well-known paramagnetic γ-Fe(Ni) phase (paramagnetic taenite).

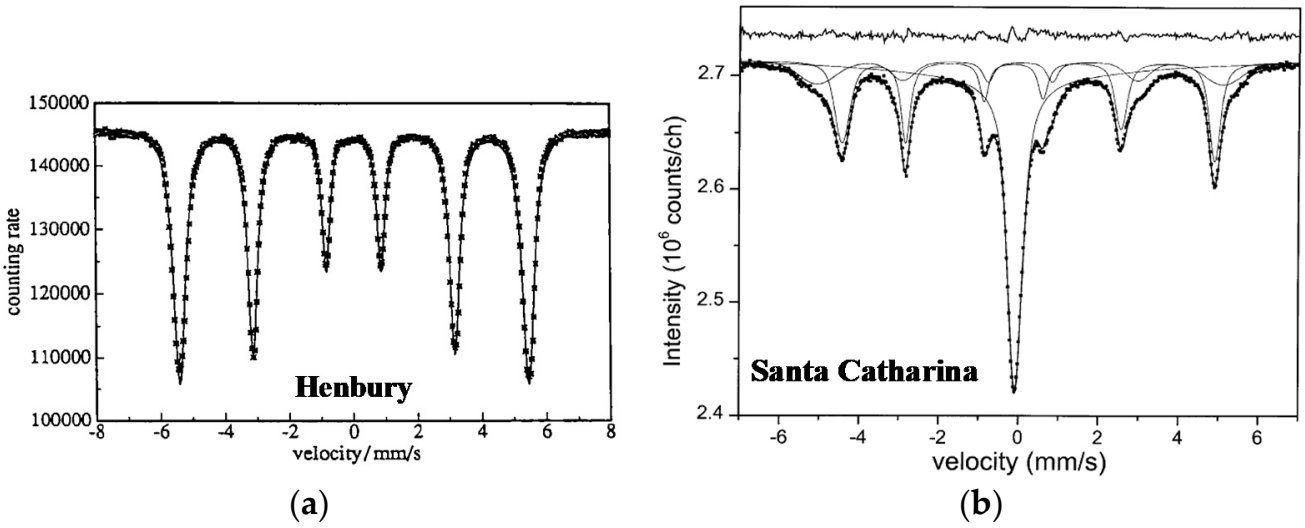

Figure 24. Room temperature Mössbauer spectra of iron meteorite: Henbury IIIAB (**a**) and Santa Catharina IAB-ung; the differential spectrum is shown on the top (**b**). Indicated spectral components are the results of the fits. Adapted from [68,69], respectively.

A comparison of the different areas of the coarse octahedrite Soledade IAB-MG by Mössbauer spectroscopy was carried out in [71]. The Fe-Ni alloy contained about 6.7 at.% Ni, indicating the α-Fe(Ni, Co) phase. The Mössbauer spectra of samples obtained from the interior and oxidized surface of Soledade measured at room temperature are shown in Figure 25. These spectra demonstrate asymmetrical six-line patterns with an additional quadrupole doublet for the oxidized sample.

A similar study was done for the interior and surface of hexahedrite from the Campo del Cielo meteorite shower in [72] (the name of this meteorite is unknown, while there were many registered iron meteorites found from this shower). This meteorite contained 94.6 wt.% Fe and 5.4 wt.% Ni. The room temperature Mössbauer spectra of the two samples are shown in Figure 26. The interior spectrum demonstrated an asymmetric six-line pattern similar to the other meteoritic Fe-Ni-Co alloys with low Ni content. In contrast, the surface spectrum mainly showed the presence of ferric compounds in the magnetic and paramagnetic states.

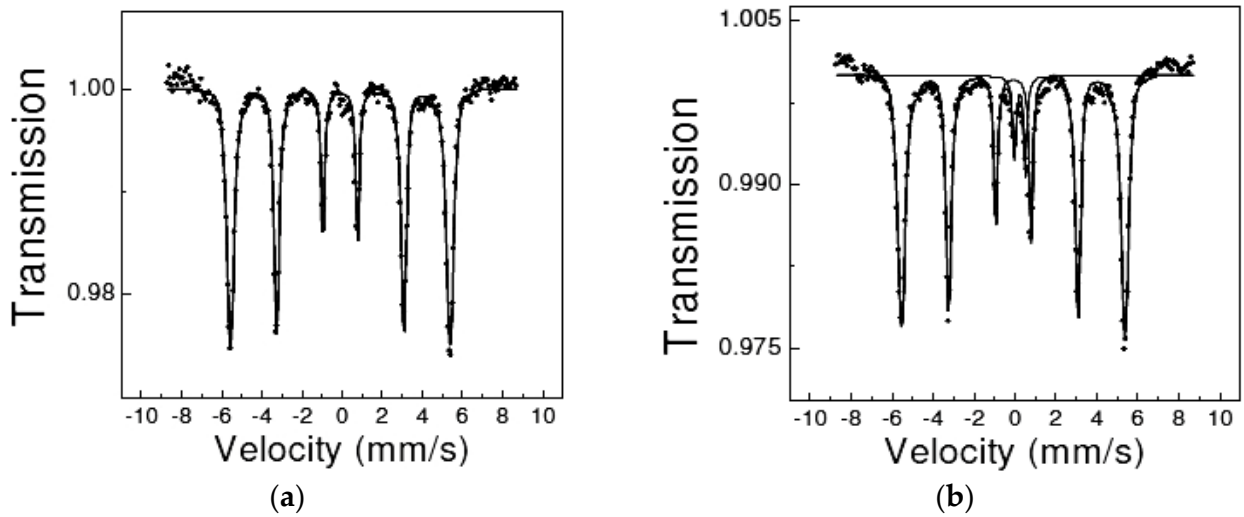

Figure 25. Room temperature Mössbauer spectra of iron meteorite Soledade IAB-MG: interior (**a**) and surface (**b**). Indicated spectral components are the results of the fits. Adapted from [71].

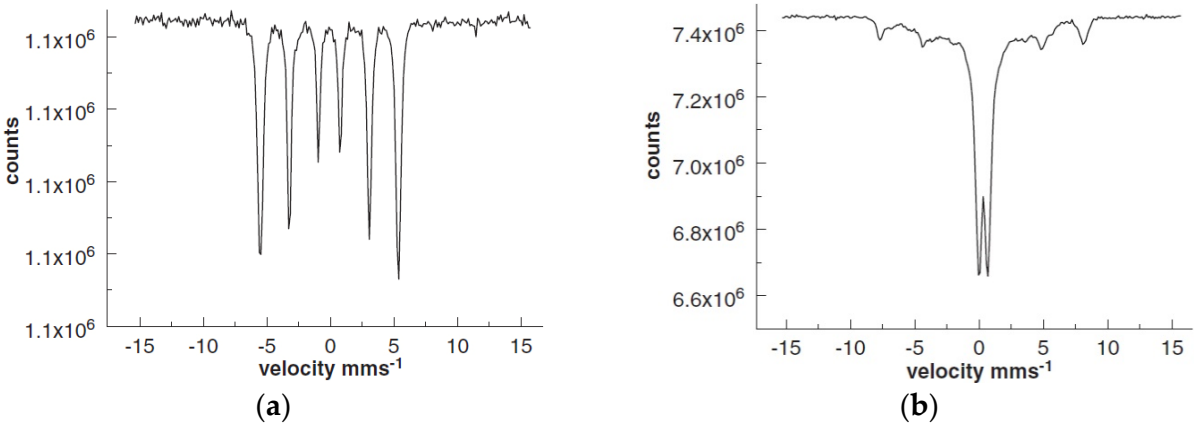

Figure 26. Room temperature Mössbauer spectra of unknown hexahedrite from Campo del Cielo meteorite shower: interior (**a**) and surface (**b**). Adapted from [72].

The study of Sikhote-Alin IIAB, Bilibino IIAB, Chinga and Dronino (both are ungrouped iron meteorites), and products of their weathering was carried out by Mössbauer spectroscopy in [73–75]. The measured Mössbauer spectra demonstrated asymmetrical six-line patterns which were fitted with different numbers of magnetic sextets. The spectra of the corrosion (weathered) products showed the presence of various ferric oxides and oxyhydroxides depending on the place of meteorite weathering. These Mössbauer spectra were measured using an SM-2201 spectrometer with a high velocity resolution but fitted in the presentation in 512-channel spectra only. Furthermore, these meteorites were re-measured to obtain the high velocity resolution Mössbauer spectra. A comparison of the Mössbauer spectra of Chinga iron-ung foil presented in 512 and 4096 channels in [76] is shown in Figure 27. The first spectrum was decomposed using three magnetic sextets to fit an asymmetrical six-line pattern, while the second spectrum was fitted with six magnetic sextets. The values of H_{eff} for these six sextets were in the range ~354–305 kOe. The Mössbauer spectra of Chinga metal fine shaving and metal powder were also fitted using six magnetic sextets with H_{eff} in the ranges ~343–296 kOe and ~354–295 kOe, respectively. These differences can be attributed to the effect of sample preparation on the phase composition.

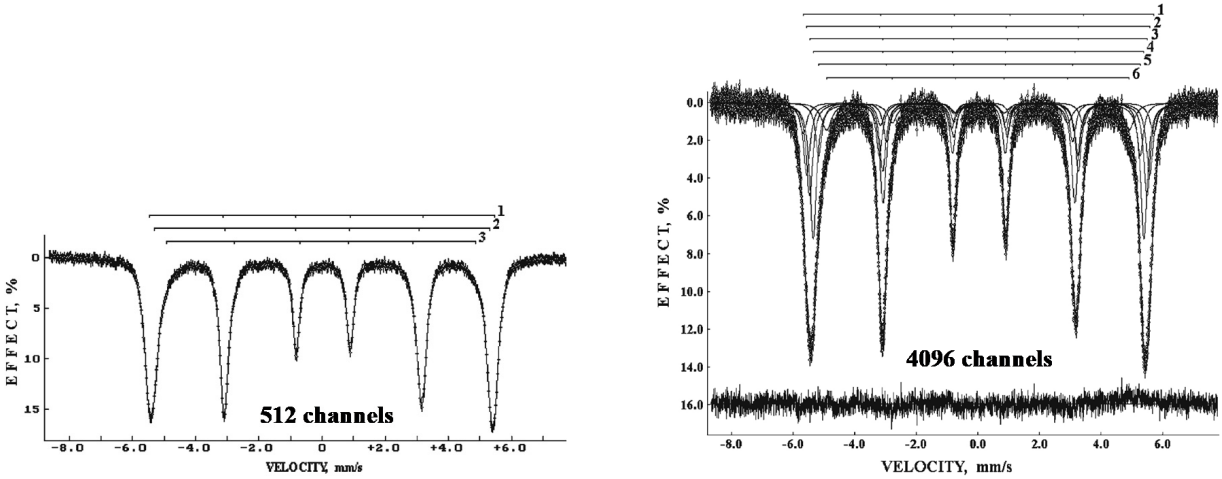

Figure 27. Room temperature Mössbauer spectra of Chinga iron-ung meteorite: the spectrum presented in 512 channels (**a**) and the spectrum presented in 4096 channels (**b**). Indicated components are the results of the best fits. The differential spectrum is shown on the bottom in (**b**). Adapted from [76].

An investigation of an iron meteorite found in Colombia named "Gaspar" was carried out by Mössbauer spectroscopy in [77]. The name "Gaspar" was not registered, but this fragment was considered as a part of the Santa Rosa IC meteorite. The authors measured the Mössbauer spectra of two samples from different sides of "Gaspar" (fragments A and B), which are shown in Figure 28. Although these spectra were asymmetrical six-line patterns, they were fitted using one magnetic sextet only with the same value of H_{eff} = 337 Oe. However, these fits cannot be considered as final and adequate because the enveloped lines could not fit the experimental points well, while the authors did not use differential spectra for quality control.

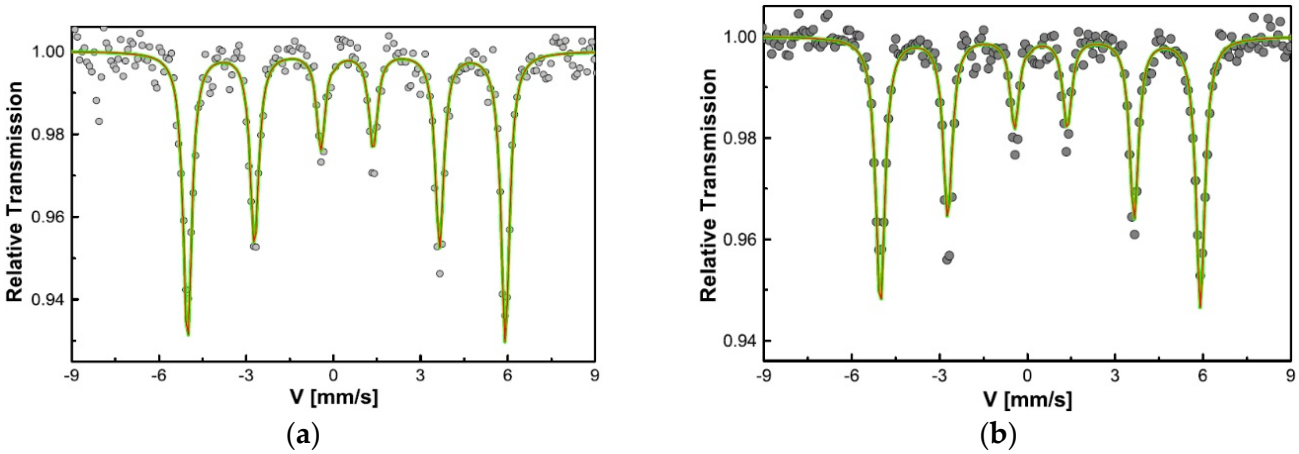

Figure 28. Room temperature Mössbauer spectra of "Gaspar" meteorite (probably, a fragment of Santa Rosa IC): side A (**a**) and side B (**b**). Adapted from [77].

Samples of Sikhote-Alin IIAB were studied by Mössbauer spectroscopy in [78,79]. The measured room temperature Mössbauer spectra in both works are shown in Figure 29 for comparison. Both spectra showed similar asymmetric six-line patterns which were fitted in different ways. The authors of [78] used a superposition of multiple magnetic sextets with different H_{eff} and hyperfine field distribution as a result of different local ^{57}Fe microenvironments due to a distribution of Ni and Co atoms in the first coordination sphere. The average value of H_{eff} was 335.7 kOe. On the other hand, the authors of [79] fitted their

spectrum using three magnetic sextets and one paramagnetic singlet. The ^{57}Fe hyperfine parameters for these sextets were δ = 0.03 mm/s, H_{eff} = 346.5 kOe, A = 25% (sextet **1**), δ = 0.02 mm/s, H_{eff} = 336.5 kOe, A = 50% (sextet **2**), δ = 0.03 mm/s, H_{eff} = 326.7 kOe, A = 23% (sextet **3**), and δ = 0 mm/s, A = 2% (singlet). These sextets were assigned to α-Fe(Ni, Co) with different Ni concentrations in the local iron microenvironment.

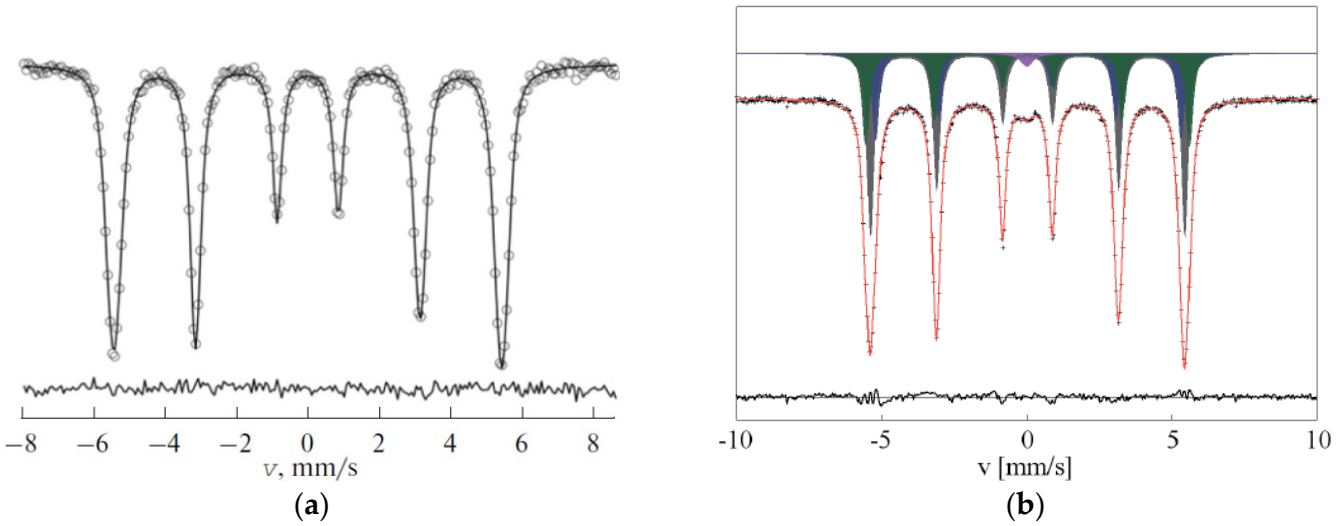

Figure 29. Comparison of the room temperature Mössbauer spectra of Sikhote-Alin IIAB measured in [78] (**a**) and in [79] (**b**). Indicated spectral components are the results of the fits. The differential spectra are shown on the bottom. Adapted from [78,79].

Various iron meteorites, namely, Landes IAB-MG, Toluca IAB-sLL, San Cristobal IAB-ung, Lime Creek IAB-ung, Santa Catharina IAB-ung, Cratheus IIC, Itutinga IIIAB, Para de Minas IVA, São João Nepomuceno IVA-an, Vitoria da Conquista IVA, Bocaiuva ungrouped, Tucson ungrouped, Gebel Kamil ungrouped, and NWA 6259 ungrouped, were studied by Mössbauer spectroscopy in [42]. Additionally, the authors studied Ni-enriched metal from São João Nepomuceno and Toluca prepared after chemical treatment of the bulk metal. Selected Mössbauer spectra measured at room temperature are shown in Figure 30.

The Ni contents in Gebel Kamil and NWA 6259 were 19.8 wt.% and 42.2 wt.%, respectively (MBD). Therefore, the authors of [42] revealed 85% of α-Fe(Ni, Co) phase, 12% of γ-Fe(Ni, Co) phase, and 3% of paramagnetic γ-Fe(Ni, Co) phase (which the authors called "antitaenite") in the Mössbauer spectrum of Gebel Kamil. In contrast, these authors obtained 12% of γ-Fe(Ni, Co) phase, 74% of γ-FeNi phase (tetrataenite), and 14% of paramagnetic γ-Fe(Ni, Co) phase for the Mössbauer spectrum of NWA 6259. Toluca and São João Nepomuceno meteorites contained ~8 wt.% Ni. Therefore, their Mössbauer spectra were fitted using one magnetic sextet assigned to the α-Fe(Ni, Co) phase. However, the Mössbauer spectra of Ni-enriched metal from both meteorites demonstrated the presence of 72% of γ-FeNi phase and 28% of paramagnetic γ-Fe(Ni, Co) phase for Toluca and 16% of α-Fe(Ni, Co) phase, 60% of γ-Fe(Ni, Co) phase, and 24% of paramagnetic γ-Fe(Ni, Co) phase for São João Nepomuceno. For the studied iron meteorites, except San Cristobal, the authors of [42] obtained the following ranges of H_{eff}: 331–339 kOe for α-Fe(Ni, Co) phase, 297–312 kOe for γ-Fe(Ni, Co) phase, and 284–295 kOe for γ-FeNi phase. As for San Cristobal, this meteorite contained 25.2 wt.% Ni. Therefore, the value of H_{eff} = 349 kOe may be assigned to the α_2-Fe(Ni, Co) phase which contained Ni in the range of 8–25 at.%, while H_{eff} = 333 kOe should be related to the α-Fe(Ni, Co) phase (the authors of [42] assigned these values of H_{eff} to kamacite and taenite, respectively, which seems to be incorrect). The δ values for the paramagnetic γ-Fe(Ni, Co) were in the range −0.08 to +0.02 mm/s.

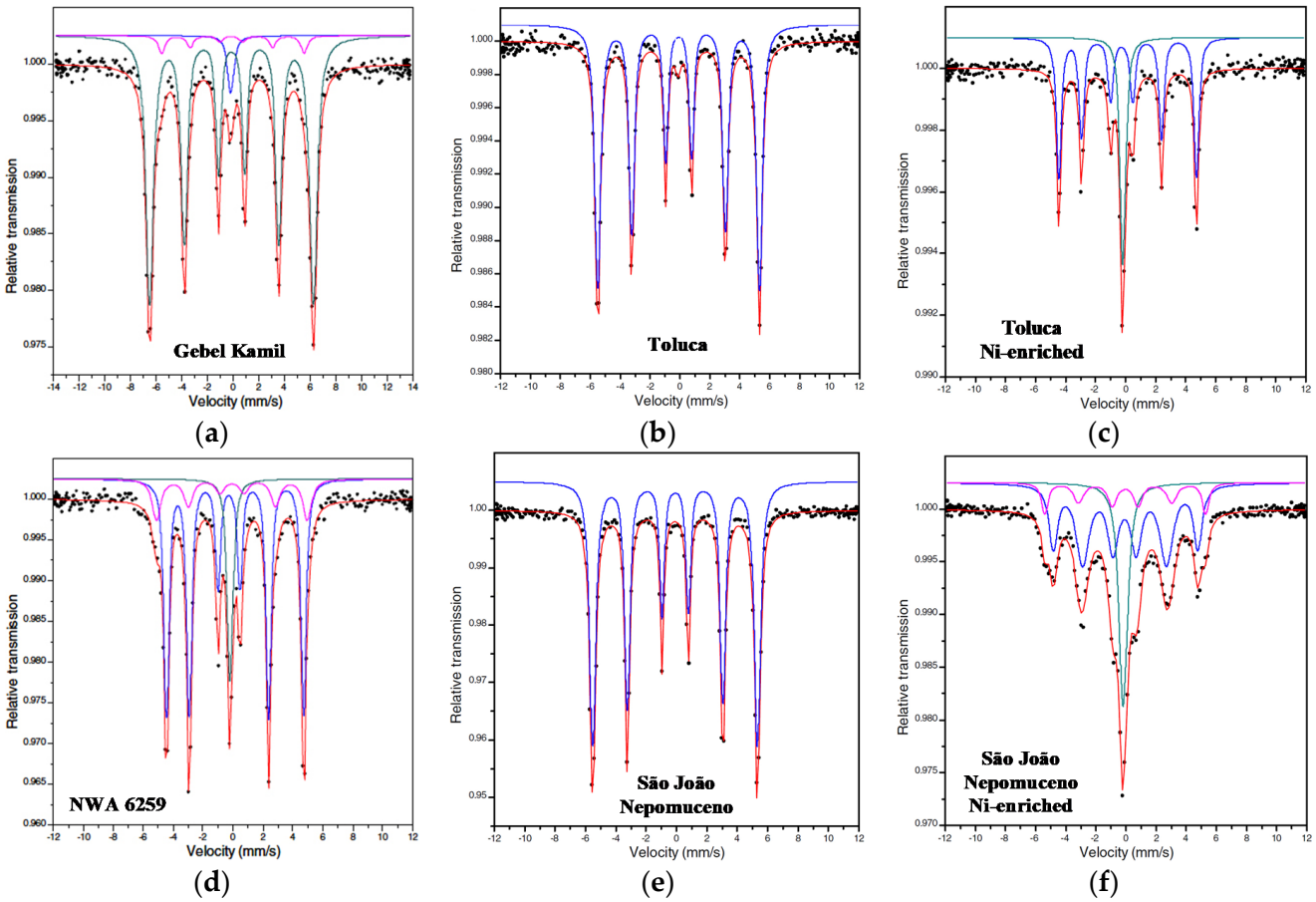

Figure 30. Room temperature Mössbauer spectra of iron meteorites: Gebel Kamil (**a**), Toluca (**b**), Toluca Ni-enriched (**c**), NWA 6259 (**d**), São João Nepomuceno (**e**), and São João Nepomuceno Ni-enriched (**f**). Indicated spectral components are the results of the fits. Adapted from [42].

The comparison of powdered samples of one fragment of Chinga iron-ung, in which visually different areas (**1**, **2**, **3**, **4**, and **5**) of the saw-cut surface were observed, was done using Mössbauer spectroscopy with a high velocity resolution (4096 channels) in [80]. The Mössbauer spectra of these samples obtained from four areas are shown in Figure 31. These spectra are six-line patterns with asymmetry, unlike that observed for Chinga foil (Figure 27b) in [76]. The new spectra were measured with larger signal-to-noise ratios and decomposed using nine magnetic sextets. The obtained distributions of the magnetic hyperfine fields shown in the histograms in Figure 32 demonstrated some differences that could be related to structural variations in different areas of the studied fragment of Chinga. Visual differences in the absorption line shape of the most negative peaks of sextets are also shown in Figure 31. These differences can be seen due to a large number of spectral points in the 4096-channel Mössbauer spectra.

A comparative study of iron meteorites Anyujskij IIAB, Sikhote-Alin IIAB, Aliskerovo IIIE-an, and Sterlitamak IIIAB was carried out using Mössbauer spectroscopy with a high velocity resolution in [81,82]. The 1024-channel Mössbauer spectra are shown in Figure 33. These spectra demonstrate similar asymmetric six-line patterns. However, these spectra were decomposed with different numbers of components; three magnetic sextets were revealed in the spectra of IIAB iron meteorites, while five magnetic sextets and one paramagnetic singlet were revealed in the spectra of IIIE-an and IIIAB iron meteorites. This may be related to different Ni contents and phase compositions in these meteorites: Anyujskij IIAB and Sikhote-Alin IIAB consisted of an α-Fe(Ni, Co) phase with ~5 at.% Ni, while Aliskerovo IIIE-an contained an α-Fe(Ni, Co) phase with ~4–7 at.% Ni, as well as probably an α_2-Fe(Ni, Co) phase with ~7–9 at.% Ni, γ-Fe(Ni, Co) phase with ~32–35 at.%

Ni, and γ-FeNi phase with 50 at.% Ni, and Sterlitamak IIIAB consisted of an α-Fe(Ni, Co) phase with ~6.5–7 at.% Ni, as well as probably an α_2-Fe(Ni, Co) phase with ~7–8 at.% Ni and γ-Fe(Ni, Co) phase with ~30–34 at.% Ni.

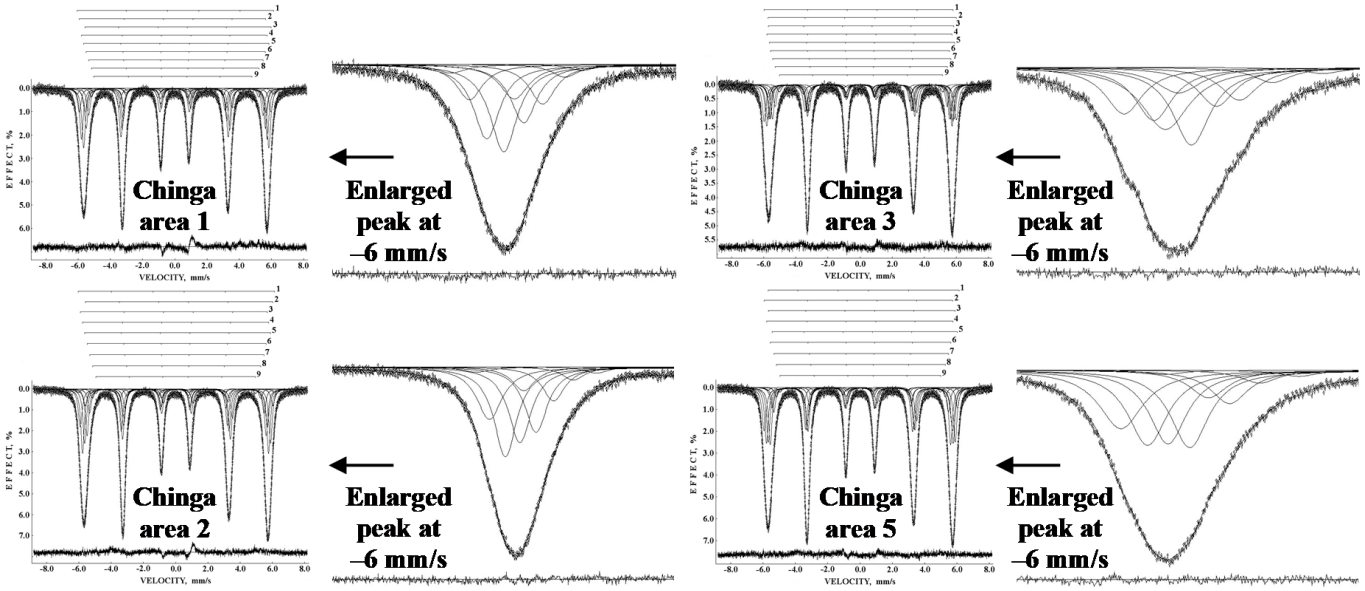

Figure 31. Comparison of the room temperature Mössbauer spectra of different powdered samples of the Chinga iron-ung meteorite obtained from areas **1**, **2**, **3**, and **5**; the most negative peaks of these spectra are enlarged. The differential spectra are shown on the bottom. Adapted from [80].

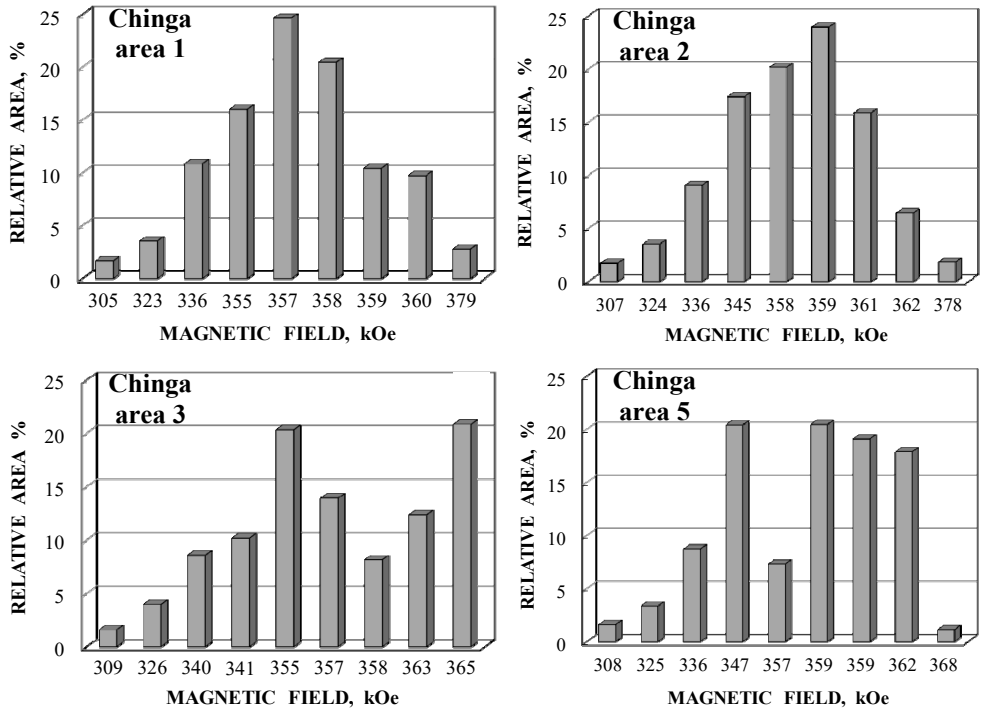

Figure 32. Comparison of histograms of the magnetic hyperfine field distributions obtained from decomposition of the Mössbauer spectra of Chinga meteorite samples shown in Figure 31. Adapted from Ref. [80].

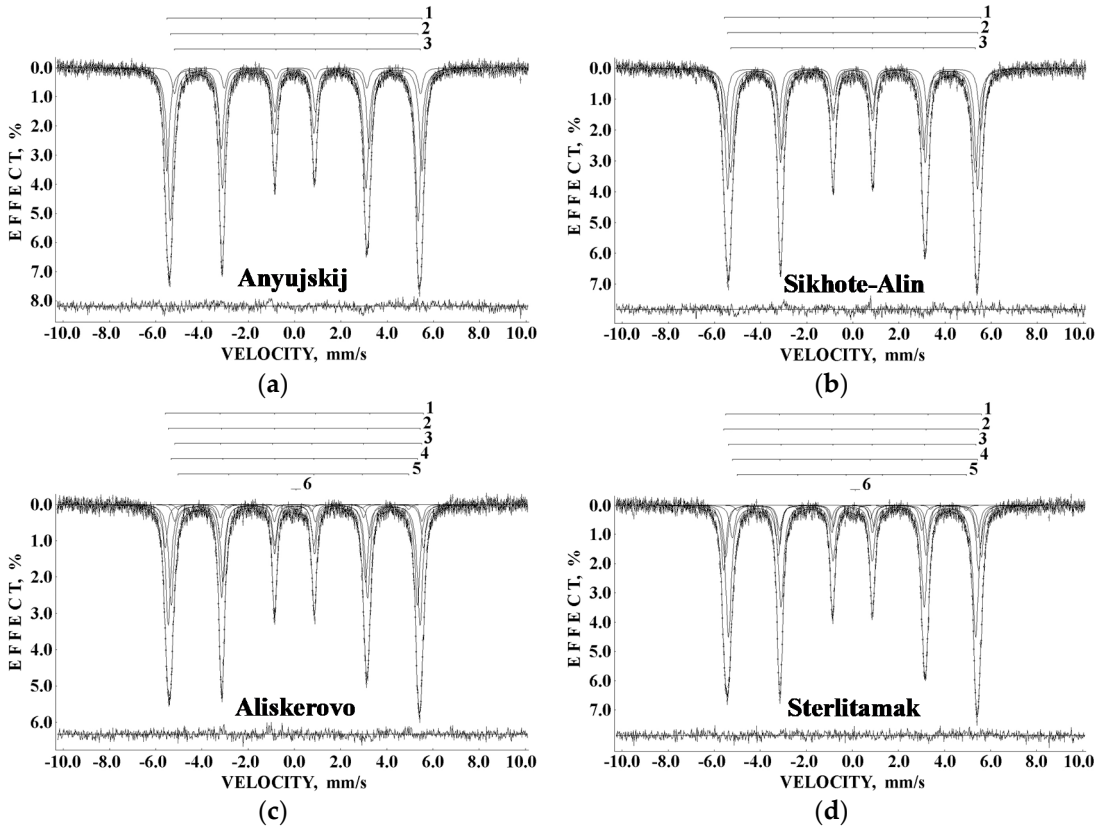

Figure 33. Room temperature Mössbauer spectra of iron meteorites measured with a high-velocity resolution (presentation in 1024 channels): (**a**) Anyujskij IIAB, (**b**) Sikhote-Alin IIAB, (**c**) Aliskerovo IIIE-an, and (**d**) Sterlitamak IIIAB. Indicated components are the results of the best fits. The differential spectra are shown on the bottom. Adapted from [81].

Therefore, the ^{57}Fe hyperfine parameters for revealed magnetic sextets were assigned in [81,82] to the following phases: (**i**) δ = 0.010 mm/s, H_{eff} = 342.3 kOe, A = 36% (sextet **1**, α-Fe(Ni, Co) phase), δ = −0.015 mm/s, H_{eff} = 332.5 kOe, A = 56% (sextet **2**, α-Fe(Ni, Co) phase), δ = 0.083 mm/s, H_{eff} = 330.0 kOe, A = 8% (sextet **3**, α-Fe(Ni, Co) phase) for Anyujskij IIAB; (**ii**) δ = 0.011 mm/s, H_{eff} = 345.1 kOe, A = 19% (sextet **1**, α-Fe(Ni, Co) phase), δ = −0.004 mm/s, H_{eff} = 336.5 kOe, A = 40% (sextet **2**, α-Fe(Ni, Co) phase), δ = −0.001 mm/s, H_{eff} = 329.7 kOe, A = 41% (sextet **3**, α-Fe(Ni, Co) phase) for Sikhote-Alin IIAB; (**iii**) δ = 0.015 mm/s, H_{eff} = 347.1 kOe, A = 14% (sextet **1**, α_2-Fe(Ni, Co) phase), δ = 0.003 mm/s, H_{eff} = 338.6 kOe, A = 43% (sextet **2**, α-Fe(Ni, Co) phase), δ = 0.036 mm/s, H_{eff} = 332.3 kOe, A = 5% (sextet **3**, α-Fe(Ni, Co) phase), δ = 0.001 mm/s, H_{eff} = 330.9 kOe, A = 35% (sextet **4**, α-Fe(Ni, Co) phase), δ = 0.006 mm/s, H_{eff} = 310.1 kOe, A = 2% (sextet **5**, γ-Fe(Ni, Co) phase) and δ = 0.071 mm/s, A = 1% (singlet **6**, paramagnetic γ-Fe(Ni, Co) phase) for Aliskerovo IIIE-an; (**iv**) δ = 0.057 mm/s, H_{eff} = 344.7 kOe, A = 16% (sextet **1**, α_2-Fe(Ni, Co) phase), δ = −0.031 mm/s, H_{eff} = 343.7 kOe, A = 20% (sextet **2**, α_2-Fe(Ni, Co) phase), δ = 0.001 mm/s, H_{eff} = 333.4 kOe, A = 50% (sextet **3**, α-Fe(Ni, Co) phase), δ = 0.024 mm/s, H_{eff} = 330.7 kOe, A = 11% (sextet **4**, α-Fe(Ni, Co) phase), δ = 0.243 mm/s, H_{eff} = 309.1 kOe, A = 2% (sextet **5**, γ-Fe(Ni, Co) phase) and δ = 0.128 mm/s, A = 1% (singlet **6**, paramagnetic γ-Fe(Ni, Co) phase) for Sterlitamak IIIAB. It should be noted that there is uncertainty in the assignment of H_{eff} in the range 340–350 kOe to α_2-Fe(Ni, Co) or α-Fe(Ni, Co) phases. Therefore, the results of chemical analysis and knowledge about Ni concentration in various phases are important for this assignment.

A re-examination of Dronino iron-ung meteorite and its weathering (oxidation) products in clay was carried out using Mössbauer spectroscopy with a high velocity resolution in [82–84]. The room temperature 2048-channel Mössbauer spectra of powdered Fe-Ni-Co alloy and extracted internal weathering product are shown in Figure 34. The

spectrum of Dronino metal earlier was measured in 512 channels and fitted using two magnetic sextets [75]. On the other hand, the newly measured spectrum presented in 2048 channels was decomposed with six magnetic sextets. The Fe-Ni-Co alloy in Dronino meteorite consisted of α-Fe(Ni, Co), α_2-Fe(Ni, Co), and γ-Fe(Ni, Co) phases and a plessite structure with Ni content in the range ~7–26.5 wt.%. The spectral components obtained from the fit had the following Mössbauer parameters: δ = 0.144 mm/s, H_{eff} = 357.1 kOe, A = ~4.4% (sextet **1**, α_2-Fe(Ni, Co) phase), δ = 0.034 mm/s, H_{eff} = 351.5 kOe, A = ~11.7% (sextet **2**, α_2-Fe(Ni, Co) phase), δ = 0.026 mm/s, H_{eff} = 341.3 kOe, A = ~54.5% (sextet **3**, α-Fe(Ni, Co) phase), δ = 0.013 mm/s, H_{eff} = 331.3 kOe, A = ~13.2% (sextet **4**, α-Fe(Ni, Co) phase), δ = 0.048 mm/s, H_{eff} = 330.4 kOe, A = ~13.9% (sextet **5**, α-Fe(Ni, Co) phase), and δ = 0.055 mm/s, H_{eff} = 307.8 kOe, A = ~2.4% (sextet **6**, γ-Fe(Ni, Co) phase).

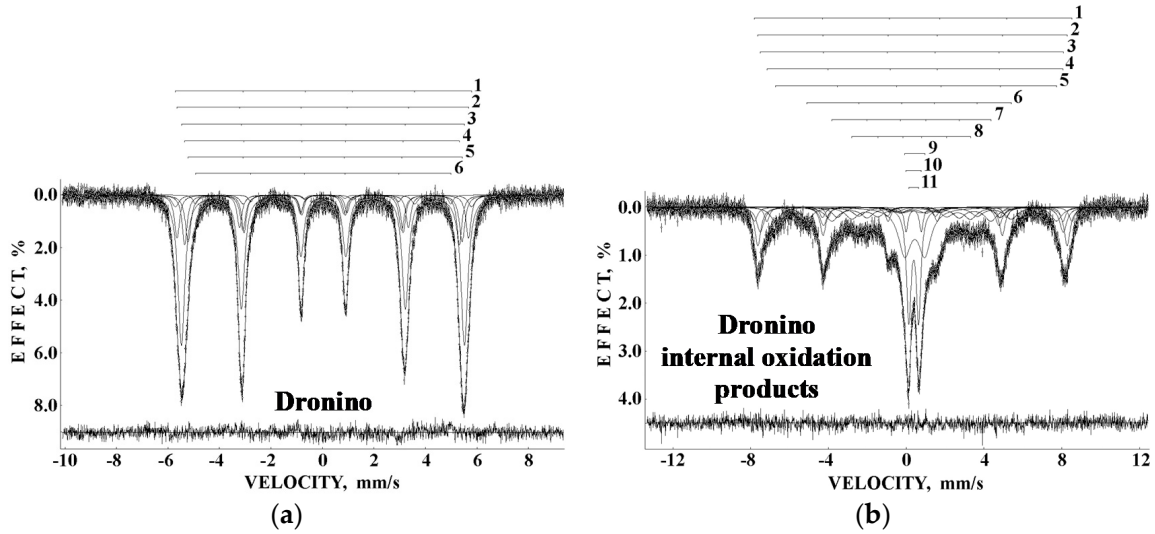

Figure 34. Room temperature 2048-channel Mössbauer spectra of Dronino iron ungrouped meteorite: powdered metallic iron alloy (**a**) and powdered internal oxidized material (**b**). Indicated components are the results of the best fits. The differential spectra are shown on the bottom. Adapted from [83].

The Mössbauer spectrum of the Dronino internal weathering product (Figure 34b) demonstrated a complex pattern which was decomposed with eight magnetic sextets and three quadrupole doublets. The magnetic sextets **1** and **3** were assigned to the octahedral [B] and tetrahedral (A) sites in γ-Fe_2O_3, respectively (δ = 0.397 mm/s, H_{eff} = 501.1 kOe, A = ~4.8% and δ = 0.277 mm/s, H_{eff} = 483.9 kOe, A = ~10.3%), sextets **2**, **4**, and **5** were related to the (A), [B1], and [B2] sites in Fe_3O_4, respectively (δ = 0.332 mm/s, H_{eff} = 494.0 kOe, A = ~13.3%; δ = 0.425 mm/s, H_{eff} = 472.8 kOe, A = ~4.2% and δ = 0.578 mm/s, H_{eff} = 449.0 kOe, A = ~8.5%), sextets **6**, **7**, and **8** were associated with α-FeOOH magnetic particles with different sizes, respectively (δ = 0.380 mm/s, H_{eff} = 326.4 kOe, A = ~8.5%; δ = 0.316 mm/s, H_{eff} = 253.9 kOe, A = ~9.8% and δ = 0.286 mm/s, H_{eff} = 189.6 kOe, A = ~8.2%), and quadrupole doublets **9**, **10**, and **11** were assigned to the paramagnetic FeOOH particles, respectively (δ = 0.444 mm/s, ΔE_Q = 1.033 mm/s, A = ~15.8%; δ = 0.389 mm/s, ΔE_Q = 0.782 mm/s, A = ~2.6%, and δ = 0.390 mm/s, ΔE_Q = 0.503 mm/s, A = ~14.1%). The fit of these and other spectra measured with a high velocity resolution in [81–84] revealed more spectral components compared to that in the low velocity resolution spectra measured in [75].

Synchrotron Mössbauer spectroscopy was applied to study the Tazewell IAB-sLH iron meteorite with a spatial resolution of ~10–20 μm in [43,44]. Therefore, the authors were able to measure the spectra of selected local areas with different phase composition. Examples of the room temperature Mössbauer spectra of the cloudy zone and plessite area of Tazewell are shown in Figure 35. The spectrum of the cloudy zone demonstrated the presence of two magnetic sextets related to kamacite (with a larger relative area) and

tetrataenite (with a smaller relative area) and a paramagnetic singlet associated by the authors with "antitaenite" (in fact, the paramagnetic γ-Fe(Ni, Co) phase). On the other hand, the spectrum of plessite area surprisingly consisted of only two components: the main magnetic sextet assigned to kamacite and a small paramagnetic singlet which should be associated with the paramagnetic taenite (because the plessite structure is a mixture of α-Fe(Ni, Co)/α_2-Fe(Ni, Co) + γ-Fe(Ni, Co) phases). The values of H_{eff} for kamacite were in the range 335.4–339.9 kOe, while those for tetrataenite varied between 284 and 289 kOe. The peak positions δ of the paramagnetic taenite were in the range between −0.004 and −0.08 mm/s.

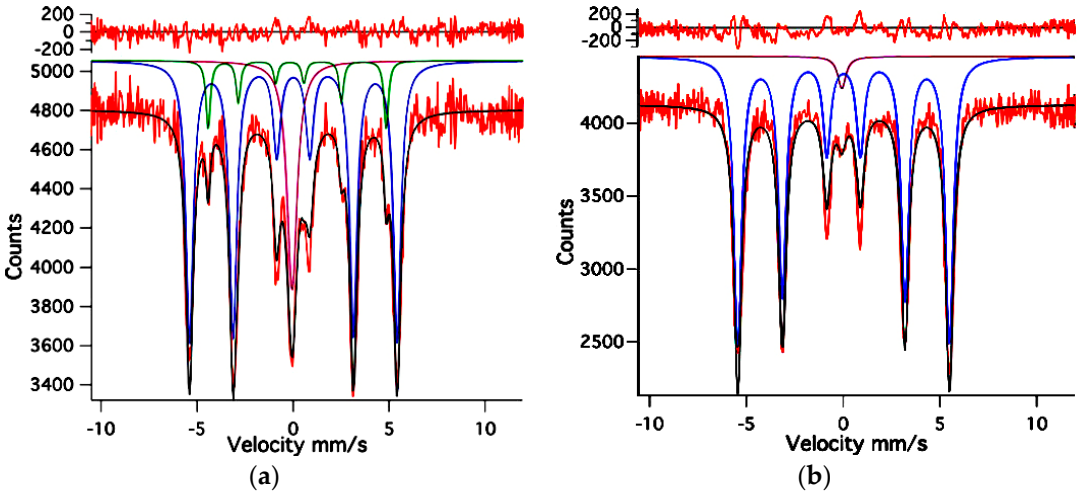

Figure 35. Room temperature synchrotron Mössbauer spectra of the Tazewell IAB-sLH iron meteorite selected areas: cloudy zone (**a**) and plessite area (**b**). Indicated spectral components are the results of the fits. The differential spectra are shown on the top. Adapted from [43].

A sample of Muonionalusta IVA iron meteorite was studied by conversion electron Mössbauer spectroscopy in [85]. The room temperature CEMS spectrum is shown in Figure 36. The authors of [85] decomposed their CEMS spectrum using four components: three magnetic sextets and one paramagnetic singlet. The Ni concentration in Muonionalusta IVA iron meteorite was determined to be about 7.9%. Therefore, magnetic sextets with parameters (**i**) δ = 0.04 mm/s, H_{eff} = 346 kOe, A = 34%, (**ii**) δ = 0.01 mm/s, H_{eff} = 337 kOe, A = 40%, and (**iii**) δ = 0.03 mm/s, H_{eff} = 328 kOe, A = 24% were related to the α-Fe(Ni, Co) phase with variations of Ni in the iron local microenvironment. A small singlet with parameters δ = 0.02 mm/s and A = 2% was assigned to the paramagnetic γ-Fe(Ni, Co) phase.

It is well known that iron meteorites contain various iron-bearing inclusions such as troilite, schreibersite, and some other compounds, in addition to the α- and γ-phases. Therefore, several papers were dedicated to the investigation of the extracted or separated compounds observed in iron meteorites. The ferromagnetic phases in graphite nodule from Canyon Diablo IAB-MG were studied by Mössbauer spectroscopy in [86]. The authors measured two Mössbauer spectra of the extracted graphite nodule material at room temperature and at 15 K (see Figure 37). The first spectrum showed the presence of three magnetic sextets and two quadrupole doublets. The magnetic sextets marked M_A and M_B with H_{eff} values of 490 kOe and 458 kOe, respectively, were related to the (A) and [B] sites in magnetite while the sextet K with δ = 0.03 mm/s and H_{eff} = 335 kOe was assigned to kamacite. One quadrupole doublet marked A with δ = 0.36 mm/s and ΔE_Q = 0.69 mm/s was associated with akaganéite, while the other quadrupole doublet E with δ = 1.17 mm/s and ΔE_Q = 2.00 mm/s was related to iron in the M2 site of enstatite. The 15 K Mössbauer spectrum consisted of magnetically split components with H_{eff} > 300 kOe.

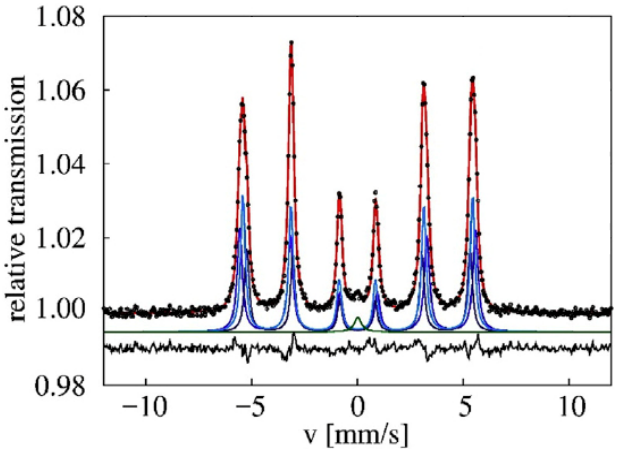

Figure 36. Conversion electron Mössbauer spectrum of Muonionalusta IVA iron meteorite measured at room temperature. Indicated spectral components are the result of the fit. The differential spectrum is shown on the bottom. Adapted from [85].

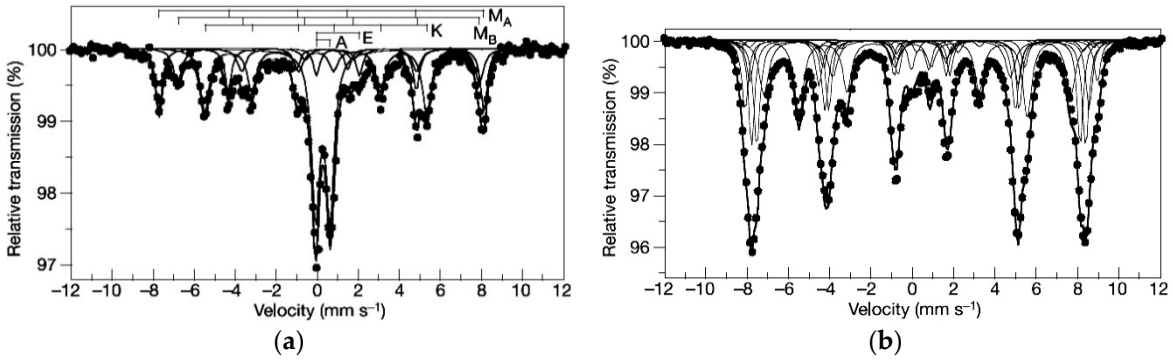

Figure 37. Mössbauer spectra of graphite nodule extracted from Canyon Diablo IAB-MG iron meteorite measured at room temperature (**a**) and at 15 K (**b**). Indicated spectral components are the results of the fits. Adapted from [86].

Troilite extracted from the iron meteorites Cape York IIIAB, Nantan IAB-MG, and Sikhote-Alin IIAB was studied by Mössbauer spectroscopy in [87–91]. The Mössbauer spectra of troilite extracted from Cape York IIIAB (called as Agpalilik) were measured in [87] at various temperatures from 77 K up to 645 K (in the temperature range 400–500 K troilite has two structural transitions). The spectrum at 645 K represented one quadrupole doublet, while the spectra at 499 K and 409 K were a six-line pattern and a superposition of three magnetic sextets, respectively. These magnetic sextets were fitted using the full static Hamiltonian. Other studies of troilite extracted from Cape York IIIAB and from Nantan IAB-MG by Mössbauer spectroscopy were carried out at very low temperatures with external magnetic field application [88–90]. These spectra were fitted without the full static Hamiltonian. In contrast, the Mössbauer spectra of troilite extracted from Sikhote-Alin IIAB measured with a high velocity resolution at 295 K and 90 K were fitted using the full static Hamiltonian [91]. These authors also revealed the spectral components assigned to nonstoichiometric troilite $Fe_{1-x}S$ (which were fitted using the hyperfine field distribution) and a paramagnetic singlet with δ = ~0.65 mm/s at 295 K, which was related to daubréelite.

The authors of [92] studied samples of troilite, kamacite, and taenite extracted from the Morasko IAB-MG iron meteorite by Mössbauer spectroscopy. They measured the room temperature spectra of these samples; however, the results obtained were partly questionable. For example, in the spectrum of extracted troilite, the authors revealed a magnetic sextet with parameters δ = 0.00 mm/s and H_{eff} = 210 kOe, which was assigned to daubréelite. However, the room temperature Mössbauer spectrum of daubréelite is a paramagnetic singlet (see, e.g., [93], in which the $FeCr_2S_4$ Mössbauer spectrum has a singlet

shape even at 170 K, and [91]). Therefore, this sextet could not be related to daubréelite, while its value of H_{eff} was the same as that obtained by the authors for cohenite in the sample of extracted taenite (e.g., H_{eff} = 199 kOe was assigned to cohenite in [7]). Moreover, the authors of [92] assigned the magnetic sextet with H_{eff} = 340 kOe to disordered taenite in the spectrum of extracted taenite, which was also incorrect, because the values of H_{eff} larger than ~329 kOe should be related to α-Fe(Ni, Co) and α_2-Fe(Ni, Co) phases, as shown above. Thus, the authors of [92] did not correctly identify the mineralogical phases.

The separates of $(Fe, Ni)_3P$ inclusions from Sikhote-Alin IIAB in the forms of massive schreibersite and rhabdite microcrystals were studied by Mössbauer spectroscopy in [94–97]. These iron nickel phosphides had a crystal structure with three non-equivalent sites M1, M2, and M3 for the metal atoms, which presented different probabilities of occupation by Fe and Ni, as well as differences in these probabilities between schreibersite and rhabdite. The Mössbauer spectra of these iron nickel phosphides extracted from Sikhote-Alin IIAB iron meteorite and measured with a high velocity resolution at 295 K and at 90 K are shown in Figure 38.

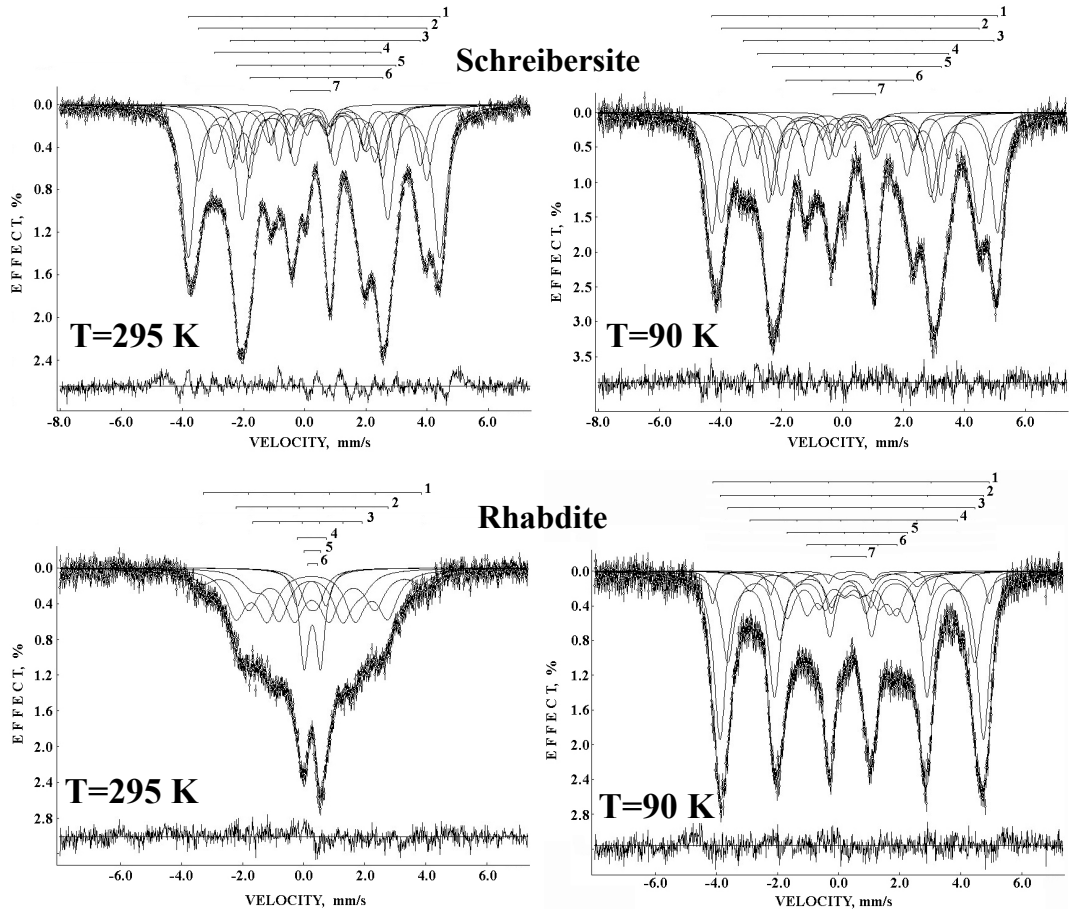

Figure 38. Mössbauer spectra of schreibersite and rhabdite microcrystals extracted from Sikhote-Alin IIAB iron meteorite measured with a high velocity resolution at 295 K and 90 K. Indicated spectral components are the results of the best fits. The differential spectra are shown on the bottom. Adapted from [96].

The room temperature spectra of schreibersite and rhabdite samples demonstrated a clear difference due to the superparamagnetic state of rhabdite microcrystals, as the spectra of rhabdite microcrystals indicated magnetically split components at lower temperatures. The magnetically split Mössbauer spectra of schreibersite and rhabdite microcrystals were better fitted using six magnetic sextets and one paramagnetic doublet. These six sextets were related to the ^{57}Fe nuclei in the M1, M2, and M3 sites in iron nickel phosphides, with two sextets per site. Using this fit, the authors of [94–97] estimated the Fe and Ni

occupancies of the M1, M2, and M3 sites in schreibersite and rhabdite from Sikhote-Alin iron meteorites, which appeared to be different for the two phosphides.

São João Nepomuceno IVA-an is an anomalous iron meteorite containing silicate inclusions. The authors of [98,99] studied the extracted orthopyroxene using Mössbauer spectroscopy in order to analyze the thermal history of meteorite by determining the Fe^{2+} populations in the M1 and M2 sites in orthopyroxene. The room temperature spectrum of extracted orthopyroxene is shown in Figure 39. This spectrum demonstrated a superposition of two quadrupole doublets related to the ^{57}Fe in M1 and M2 sites in orthopyroxene with the following Mössbauer parameters: δ = 1.23 mm/s, ΔE_Q = 2.24 mm/s, A = 10% (M1) and δ = 1.16 mm/s, ΔE_Q = 2.12 mm/s, A = 90% (M2). The authors measured Mössbauer spectra in the temperature range 300–25 K. On the basis of the Mössbauer relative areas and microprobe analysis, the authors determined the values of K_D = 0.083 and T_{Cl} = 770 K for orthopyroxene extracted from São João Nepomuceno iron meteorite.

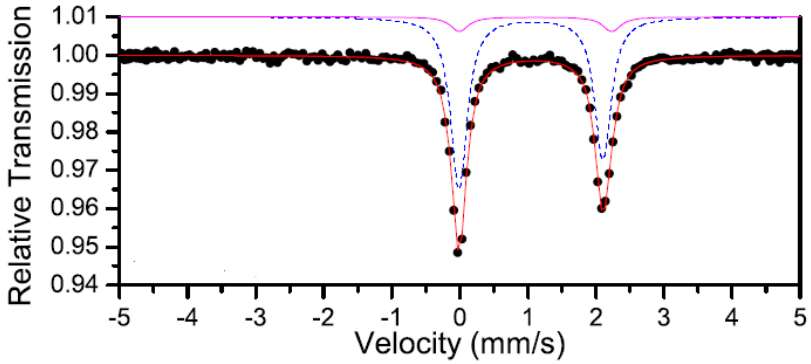

Figure 39. Room temperature Mössbauer spectrum of orthopyroxene extracted from São João Nepomuceno IVA-an iron meteorite. Indicated spectral components are the result of the fit. Adapted from [99].

5. Lunar and Martian Matter

5.1. Lunar Soils and Rocks

Investigation of Lunar material became possible due to successful return missions to the Moon in 1969–1976 by two space programs: Apollo (USA) and Luna (the former USSR). Apollo missions were crewed, and the first two men appeared on the Moon on July 21, 1969 (Apollo 11). Astronauts collected Lunar soils and rocks from different parts of the Moon near the places of six Apollo mission landings, with a total weight of 380 kg, and delivered Lunar matter to the Earth. Luna space missions to the Moon were uncrewed and equipped with return modules which delivered Lunar material to the Earth with a total weight of about 320 g. Therefore, intensive studies of delivered Lunar material by various techniques including Mössbauer spectroscopy were started in 1969 by various research groups (some of these studies were reviewed in [100]).

Some of the first Mössbauer spectra of Lunar samples were measured in [101–105]. The authors studied Lunar soil and rock samples using transmission and backscattering geometries. The room temperature Mössbauer spectra of two Lunar fines are shown in Figure 40. These spectra are typical for Lunar fines. The fits of the various fines spectra demonstrated the presence of the following components: (**i**) magnetic sextet δ = 0.07 mm/s, H_{eff} = 334 kOe, (**ii**) magnetic sextet δ = 0.75 mm/s, H_{eff} = 310 kOe, (**iii**) quadrupole doublet δ = 1.15 mm/s, ΔE_Q = 2.71 mm/s, (**iv**) quadrupole doublet δ = 1.12 mm/s, ΔE_Q = 1.97 mm/s, and (**v**) quadrupole doublet δ = 1.07 mm/s, ΔE_Q = 0.71 mm/s. These components were assigned to (**i**) metallic iron alloy, (**ii**) troilite, (**iii**) Fe^{2+} in the M1 sites in clinopyroxenes and olivine, (**iv**) Fe^{2+} in iron-bearing glasses and in the M2 sites in clinopyroxene, and (**v**) ilmenite. These spectra demonstrated a relatively large content of ilmenite.

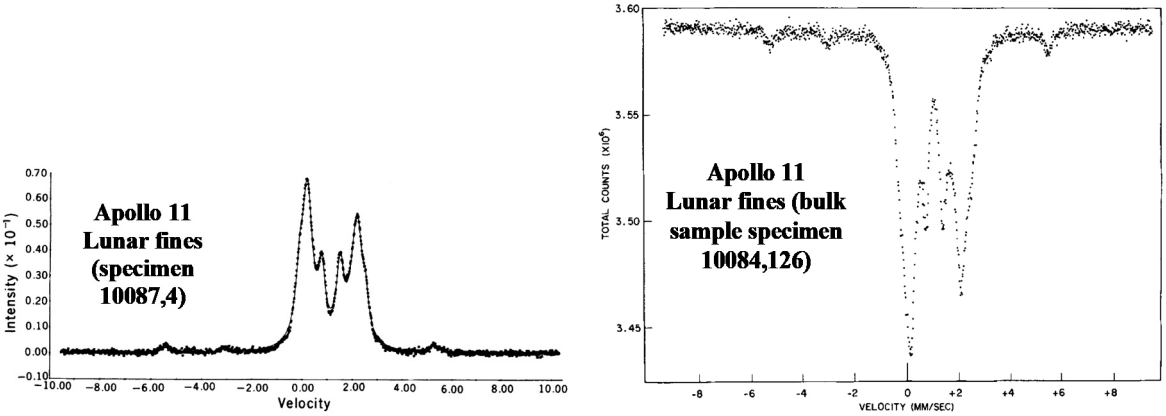

Figure 40. Mössbauer spectra of Lunar fines (Apollo 11) measured at room temperature: unsieved sample, specimen 10087,4 (backscattering geometry) (**a**) and specimen 10084,126, from the 140/170 sieve size fraction (transmission geometry) (**b**). Adapted from [101,103].

The backscattered Mössbauer spectra of Lunar gabbroic rock and vesicular basalt measured at room temperature are shown in Figure 41. These spectra also demonstrated a large contribution of ilmenite (two peaks in the middle of the spectrum with a small quadrupole doublet), in addition to silicates and probably glasses [102]. However, the relative part of ilmenite in gabbroic rock was smaller than that in vesicular basalt.

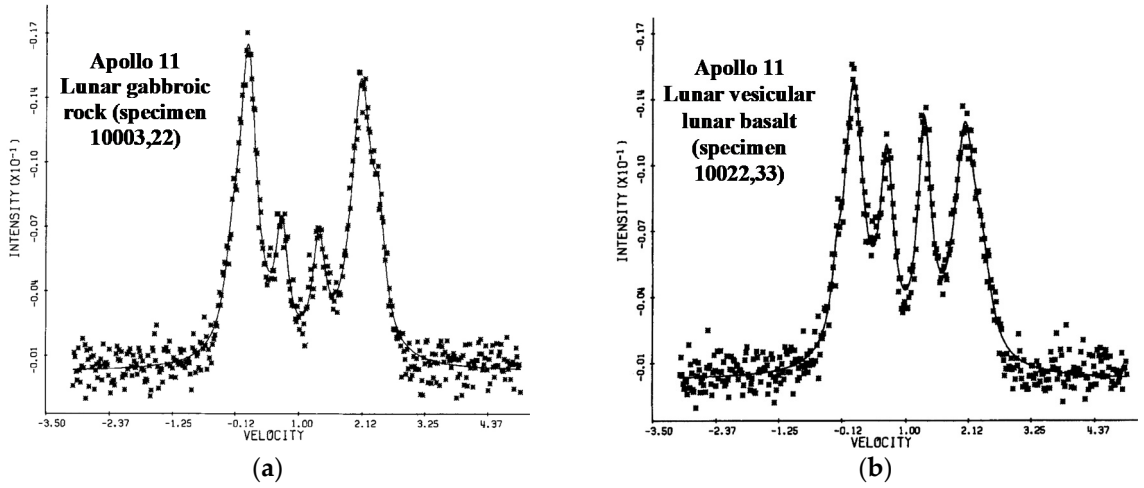

Figure 41. Mössbauer spectra of Lunar samples (Apollo 11) measured at room temperature in the small velocity range and backscattering geometry: gabbroic rock, specimen 10003,22 (**a**) and vesicular basalt, specimen 10022,33 (**b**). Adapted from [102].

The transmission Mössbauer spectra of two rock samples delivered by the Apollo 12 mission are shown in Figure 42. These spectra showed that the components in both rocks were similar: silicate phases and ilmenite, metallic iron alloy, and troilite. However, the relative contents of these phases were different for specimens 12002 and 12063 [105]. For example, ilmenite contents were ~7% (12002) and ~14% (12063), while olivine contents were ~25% (12002) and ~14% (12063). On the other hand, the contents of metallic iron alloy and of troilite are very close, respectively, in specimens 12002 and 12063, while pyroxene content differed by about 5% only. The authors compared the Mössbauer spectra of several rocks from the Apollo 12 mission and observed some similarities and differences. Moreover, these spectra were compared with those of rocks from the Apollo 11 mission, and the authors found some differences.

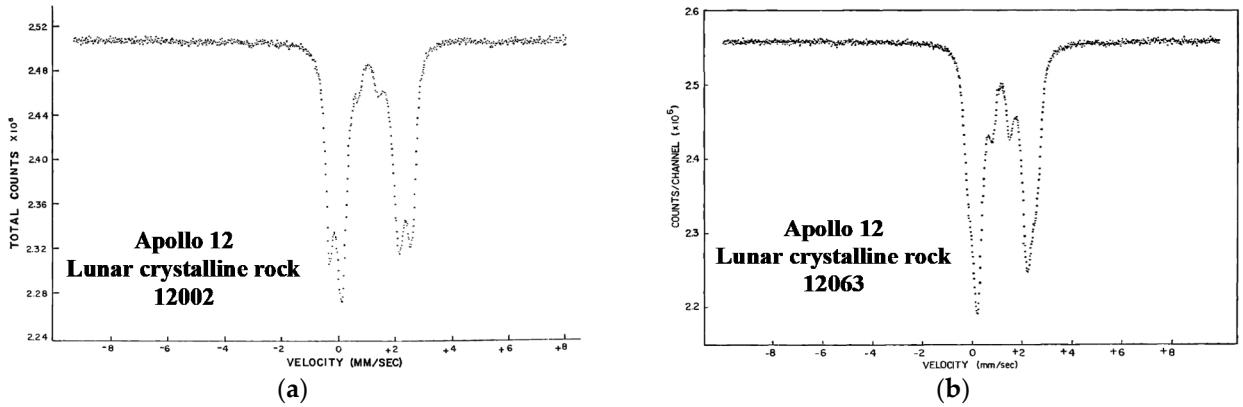

Figure 42. Mössbauer spectra of Lunar crystalline rocks (Apollo 12) measured at room temperature in transmission geometry: specimen 12002 (**a**) and specimen 12063 (**b**). Adapted from [105].

Some other investigations of Lunar soil and rocks delivered by the Apollo 11 mission using Mössbauer spectroscopy were done in [106,107]. The authors of [106] studied Lunar fines (specimen 10084,89) and light and heavy dust separated from the fines. The room temperature Mössbauer spectra of these samples are shown in Figure 43. All these spectra demonstrated the presence of large contents of pyroxene (components related to the M1 and M2 sites were identified) and ilmenite (components marked **1**, **2**, and **3** in Figure 43). A component corresponding to a metallic iron alloy was found in fines and light dust, while troilite was found in the spectrum of light dust only. The authors explained the absence of metallic iron alloy in the heavy dust spectrum as being due to removal during sample preparation.

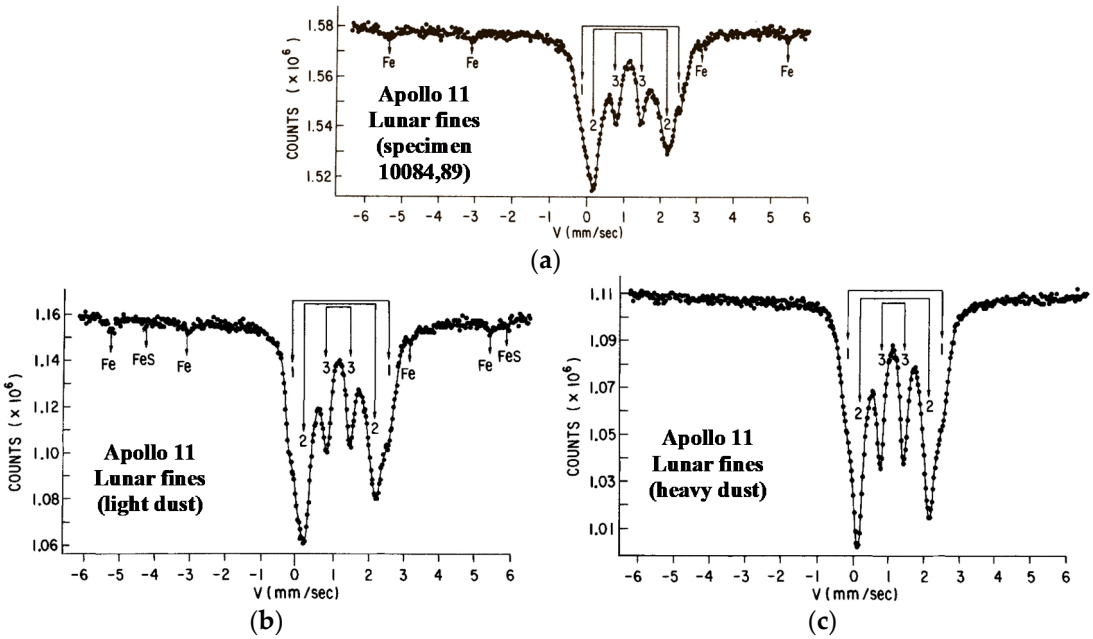

Figure 43. Mössbauer spectra of Lunar fines (Apollo 11) measured at room temperature: specimen 10084,89 (**a**), light dust from fines (**b**), and heavy dust from fines (**c**). **Fe** is metallic iron alloy, **FeS** is troilite, **1** represents the M1 sites in pyroxene, **2** represents the M2 sites in pyroxene, and **3** is ilmenite. Adapted from [106].

The authors of [106] measured Mössbauer spectra of their various Lunar samples at low temperatures down to liquid helium temperature. They deduced similar ^{57}Fe hyperfine parameters for pyroxene and for ilmenite in the studied sample at both 295 K and 77 K. The room temperature parameters were as follows: δ = 1.14 mm/s, ΔE_Q = 2.64 mm/s

(the M1 sites in pyroxene), δ = 1.10 mm/s, ΔE_Q = 1.96 mm/s (the M2 sites in pyroxene), and δ = 1.07 mm/s, ΔE_Q = 0.74 mm/s (ilmenite) for Lunar fines and δ = 1.11 mm/s, ΔE_Q = 2.58 mm/s (the M1 sites in pyroxene), δ = 1.08 mm/s, ΔE_Q = 1.98 mm/s (the M2 sites in pyroxene), and δ = 1.02 mm/s, ΔE_Q = 0.72 mm/s (ilmenite) for Lunar rocks.

Furthermore, the large number of Lunar samples delivered by Apollo missions 11, 12, 14, 15, 16, and 17 were studied by Mössbauer spectroscopy in order to determine the iron-bearing phases and ratios of their contents in [107]. The room temperature Mössbauer spectra of basalt, specimen 70017, and poikilitic rock, specimen 60315, are shown in Figure 44. These spectra demonstrated that the basalt sample contained a small amount of troilite and large amounts of pyroxene (components related to the M1 and M2 sites) and ilmenite, while poikilitic rock additionally contained metallic iron alloy and olivine. However, the content of ilmenite was substantially smaller in the latter sample.

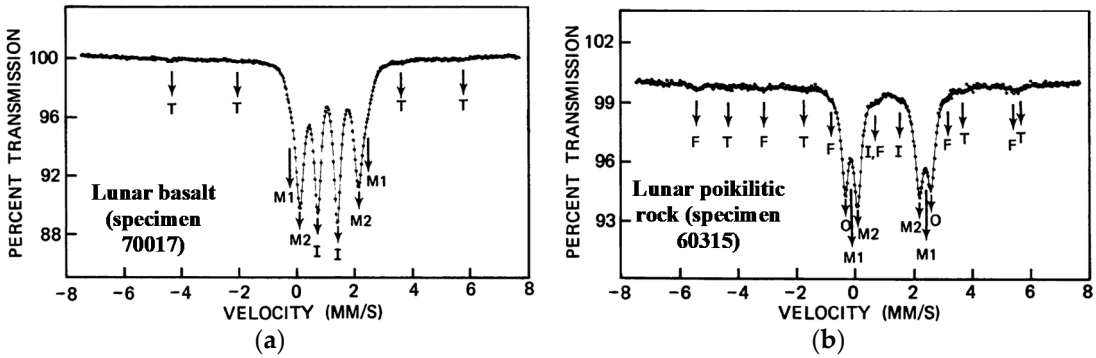

Figure 44. Mössbauer spectra of Lunar samples measured at room temperature: basalt, specimen 70017 (**a**) and poikilitic rock, specimen 60315 (**b**). **F** is metallic iron alloy, **T** is troilite, **O** is olivine, **M1** represents the M1 sites in pyroxene, **M2** represents the M2 sites in pyroxene, and **I** is ilmenite. Adapted from [107].

The results of various other studies of Lunar soils, rocks, fines, glasses, etc. from Apollo missions using Mössbauer spectroscopy were discussed in various papers (see, e.g., [108–119]). These results indicated the presence of silicate phases, mainly pyroxene and sometimes olivine, ilmenite, troilite, and metallic iron alloy in different quantities depending on the sample. In addition to Apollo samples, studies of Lunar soils delivered by Luna missions were also carried out by Mössbauer spectroscopy (see, e.g., [120–132]).

A comparison of the Mössbauer spectra of Lunar fines delivered by Luna-16 and Luna-20 return missions was carried out in [121]. The room temperature spectra of Lunar fines specimens L1627,2, L1627,9, and L2015,2 measured in the large velocity range are shown in Figure 45a. These spectra demonstrated the presence of magnetic sextet with $H_{eff} \approx 330$ kOe in specimens L1627,2 and L1627,9, which is characteristic for ferromagnetic Fe-Ni alloy. However, this magnetic sextet was not revealed in the spectrum of specimen L2015,2. The central (paramagnetic) parts of these spectra were slightly different for the studied fines. Therefore, the authors measured the Mössbauer spectra of specimens L1627,2 and L2015,2 in comparison with the Lunar soil, specimen 15601,104, from the Apollo 15 mission, in the small velocity range (Figure 45b). The central part of these spectra indicated the presence of at least a superposition of three quadrupole doublets with different relative areas (in fact, with different iron content in these phases) but with the same isomer shift and quadrupole splitting for the studied samples. The authors of [121] believed that these quadrupole doublets could be assigned to orthopyroxenes, clinopyroxenes, olivine, ilmenite, glassy phases, and superparamagnetic iron. Parameters for ilmenite were δ = 0.70 mm/s and ΔE_Q = 1.06 mm/s. Different contents of ilmenite in specimens L1627,2, L2015,2, and 15601,104 were visible in the spectra (shown in Figure 45b) due to different contributions of the quadrupole doublet related to ilmenite. On the other hand, the authors did not reveal any spectral component which could be related to ferric compound.

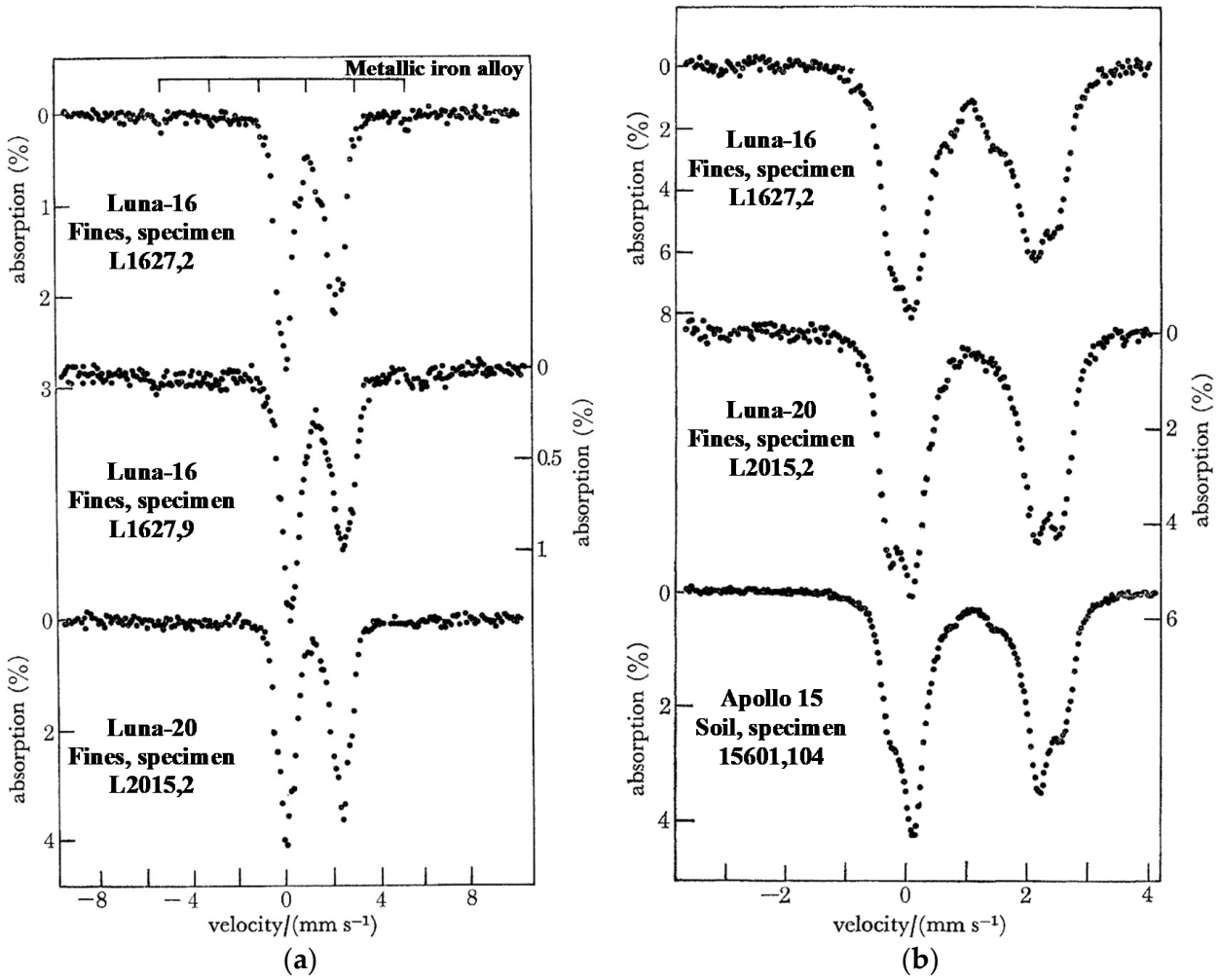

Figure 45. Room temperature Mössbauer spectra of Lunar fines from Luna-16 and Luna-20 and of Lunar soil from Apollo 15: specimens L1627,2, L1627,9 (Luna-16) and L2015,2 (Luna-20), large velocity range (**a**) and specimens L1627,2 (Luna-16), L2015,2 (Luna-20) and 15601,104 (Apollo 15), small velocity range (**b**). Adapted from [121].

5.2. Martian Surface

The study of the surface of Mars by means of Mössbauer spectroscopy became possible with development of the miniaturized spectrometer MIMOS II (see [133–135]). Two robotic rovers of NASA's Mars Exploration Rover Missions named Spirit and Opportunity were equipped with MIMOS II spectrometers that recorded the backscattered Mössbauer spectra of the surface targets. These rovers landed on Mars at two different locations: on January 4, 2004 at the Gusev Crater (Spirit) and on January 25, 2004 at the Miridiani Planum (Opportunity). The measured Mössbauer spectra transferred to the Earth were fitted and demonstrated the presence of spectral components that could be related to olivine and possibly pyroxene, the paramagnetic ferric compounds, and magnetically split ferric compounds [136–138].

The first Mössbauer spectrum measured on the Mars surface (Gusev Crater) by Spirit rover is shown in Figure 46a. This spectrum demonstrated the presence of three quadrupole doublets that were assigned to olivine, probably pyroxene and ferric compound. Another spectrum of Adirondack rock (also Gusev Crater) demonstrated the same three quadrupole doublets and an additional two magnetic sextets that were assigned to the tetrahedral (A) and octahedral [B] sites in magnetite (Figure 46b). These Mössbauer spectra indicated that the Mars surface and rocks contained olivine and pyroxene, as well as some ferric compounds.

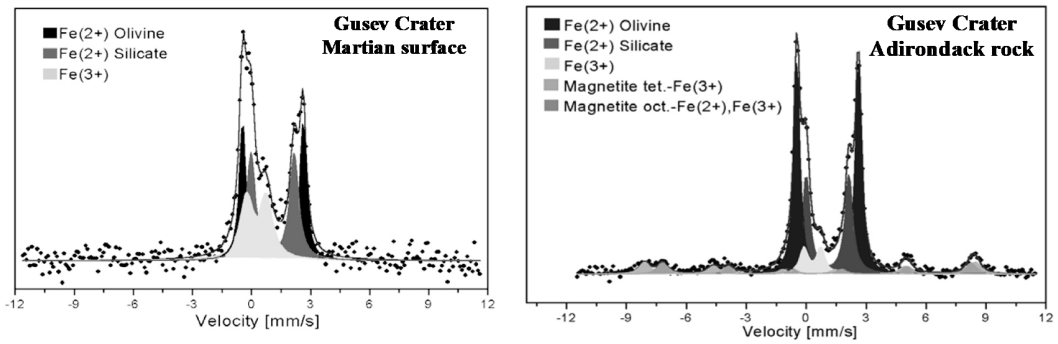

Figure 46. Mössbauer spectra from Gusev Crater, Mars: Martian surface (**a**) and Adirondack rock (**b**). T is in the range 200–280 K. Adapted from [138].

On the other side of Mars, at the Miridiani Planum, the second rover Opportunity measured the Mössbauer spectrum of outcropped target "El Capitan", which was different from the spectra measured at the Gusev Crater (see Figure 47). This spectrum demonstrated the presence of basaltic components (olivine and pyroxene), as well as jarosite (K, Na)$Fe_3(SO_4)_2(OH)_6$ and paramagnetic and magnetic ferric compounds (the latter was associated with hematite). Observation of jarosite was the most important because this mineral contains hydroxyl groups, which was a direct confirmation of aqueous alteration processes and the presence of water at this site of Mars in the past.

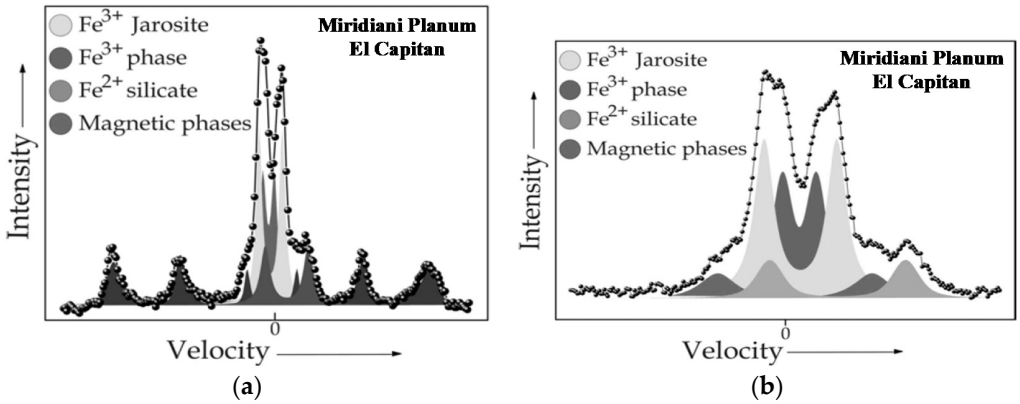

Figure 47. Mössbauer spectra of outcropped target "El Capitan" from Miridiani Planum, Mars measured in the large velocity range (**a**) and in the small velocity range (**b**). Adapted from [138].

In addition to jarosite, goethite α-FeOOH was found in the Mössbauer spectra of rock "Clovis" in the Columbia Hills at the Gusev Crater [139]. Two Mössbauer spectra measured at slightly different temperature ranges are shown in Figure 48. These spectra demonstrated the presence of goethite in the magnetic and paramagnetic states, thus testifying to the presence of water on Mars in the past.

Various Mössbauer measurements of soils and rocks by two rovers at the Gusev Crater and Miridiani Planum were considered, e.g., in [140–144]. The authors determined the iron-bearing minerals in these soils and rocks and obtained the modal phase analyses of the studied materials. The iron-bearing phases detected at the Gusev Crater by Spirit rover Mössbauer spectrometer were olivine, pyroxene, ilmenite, magnetite, chromite, nanophase ferric oxide, Fe^{3+}-sulfate, hematite, goethite, and pyrite/marcasite. The iron-bearing phases identified by Mössbauer spectroscopy with the Opportunity rover at the Meridiani Planum were jarosite, hematite, olivine, pyroxene, magnetite, nanophase ferric oxides, an unassigned ferric phase, and metallic iron alloy (kamacite). Selected Mössbauer spectra of various soils and rocks from the Gusev Crater are shown in Figure 49.

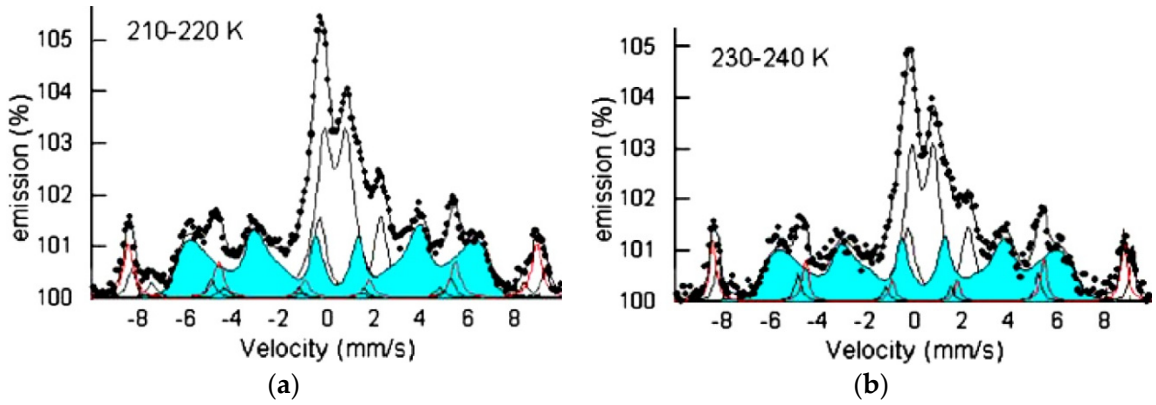

Figure 48. Mössbauer spectra of rock "Clovis" in the Columbia Hills at the Gusev Crater, Mars, measured at two temperature ranges: 210–220 K (**a**) and 230–240 K (**b**). Indicated spectral components are the results of the fits. Adapted from [139].

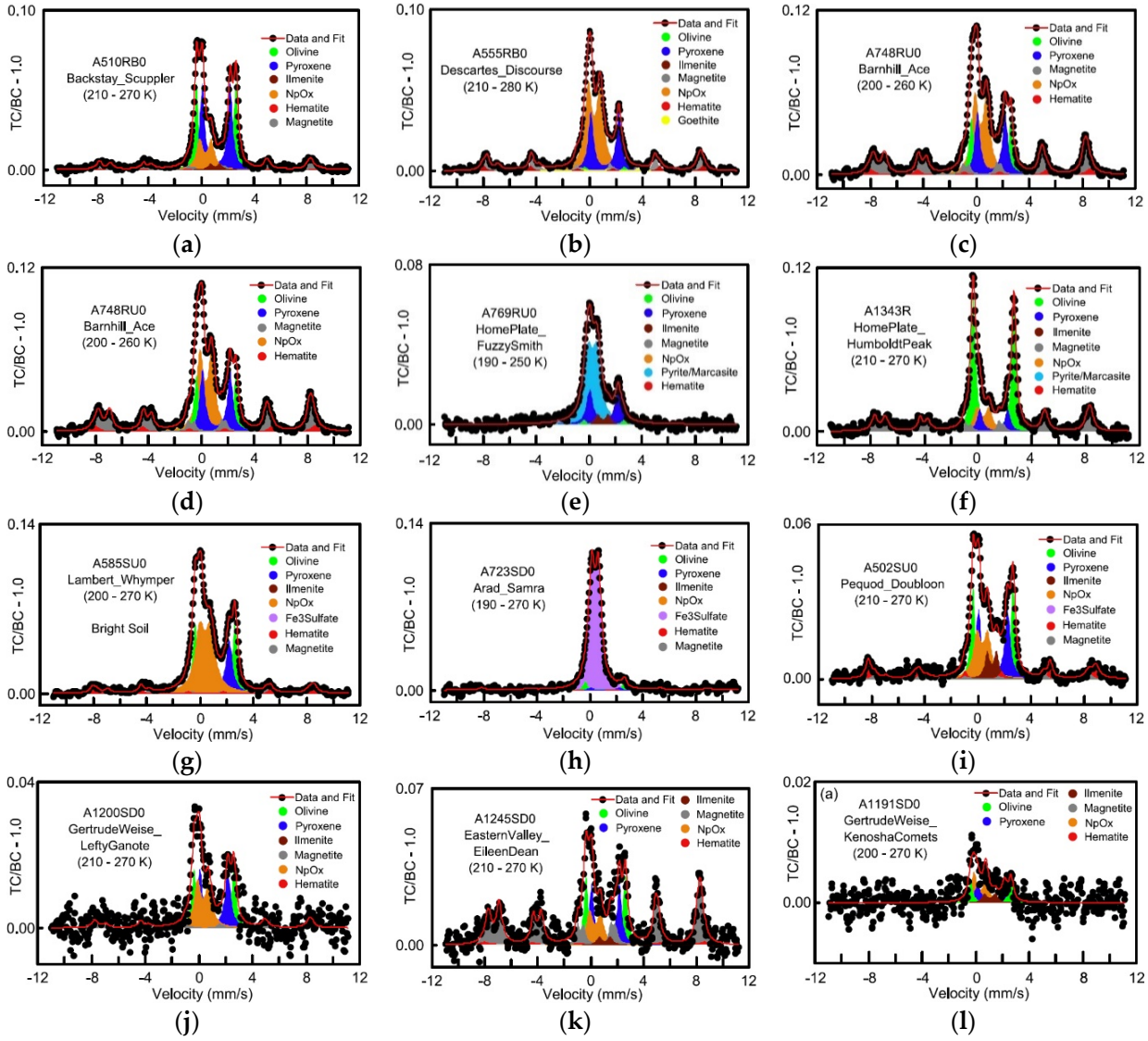

Figure 49. Selected Mössbauer spectra of Mars rocks (**a**–**c**), outcrop rock (**d**), float rocks (**e**,**f**), and soils (**g**–**l**) measured by Spirit rover at the Gusev Crater. **NpOx** means nanophase ferric oxide, **Fe3Sulfate** means Fe^{3+}-bearing sulfate. Adapted from [143].

Some particular studies by Mössbauer spectroscopy were carried out for investigations of Martian hematite [145,146], mineralogy of several Martian cobbles [147,148], shergottite-like basalt on Mars [149], and Martian olivine and pyroxene [150]. It is interesting to observe that the chemical and mineralogical data for Martian shergottite-like basalt were similar to those for Martian meteorites shergottites found on Earth, especially for Elephant Moraine (EETA) 79001 (see Mössbauer data in Section 2.4 and [26]) and Queen Alexandra Range 94201.

Some cobbles named the Arkansas group, studied using Opportunity rover Mössbauer spectrometer at the Miridiani Planum on Mars [147,148], demonstrated the spectra shown in Figure 50. These spectra indicated the presence of one magnetic sextet (except Antistasi) and four quadrupole doublets with different contributions. The fits of Mössbauer spectra deduced the ^{57}Fe hyperfine parameters which were related to the following iron-bearing phases: (**i**) hematite (δ = 0.37 mm/s, H_{eff} = 520 kOe, A = 8% for Arkansas and δ = 0.37 mm/s, H_{eff} = 519 kOe, A = 5% for Joseph McCoy), (**ii**) olivine (δ = 1.14 mm/s, ΔE_Q = 2.99 mm/s, A = 26% for Antistasi, δ = 1.14 mm/s, ΔE_Q = 3.00 mm/s, A = 7% for Arkansas and δ = 1.14 mm/s, ΔE_Q = 2.96 mm/s, A = 39% for Joseph McCoy), (**iii**) pyroxene (δ = 1.15 mm/s, ΔE_Q = 2.14 mm/s, A = 48% for Antistasi, δ = 1.15 mm/s, ΔE_Q = 2.23 mm/s, A = 11% for Arkansas and δ = 1.15 mm/s, ΔE_Q = 2.12 mm/s, A = 34% for Joseph McCoy), (**iv**) nanophase ferric oxide (δ = 0.37 mm/s, ΔE_Q = 1.10 mm/s, A = 23% for Antistasi, δ = 0.36 mm/s, ΔE_Q = 1.03 mm/s, A = 72% for Arkansas and δ = 0.38 mm/s, ΔE_Q = 1.03 mm/s, A = 20% for Joseph McCoy), and (**v**) ilmenite (δ = 1.08 mm/s, ΔE_Q = 0.80 mm/s, A = 2% for Antistasi, δ = 1.07 mm/s, ΔE_Q = 0.81 mm/s, A = 2% for Arkansas and δ = 1.07 mm/s, ΔE_Q = 0.81 mm/s, A = 2% for Joseph McCoy). The authors related the Arkansas group cobbles to the Meridiani outcrop with an additional basaltic or basaltic soil component.

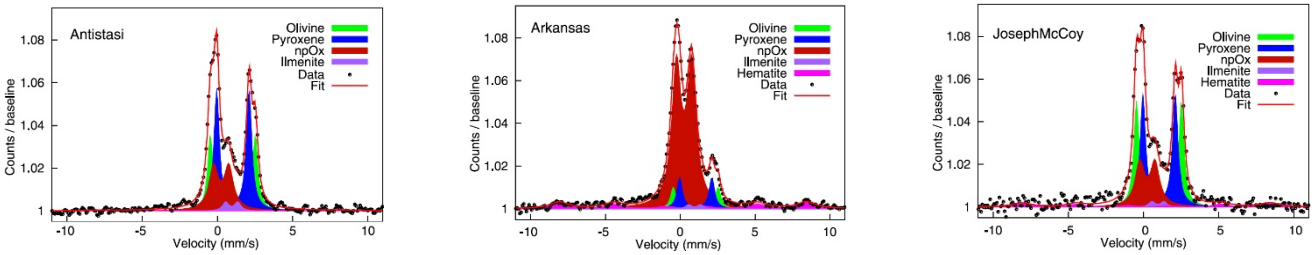

Figure 50. Mössbauer spectra of cobbles from Arkansas group at the Meridiani Planum, Mars: Antistasi (**a**), Arkansas (**b**), and Joseph McCoy (**c**) measured by Opportunity rover. **NpOx** means nanophase ferric oxide. Adapted from [148].

Another cobble group, named Barberton, which was also observed at the Miridiani Planum by Opportunity rover, demonstrated different Mössbauer spectra [148]. Two of them measured for Barberton and Kasos cobbles are shown in Figure 51. These Mössbauer spectra demonstrated the presence of two magnetic sextets and three quadrupole doublets.

The obtained ^{57}Fe hyperfine parameters from the simultaneous fit of these spectra were assigned by the authors of [148] to the following iron-bearing phases: (**i**) kamacite (δ = 0.01 mm/s, H_{eff} = 345 kOe, A = 11% for Barberton and δ = 0.00 mm/s, H_{eff} = 346 kOe, A = 5% for Kasos), (**ii**) troilite (δ = 0. 75 mm/s, H_{eff} = 313 kOe, A = 3% for Barberton and δ = 0.74 mm/s, H_{eff} = 316 kOe, A = 14% for Kasos), (**iii**) olivine (δ = 1.16 mm/s, ΔE_Q = 3.03 mm/s, A = 48% for Barberton and δ = 1.17 mm/s, ΔE_Q = 3.03 mm/s, A = 32% for Kasos), (**iv**) pyroxene (δ = 1.15 mm/s, ΔE_Q = 2.15 mm/s, A = 32% for Barberton and δ = 1.16 mm/s, ΔE_Q = 2.16 mm/s, A = 41% for Kasos), and (**v**) nanophase ferric oxide (δ = 0.38 mm/s, ΔE_Q = 0.88 mm/s, A = 6% for Barberton and δ = 0.39 mm/s, ΔE_Q = 0.97 mm/s, A = 8% for Kasos). The presence of kamacite and troilite in these cobbles may indicate their meteoritical origin. Therefore, the authors of [147,148] associ-

ated the Barberton group cobbles with meteorites with an overall chemistry and mineralogy consistent with a mesosiderite silicate clast composition.

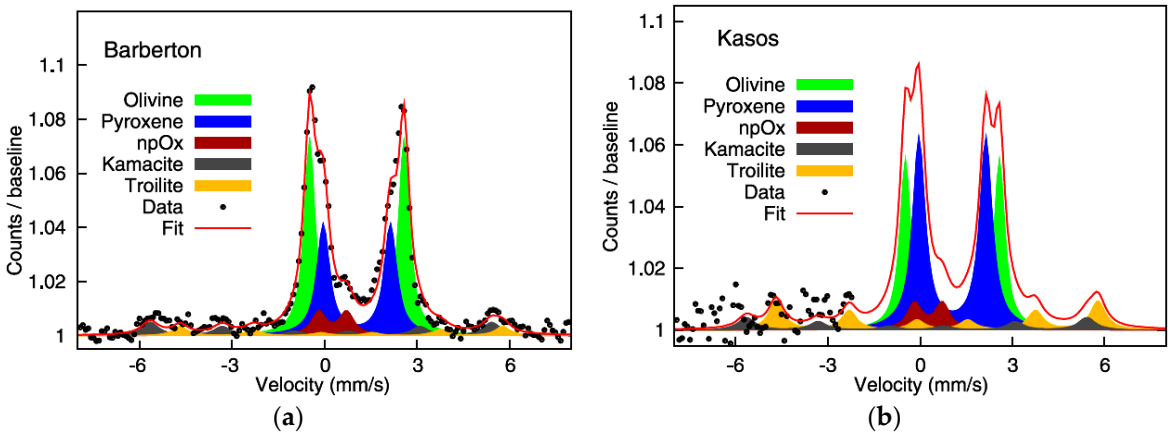

Figure 51. Mössbauer spectra of cobbles from the Barberton group: Barberton (**a**) and Kasos (**b**), measured by Opportunity rover at the Meridiani Planum, Mars. **NpOx** means nanophase ferric oxide. Adapted from [148].

Moreover, Opportunity rover discovered the first iron meteorite at the Meridiani Planum, Mars which was named Maridiani Planum. The Mössbauer spectrum of the brushed part of Meridiani Planum is shown in Figure 52 [151] and demonstrates the presence of a magnetic sextet and paramagnetic doublet with the following parameters (for the temperature range 220–230 K): (**i**) δ = 0.01 mm/s, H_{eff} = 343 kOe, A = 91% and (**ii**) δ = 0.34 mm/s, ΔE_Q = 0.75 mm/s, A = 9%. The magnetic sextet was assigned to kamacite (the Ni content was ~7 wt.%). The paramagnetic doublet was associated with paramagnetic ferric compound.

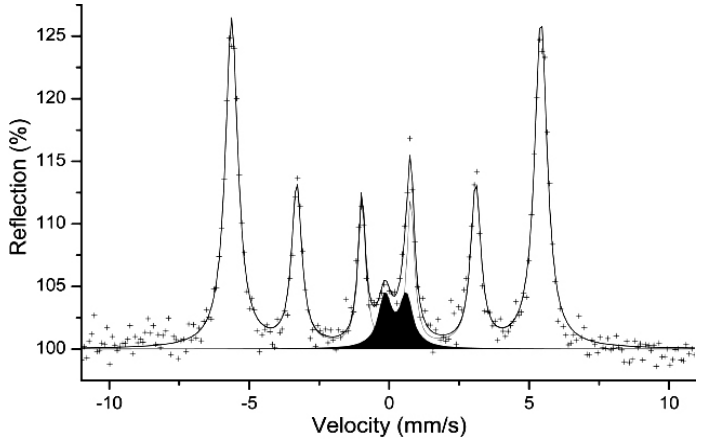

Figure 52. Mössbauer spectrum of the Meridiani Planum iron meteorite observed at the Meridiani Planum, Mars and measured using Opportunity rover in the temperature range 220–230 K. Indicated spectral components are the result of the fit. Adapted from [151].

6. Conclusions

About 60 years of successful applications of ^{57}Fe Mössbauer spectroscopy in the investigation of extraterrestrial materials have demonstrated the great utility of this technique in the study of various iron-bearing minerals and phases. Almost all groups/clans of meteorites have been investigated by Mössbauer spectroscopy. Lunar soils and rocks were also studied by Mössbauer spectroscopy after delivery to the Earth by returned Lunar space missions. In the case of Mars, two rovers Spirit and Opportunity equipped with miniaturized Mössbauer spectrometers measured the Mössbauer spectra in situ of Martian soils and rocks, as well as meteorites that fell on Mars. The application of synchrotron

Mössbauer spectroscopy demonstrated the unique possibility of measuring the selective spectra of thin slices of meteorite with a spatial resolution ~10–20 μm. Mössbauer spectroscopy with a high velocity resolution demonstrates the possibility to excavate spectral components including minor ones which cannot be extracted correctly from the spectra measured using conventional spectrometers.

The main results which can be obtained using Mössbauer spectroscopy of extraterrestrial materials include the following: (**i**) decomposition of the Mössbauer spectra of various materials with determination of the ^{57}Fe hyperfine and other Mössbauer parameters; (**ii**) determination of the iron-bearing phases/minerals using the ^{57}Fe hyperfine parameters; (**iii**) comparison of the ^{57}Fe hyperfine parameters for the same phases/minerals in different meteorites/planetary materials in order to analyze the microstructural variations in the iron local microenvironments and evaluate similarities and differences in their formation and evolution; (**iv**) modal phase analysis of the iron-bearing phases/minerals and its comparison for different samples; (**v**) determination of the Fe^{2+} partitioning among the M1 and M2 sites in silicate crystals (olivine, orthopyroxene and clinopyroxene), as well as iron occupancies of the M1, M2, and M3 sites in iron nickel phosphides (and in any other extraterrestrial crystals consisting of non-equivalent sites for iron); (**vi**) estimation of the distribution coefficient and the temperature of equilibrium cation distribution for olivines and orthopyroxenes in order to analyze their thermal history (with a thermal history of extraterrestrial materials containing these silicates); (**vii**) investigation of the processes of terrestrial and extraterrestrial weathering of meteorites and planetary materials, as well as the fusion crust formation; (**viii**) estimation of the terrestrial age of meteorites; (**ix**) classification of meteorites using Mössbauer parameters.

Therefore, Mössbauer spectroscopy will be further used for the study of meteorites and planetary materials. However, to obtain reliable results, it is necessary to use the most appropriate Mossbauer spectrometers and carry out measurements with high quality and precision that can produce the high-quality spectra. Moreover, the most careful studies should be done using other powerful complementary techniques such as X-ray diffraction, scanning electron microscopy with energy/wavelength dispersive spectroscopy, electron microprobe analysis, magnetization measurements, and optical microscopy (metallography). A multidisciplinary approach to study extraterrestrial materials that also includes Mössbauer spectroscopy is most successful because there is the possibility of verifying the quality of the data by comparing the analyses performed with different techniques.

Author Contributions: Conceptualization, Methodology, Validation, Writing-Original Draft Preparation, Supervision, M.I.O.; Data Curation, Validation, Writing-Review & Editing, A.A.M., M.V.G. All authors have read and agreed to the published version of the manuscript.

Funding: This work was supported by the Ministry of Science and Higher Education of the Russian Federation, project No. FEUZ-2020-0060. The Zavaritsky Institute of Geology and Geochemistry of the Ural Branch of the Russian Academy of Sciences is supported by the Ministry of Science and Higher Education of the Russian Federation, project No. AAAA-A19-119071090011-6 (A.A.M.).

Conflicts of Interest: The authors declare no conflict of interest.

References

1. Maksimova, A.A.; Oshtrakh, M.I. Applications of Mössbauer spectroscopy in meteoritical and planetary science, Part I: Undifferentiated meteorites. *Minerals* **2021**, *11*, 612. [CrossRef]
2. Weisberg, M.K.; McCoy, T.J.; Krot, A.N. Systematics and evaluation of meteorite classification. In *Meteorites and the Early Solar System II.*; Lauretta, D.S., McSween, H.Y., Jr., Eds.; The University of Arizona Press: Tucson, AZ, USA, 2006; pp. 19–52.
3. Mittlefehldt, D.W. Asteroid (4) vesta: I. The howardite-eucrite-diogenite (HED) clan of meteorites. *Chem. Erde* **2015**, *75*, 155–183. [CrossRef]
4. Rubin, A.E. Mineralogy of meteorite groups. *Meteorit. Planet. Sci.* **1997**, *32*, 231–247. [CrossRef]
5. Rubin, A.E.; Ma, C. Meteoritic minerals and their origins. *Chem. Erde* **2017**, *77*, 325–385. [CrossRef]
6. Burns, R.G.; Martinez, S.L. Mössbauer spectra of olivine-rich achondrites: Evidence of preterrestrial redox reactions. In *Proceedings of the 21st Lunar and Planetary Science Conference, Houston, TX, USA, 12–16 March 1990*; Lunar and Planetary Institute: Houston, TX, USA, 1991; Volume 21, pp. 331–340.

7. Gismelseed, A.M.; Abdu, Y.A.; Shaddad, M.H.; Verma, H.C.; Jenniskens, P. Fe-bearing phases in a ureilite fragment from the asteroid 2008 TC_3 (=Almahata Sitta meteorites): A combined Mössbauer spectroscopy and X-ray diffraction study. *Meteorit. Planet. Sci.* **2014**, *49*, 1485–1493. [CrossRef]
8. Maliszewski, A.; Szlachta, K.; Gałązka-Friedman, J.; Bakun-Czubarow, N. Mössbauer studies of Polish enstatite meteorite—Zakłodzie. *Hyperfine Interact.* **2008**, *186*, 121–125. [CrossRef]
9. Dunlap, R.A. A Mössbauer effect investigation of the enstatite chondrite from Abee, Canada. *Hyperfine Interact.* **1997**, *110*, 209–215. [CrossRef]
10. Kruse, O. Mössbauer and X-ray study of the effects of vacancy concentration in synthetic hexagonal pyrrhotites. *Am. Mineral.* **1990**, *75*, 755–763.
11. Abdu, Y.A.; Azevedo, I.S.; Stewart, S.J.; López, A.; Varela, M.E.; Kurat, G.; Scorzelli, R.B. Mössbauer study of glasses in meteorites: The D'Orbigny angrite and Cachari eucrite. *Hyperfine Interact.* **2005**, *166*, 543–547. [CrossRef]
12. Abdu, Y.A.; Scorzelli, R.B.; Varela, M.E.; Kurat, G.; Azevedo, I.S.; Stewart, S.J.; Hawthorne, F.C. Druse clinopyroxene in D'Orbigny angritic meteorite studied by single-crystal X-ray diffraction, electron microprobe analysis, and Mössbauer spectroscopy. *Meteorit. Planet. Sci.* **2009**, *44*, 581–587. [CrossRef]
13. Vieira, V.W.A.; Knudsen, J.M.; Roy-Poulsen, N.O.; Campsie, J. Mössbauer spectroscopy of pyroxenes from two meteorites (achondrites). *Phys. Scr.* **1983**, *27*, 437–444. [CrossRef]
14. Zbik, M.; Yakovlev, O.I.; Polosin, A.V. The melting crust of the Stannern eucrite. *Geochem. Int.* **1989**, *26*, 108–115.
15. Costa, T.V.V.; Vieira, V.W.; de Araújo, M.A.B. Low temperature Mössbauer spectra of the Ibitira meteorite (achondrite). *Phys. Scr.* **1989**, *40*, 702–704. [CrossRef]
16. Solberg, T.C.; Burns, R.G. Iron Mössbauer spectral study of weathered Antarctic and SNC meteorites. In *Proceedings of the 19th Lunar and Planetary Science Conference, Houston, TX, USA, 14–18 March 1988*; Lunar and Planetary Institute: Houston, TX, USA, 1989; Volume 19, pp. 313–322.
17. Costa, T.V.V.; Vieira, V.W.; de Araújo, M.A.B. Analysis of impact-induced Fe^{2+} disorder in the pyroxene of the Ibitira meteorite. *Hyperfine Interact.* **1991**, *67*, 463–466. [CrossRef]
18. Gismelseed, A.M.; Khangi, F.; Ibrahim, A.; Yousif, A.A.; Worthing, M.A.; Rais, A.; Elzain, M.E.; Brooks, C.K.; Sutherland, H.H. Studies on AI Kidirate and Kapoeta meteorites. *Hyperfine Interact.* **1994**, *91*, 551–555. [CrossRef]
19. Tripathi, R.P.; Sharma, S.K.; Shrivastava, K.L.; Verma, H.C. Mössbauer spectroscopic studies of the Piplia Kalan (eucrite) and Lohawat (howardite) meteorites. *Meteorit. Planet. Sci.* **2000**, *35*, 201–204. [CrossRef]
20. Bhatia, B.; Patel, K.R.; Tripathi, R.P.; Layek, S.; Verma, H.C. Implication of Mössbauer spectra on the mixing model of eucrites and diogenites (resulting in howardites). *Curr. Sci.* **2015**, *109*, 331–337.
21. Verma, H.C.; Tewari, V.C.; Paliwal, B.S.; Tripathi, R.P. Preferential occupation of pyroxene sites by iron in diogenite meteorites. *Hyperfine Interact.* **2008**, *186*, 181–186. [CrossRef]
22. Chandra, U.; Parthasarathy, G.; Chandra Shekar, N.V.; Sahu, P.C. X-ray diffraction, Mössbauer spectroscopic and electrical resistivity studies on Lohawat meteorite under high-pressure up to 9 GPa. *Chem. Erde* **2013**, *73*, 197–203. [CrossRef]
23. Chandra, U.; Pandey, K.K.; Parthasarathy, G.; Sharma, S.M. High-pressure investigations on Piplia Kalan eucrite meteorite using in-situ X-ray diffraction and ^{57}Fe Mössbauer spectroscopic technique up to 16 GPa. *Geosci. Front.* **2016**, *7*, 265–271. [CrossRef]
24. Abdu, Y.A.; Hawthorne, F.C. Mössbauer spectroscopy of pyroxene in the light-dark structure of the Kapoeta meteorite: Implications for thermal history of the Kapoeta parent body. *J. Phys. Conf. Ser.* **2017**, *869*, 012096. [CrossRef]
25. Maksimova, A.A.; Unsalan, O.; Chukin, A.V.; Karabanalov, M.S.; Jenniskens, P.; Felner, I.; Semionkin, V.A.; Oshtrakh, M.I. The interior and the fusion crust in Sariçiçek howardite: Study using X-ray diffraction, magnetization measurements and Mössbauer spectroscopy. *Spectrochim. Acta Part A Molec. Biomolec. Spectrosc.* **2020**, *228*, 117819. [CrossRef] [PubMed]
26. Vieira, V.W.A.; Costa, T.V.V.; Jensen, H.G.; Knudsen, J.M.; Olsen, M.; Vistisen, L. Oxidation state of iron in SNC meteorites as studied by Mössbauer spectroscopy. *Phys. Scr.* **1986**, *33*, 180–186. [CrossRef]
27. Vistisen, L.; Petersen, D.; Madsen, M.B. Mössbauer spectroscopy showing large-scale inhomogeneity in the presumed Martian meteorite Zagami. *Phys. Scr.* **1992**, *46*, 94–96. [CrossRef]
28. Dyar, D.M. Ferric iron in SNC meteorites as determined by Mössbauer spectroscopy: Implications for Martian landers and Martian oxygen fugacity. *Meteorit. Planet. Sci.* **2003**, *38*, 1733–1752. [CrossRef]
29. Dyar, M.D.; Treiman, A.H.; Pieters, C.M.; Hiroi, T.; Lane, M.D.; O'Connor, V. MIL 03346, the most oxidized Martian meteorite: A first look at spectroscopy, petrography, and mineral chemistry. *J. Geophys. Res.* **2005**, *110*, E09005.
30. Treiman, A.H.; Dyar, M.D.; McCanta, M.; Noble, S.K.; Pieters, C.M. Martian dunite NWA 2737: Petrographic constraints on geological history, shock events, and olivine color. *J. Geophys. Res.* **2007**, *112*, E04002. [CrossRef]
31. Pieters, C.M.; Klima, R.L.; Hiroi, T.; Dyar, M.D.; Lane, M.D.; Treiman, A.H.; Noble, S.K.; Sunshine, J.M.; Bishop, J.L. Martian dunite NWA 2737: Integrated spectroscopic analyses of brown olivine. *J. Geophys. Res.* **2008**, *113*, E06004. [CrossRef]
32. Oshtrakh, M.I.; Maksimova, A.A.; Chukin, A.V.; Petrova, E.V.; Jenniskens, P.; Kuzmann, E.; Grokhovsky, V.I.; Homonnay, Z.; Semionkin, V.A. Variability of Chelyabinsk meteoroid stones studied by Mössbauer spectroscopy and X-ray diffraction. *Spectrochim. Acta Part A Molec. Biomolec. Spectrosc.* **2019**, *219*, 206–224. [CrossRef]
33. Quintiliani, M.; Andreozzi, G.B.; Skogby, H. Synthesis and Mössbauer characterization of $Fe_{1+x}Cr_{2-x}O_4$ ($0 \leq x \leq 2/3$) spinel single crystals. *Period. Mineral.* **2011**, *80*, 39–55.

34. Lenaz, D.; Andreozzi, G.B.; Bidyananda, M.; Princivalle, F. Oxidation degree of chromite from Indian ophiolites: A crystal chemical and ^{57}Fe Mössbauer study. *Period. Mineral.* **2014**, *83*, 241–255.
35. Gunnlaugsson, H.P.; Koch, C.B.; Bharuth-Ram, K.; Dietrich, M.; Helgason, Ö.; Madsen, M.B.; Mantovan, R.; Naidoo, D.; Steinthorsson, S.; Vistisen, L.; et al. Disordered chromite in the Martian meteorite Allan Hills 84001. *Hyperfine Interact.* **2008**, *186*, 9–14. [CrossRef]
36. Dyar, M.D.; Glotch, T.D.; Lane, M.D.; Wopenka, B.; Tucker, J.M.; Seaman, S.J.; Marchand, G.J.; Klima, R.; Hiroi, T.; Bishop, J.L.; et al. Spectroscopy of Yamato 984028. *Polar Sci.* **2011**, *4*, 530–549. [CrossRef]
37. Domeneghetti, M.C.; Fioretti, A.M.; Cámara, F.; McCammon, C.; Alvaro, M. Thermal history of nakhlites: A comparison between MIL 03346 and its terrestrial analogue Theo's flow. *Geochim. Cosmochim. Acta* **2013**, *121*, 571–581. [CrossRef]
38. Patrusheva, D.G.; Oshtrakh, M.I.; Petrova, E.V.; Grokhovsky, V.I.; Semionkin, V.A. ^{57}Fe hyperfine interactions in M1 and M2 sites of olivine from Omolon meteorite: Study using Mössbauer spectroscopy. *Hyperfine Interact.* **2010**, *197*, 295–300. [CrossRef]
39. Oshtrakh, M.I.; Petrova, E.V.; Grokhovsky, V.I.; Chukin, A.V.; Shtoltz, A.K.; Semionkin, V.A. Study of olivines from Omolon and Seymchan meteorites using X-ray diffraction and Mössbauer spectroscopy with a high velocity resolution. In *Proceedings of the International Conference Mössbauer Spectroscopy in Materials Science 2012, Olomouc, Czech Republic, 11–15 June 2012*; Tuček, J., Machala, L., Eds.; AIP Conference Proceedings: Melville, NY, USA, 2012; Volume 1489, pp. 154–163.
40. Oshtrakh, M.I.; Petrova, E.V.; Grokhovsky, V.I.; Semionkin, V.A. Variations in quadrupole splitting of the ^{57}Fe in the M1 and M2 sites of meteoritic olivines with different origin. *Hyperfine Interact.* **2013**, *222*, 61–66. [CrossRef]
41. Gutlich, P.; Bill, E.; Trautwein, A. *Mössbauer Spectroscopy and Transition Metal Chemistry. Fundamentals and Applications*; Springer: Berlin/Heidelberg, Germany; Dordrecht, The Netherlands; London, UK; New York, NY, USA, 2011; pp. 1–569. ISBN 978-3-540-88427-9.
42. Dos Santos, E.; Gattacceca, J.; Rochette, P.; Scorzelli, R.B.; Fillion, G. Magnetic hysteresis properties and ^{57}Fe Mössbauer spectroscopy of iron and stony-iron meteorites: Implications for mineralogy and thermal history. *Phys. Earth Planet. Inter.* **2015**, *242*, 50–64. [CrossRef]
43. Blukis, R.; Rüffer, R.; Chumakov, A.I.; Harrison, R.J. A high spatial resolution synchrotron Mössbauer study of the Tazewell IIICD and Esquel pallasite meteorites. *Meteorit. Planet. Sci.* **2017**, *52*, 925–936. [CrossRef]
44. Nichols, C.I.O.; Bryson, J.F.J.; Blukis, R.; Herrero-Albillos, J.; Kronast, F.; Rüffer, R.; Chumakov, A.I.; Harrison, R.J. Variations in the magnetic properties of meteoritic cloudy zone. *Geochem. Geophys. Geosyst.* **2020**, *21*, e2019GC008798. [CrossRef]
45. Oshtrakh, M.I.; Maksimova, A.A.; Goryunov, M.V.; Petrova, E.V.; Felner, I.; Chukin, A.V.; Grokhovsky, V.I. Study of metallic Fe-Ni-Co alloy and stony part isolated from Seymchan meteorite using X-ray diffraction, magnetization measurement and Mössbauer spectroscopy. *J. Mol. Struct.* **2018**, *1174*, 112–121. [CrossRef]
46. Lafleur, L.D.; Goodman, C.D.; King, E.A. Mössbauer investigation of shocked and unshocked iron meteorites and fayalite. *Science* **1968**, *162*, 1268–1270. [CrossRef]
47. Petersen, J.F.; Aydin, M.; Knudsen, J.M. Mössbauer spectroscopy of an ordered phase (superstructure) of FeNi in an iron meteorite. *Phys. Lett. A* **1977**, *62*, 192–194. [CrossRef]
48. Albertsen, J.F.; Jensen, J.B.; Knudsen, J.M. Structure of taenite in two iron meteorites. *Nature* **1978**, *273*, 453–454. [CrossRef]
49. Albertsen, J.F.; Aydin, M.; Knudsen, J.M. Mössbauer effect studies of taenite lamellae of an iron meteorite Cape York (III. A). *Phys. Scr.* **1978**, *17*, 467–472. [CrossRef]
50. Danon, J.; Scorzelli, R.; Azevedo, I.S.; Curvello, W.; Albertsen, J.F.; Knudsen, J.M. Iron-nickel 50-50 superstructure in the Santa Catharina meteorite. *Nature* **1979**, *277*, 283–284. [CrossRef]
51. Danon, J.; Scorzelli, R.; Azevedo, I.S.; Laugier, J.; Chamberod, A. Santa Catharina meteorite and phase composition of irradiated Fe-Ni invar alloys. *Nature* **1980**, *284*, 237–238. [CrossRef]
52. Albertsen, J.F.; Knudsen, J.M.; Roy-Poulsen, N.O.; Vistisen, L. Meteorites and thermodynamic equilibrium in f.c.c. iron-nickel alloys (25–50% Ni). *Phys. Scr.* **1980**, *22*, 171–175. [CrossRef]
53. Danon, J.; Scorzelli, R.; Azevedo, I.S. Mössbauer studies of the Fe-Ni ordered phase (superstructure $L1_0$) in meteorites. *J. Phys. Colloq.* **1980**, *41*, C1-363–364. [CrossRef]
54. Albertsen, J.F. Tetragonal lattice of tetrataenite (ordered Fe-Ni, 50–50) from 4 meteorites. *Phys. Scr.* **1981**, *23*, 301–306. [CrossRef]
55. Jago, R.A.; Clark, P.E.; Rossiter, P.L. The Santa Catharina meteorite and the equilibrium state of Fe-Ni alloys. *Phys. Status Solidi A* **1982**, *74*, 247–254. [CrossRef]
56. Larsen, L.; Roy-Poulsen, H.; Roy-Poulsen, N.O.; Vistisen, L.; Knudsen, J.M. Order-disorder transitions in iron-nickel (50–50%) alloys from iron meteorites as studied by Mössbauer spectroscopy. *Phys. Rev. Lett.* **1982**, *48*, 1054–1056. [CrossRef]
57. Albertsen, J.F.; Nielsen, H.P.; Buchwald, V.F. On the fine structure of meteoritical taenite/tetrataenite and its interpretation. *Phys. Scr.* **1983**, *27*, 314–320. [CrossRef]
58. Christiansen, A.; Laisen, L.; Roy-Poulsen, H.; Roy-Poulsen, N.O.; Vistisen, L. Iron-nickel alloys in a taenite lamella from the iron meteorite Cape York as measured by conversion electron Mössbauer spectroscopy. *Phys. Scr.* **1984**, *29*, 94–96. [CrossRef]
59. Scorzelli, R.B.; Danon, J. Mössbauer spectroscopy and X-ray diffraction studies of Fe-Ni order-disorder processes in a 35% Ni meteorite (Santa Catharina). *Phys. Scr.* **1985**, *32*, 143–148. [CrossRef]
60. Scorzelli, R.B.; Danon, J.; Da Silva, E.G. Solid state transformations in Fe-Ni alloys from meteorites in powder form. *Hyperfine Interact.* **1986**, *28*, 979–983. [CrossRef]

61. Roy-Poulsen, H.; Knudsen, J.M.; Larsen, L.; Roy-Poulsen, N.O.; Vistisen, L. A study of Ni-rich iron meteorites. *Hyperfine Interact.* **1986**, *29*, 1089–1092. [CrossRef]
62. Scorzelli, R.; Azevedo, I.S.; Danon, J.; Meyers, M.A. Mössbauer study of shock-induced effects in the ordered alloy $Fe_{50}Ni_{50}$ in meteorites. *J. Phys. F: Metal Phys.* **1987**, *17*, 1993–1997. [CrossRef]
63. Aramu, F.; Brovetto, P.; Delunas, A.; Maxia, V.; Murgia, M. Study by Mössbauer spectroscopy of an iron meteorite. *Il Nuovo Cim.* **1990**, *12D*, 1021–1024. [CrossRef]
64. De Grave, E.; Vandenberghe, R.E.; De Bakker, P.M.A.; Van Alboom, A.; Vochten, R.; Van Tassel, R. Temperature dependence of the Mössbauer parameters of the Fe-Ni phases in the Santa Catharina meteorite. *Hyperfine Interact.* **1992**, *70*, 1009–1012. [CrossRef]
65. De Grave, E.; Pollard, R.J.; Vandenberghe, R.E.; De Bakker, P.M.A. The effect of high external magnetic fields on the hyperfine interactions in the Fe-Ni phases of the Santa Catharina meteorite. *Hyperfine Interact.* **1994**, *94*, 2349–2353. [CrossRef]
66. Ouseph, P.J.; Groskreutz, H.E.; Johnson, A.A. Mössbauer spectra for iron bearing phases in the meteorite Toluca. *Meteoritics* **1979**, *14*, 97–108. [CrossRef]
67. Scorzelli, R.B.; Pereira, R.A.; Perez, C.A.C.; Fernandes, A.A.R. Phase composition and structure of Fe-Ni alloys in a unique Antarctic meteorite Yamato 791694. *Hyperfine Interact.* **1994**, *94*, 2343–2347. [CrossRef]
68. Böttger, C.; Campbell, S.J.; Wu, E.; Smith, R.G. Mössbauer and X-ray studies of an iron meteorite sample. *Hyperfine Interact.* **1994**, *91*, 563–569. [CrossRef]
69. Rancourt, D.G.; Lagarec, K.; Densmore, A.; Dunlap, R.A.; Goldstein, J.I.; Reisener, R.I.; Scorzelli, R.B. Experimental proof of the distinct electronic structure of a new meteoritic Fe-Ni alloy phase. *J. Magn. Magn. Mater.* **1999**, *191*, L255–L260. [CrossRef]
70. Rancourt, D.G.; Scorzelli, R.B. Low-spin γ-Fe-Ni (γ_{LS}) proposed as a new mineral in Fe-Ni-bearing meteorites: Epitaxial intergrowth of γ_{LS} and tetrataenite as a possible equilibrium state at ~20–40 at% Ni. *J. Mag. Mag. Mater.* **1995**, *150*, 30–36. [CrossRef]
71. Paduani, C.; Pérez, C.A.S.; Ardisson, J.D. A Mössbauer effect study of the Soledade meteorite. *Braz. J. Phys.* **2005**, *35*, 667–669. [CrossRef]
72. Cabanillas, E.D.; Palacios, T.A. An hexahedrite meteorite from the Campo del Cielo Fall. *Planet. Space Sci.* **2006**, *54*, 303–309. [CrossRef]
73. Oshtrakh, M.I.; Milder, O.B.; Grokhovsky, V.I.; Semionkin, V.A. Hyperfine interactions in iron meteorites: Comparative study by Mössbauer spectroscopy. *Hyperfine Interact.* **2004**, *158*, 365–370. [CrossRef]
74. Grokhovsky, V.I.; Oshtrakh, M.I.; Milder, O.B.; Semionkin, V.A. Mössbauer study of iron meteorites and their corrosion products. *Bull. Russ. Acad. Sci. Phys.* **2005**, *69*, 1710–1716.
75. Grokhovsky, V.I.; Oshtrakh, M.I.; Milder, O.B.; Semionkin, V.A. Mössbauer spectroscopy of iron meteorite Dronino and products of its corrosion. *Hyperfine Interact.* **2005**, *166*, 671–677. [CrossRef]
76. Oshtrakh, M.I.; Grokhovsky, V.I.; Abramova, N.V.; Semionkin, V.A.; Milder, O.B. Iron-nickel alloy from iron meteorite Chinga studied using Mössbauer spectroscopy with high velocity resolution. *Hyperfine Interact.* **2009**, *190*, 135–142. [CrossRef]
77. Torres, L.M.F.; Alcazar, G.A.P. Structural and magnetic characterization of the "GASPAR" meteorite from Betéitiva, Boyacá, Colombia. *Hyperfine Interact.* **2014**, *224*, 289–298. [CrossRef]
78. Badjukov, D.D.; Rusakov, V.S.; Kupin, Y.G. Shock Wave-induced interaction between meteoritic iron and silicates. *Petrology* **2012**, *20*, 347–355. [CrossRef]
79. Cesnek, M.; Štefánik, M.; Kmječ, T.; Miglierini, M. Iron meteorite fragment studied by atomic and nuclear analytical methods. In *Proceedings of the International Conference Mössbauer Spectroscopy in Materials Science 2016, Liptovský Ján, Slovakia, 23–27 May 2016*; Tuček, J., Miglierini, M., Eds.; AIP Conference Proceedings, AIP Publishing: Melville, NY, USA, 2016; Volume 1781, p. 020015.
80. Oshtrakh, M.I.; Goryunov, M.V.; Grokhovsky, V.I.; Chukin, A.V.; Shtolz, A.K.; Semionkin, V.A. Study of visually different areas in the Chinga iron meteorite fragment using Mössbauer spectroscopy with a high velocity resolution. *Hyperfine Interact.* **2013**, *219*, 25–31. [CrossRef]
81. Goryunov, M.V.; Oshtrakh, M.I.; Chukin, A.V.; Grokhovsky, V.I.; Semionkin, V.A. Comparative study of Aliskerovo, Anyujskij, Sikhote-Alin and Sterlitamak iron meteorites using Mössbauer spectroscopy. *Hyperfine Interact.* **2016**, *237*, 15. [CrossRef]
82. Goryunov, M.V.; Yakovlev, G.A.; Chukin, A.V.; Grokhovsky, V.I.; Semionkin, V.A.; Oshtrakh, M.I. Iron meteorites and their weathering products: Mössbauer spectroscopy with a high velocity resolution of the iron-bearing minerals. *Eur. J. Mineral.* **2016**, *28*, 601–610. [CrossRef]
83. Oshtrakh, M.I.; Yakovlev, G.A.; Grokhovsky, V.I.; Semionkin, V.A. Re-examination of Dronino iron meteorite and its weathering products using Mössbauer spectroscopy with a high velocity resolution. *Hyperfine Interact.* **2016**, *237*, 42. [CrossRef]
84. Yakovlev, G.A.; Chukin, A.V.; Grokhovsky, V.I.; Semionkin, V.A.; Oshtrakh, M.I. Study of Dronino iron meteorite weathering in clay sand using Mössbauer spectroscopy. *Croat. Chem. Acta* **2016**, *89*, 117–124. [CrossRef]
85. Stefanik, M.; Cesnek, M.; Sklenka, L.; Kmjec, T.; Miglierini, M. Neutron activation analysis of meteorites at the VR-1 training reactor. *Rad. Phys. Chem.* **2020**, *171*, 108675. [CrossRef]
86. Coey, J.M.D.; Venkatesan, M.; Fitzgerald, C.B.; Douvalis, A.P.; Sanders, I.S. Ferromagnetism of a graphite nodule from the Canyon Diablo meteorite. *Nature* **2002**, *420*, 156–159. [CrossRef]
87. Kruse, O.; Ericsson, T. A Mössbauer investigation of natural troilite from the Agpalilik meteorite. *Phys. Chem. Minerals* **1988**, *15*, 509–513. [CrossRef]

88. Čuda, J.; Kohout, T.; Tuček, J.; Haloda, J.; Filip, J.; Prucek, R.; Zboril, R. Low-temperature magnetic transition in troilite: A simple marker for highly stoichiometric FeS systems. *J. Geophys. Res.* **2011**, *116*, B11205.
89. Čuda, J.; Kohout, T.; Tuček, J.; Filip, J.; Malina, O.; Krizek, M.; Zboril, R. In-field ^{57}Fe Mössbauer spectroscopy below spin-flop transition in powdered troilite (FeS) mineral. In *Proceedings of the International Conference Mössbauer Spectroscopy in Materials Science 2014, Hlohovec u Břeclavi, Czech Republic, 26–30 May 2014*; Tuček, J., Miglierini, M., Eds.; AIP Conference Proceedings: Melville, NY, USA, 2014; Volume 1622, pp. 8–11.
90. Čuda, J.; Kohout, T.; Tuček, J.; Filip, J.; Medrík, I.; Mashlan, M.; Zboril, R. Mössbauer study and magnetic measurement of troilite extract from Natan iron meteorite. In *Mössbauer Spectroscopy, Proceedings of the International Conference Mössbauer Spectroscopy in Materials Science 2012, Olomouc, Czech Republic, 11–15 June 2012*; Tuček, J., Machala, L., Eds.; AIP Conference Proceedings: Melville, NY, USA, 2012; Volume 1489, pp. 145–153.
91. Oshtrakh, M.I.; Klencsár, Z.; Petrova, E.V.; Grokhovsky, V.I.; Chukin, A.V.; Shtoltz, A.K.; Maksimova, A.A.; Felner, I.; Kuzmann, E.; Homonnay, Z.; et al. Iron sulfide (troilite) inclusion extracted from Sikhote-Alin iron meteorite: Composition, structure and magnetic properties. *Mat. Chem. Phys.* **2016**, *174*, 100–111. [CrossRef]
92. Wojnarowska, A.; Dziel, T.; Gałązka-Friedman, J.; Karwowski, Ł. New mineralogical phases identified by Mössbauer measurements in Morasko meteorite. *Hyperfine Interact.* **2008**, *186*, 167–171. [CrossRef]
93. Klencsár, Z.; Kuzmann, E.; Homonnay, Z.; Vértes, A.; Simopoulos, A.; Devlin, E.; Kallias, G. Interplay between magnetic order and the vibrational state of Fe in $FeCr_2S_4$. *J. Phys. Chem. Solids* **2003**, *64*, 325–331. [CrossRef]
94. Oshtrakh, M.I.; Larionov, M.Y.; Grokhovsky, V.I.; Semionkin, V.A. Study of iron meteorite Sikhote-Alin and extracted iron-nickel phosphides using Mössbauer spectroscopy with high velocity resolution. *Hyperfine Interact.* **2008**, *186*, 53–59. [CrossRef]
95. Oshtrakh, M.I.; Larionov, M.Y.; Grokhovsky, V.I.; Semionkin, V.A. Temperature dependent high velocity resolution Mössbauer spectroscopic study of iron nickel phosphide microcrystals (rhabdites) extracted from Sikhote-Alin iron meteorite. *J. Alloys Comp.* **2011**, *509*, 1781–1784. [CrossRef]
96. Oshtrakh, M.I.; Larionov, M.Y.; Grokhovsky, V.I.; Semionkin, V.A. An analysis of Fe and Ni distribution in M1, M2 and M3 sites of iron nickel phosphides extracted from Sikhote-Alin Meteorite using Mössbauer spectroscopy with a high velocity resolution. *J. Mol. Struct.* **2011**, *993*, 38–42. [CrossRef]
97. Oshtrakh, M.I.; Larionov, M.Y.; Grokhovsky, V.I.; Semionkin, V.A. Study of rhabdite (iron nickel phosphide) microcrystals extracted from Sikhote-Alin iron meteorite by magnetization measurements and Mössbauer spectroscopy. *Mat. Chem. Phys.* **2011**, *130*, 373–380. [CrossRef]
98. Dos Santos, E.; Scorzelli, R.B.; Varela, M.E.; Munayco, P. Fe^{2+}-Mg order–disorder study in orthopyroxenes from São João Nepomuceno (IVA) iron meteorite. *Hyperfine Interact.* **2014**, *224*, 251–256. [CrossRef]
99. Dos Santos, E.; Scorzelli, R.B.; Varela, M.E. Cation distribution in orthopyroxenes from São João Nepomuceno iron meteorite inferred from ^{57}Fe Mössbauer spectroscopy: Implications for thermal history and origin of IVA parent body. *Meteorit. Planet. Sci.* **2018**, *53*, 2249–2258. [CrossRef]
100. Hafner, S.S. Mössbauer spectroscopy in lunar geology and mineralogy. In *Mössbauer Spectroscopy*; Gonser, U., Ed.; Springer: Berlin/Heidelberg, Germany; New York, NY, USA, 1975; pp. 167–199.
101. Herzenberg, C.L.; Riley, D.L. Mössbauer spectrometry of lunar samples. *Science* **1970**, *167*, 683–686. [CrossRef]
102. Herzenberg, C.L.; Riley, D.L. Analysis of first returned lunar samples by Mössbauer spectrometry. In *Proceedings of the Apollo 11 Lunar Science Conference, Houston, TX, USA, 5–8 January 1970*; Levinson, A.A., Ed.; Pergamon Press: New York, NY, USA, 1970; Volume 3, (Suppl. 1), pp. 2221–2241.
103. Herzenberg, C.L.; Riley, D.L. Mössbauer spectrometry of lunar samples from the Apollo 11 mission. In *Mössbauer Effect Methodology, Proceedings of the Sixth Symposium on Mössbauer Effect Methodology, New York, NY, USA, 25 January 1970*; Gruverman, I.J., Ed.; Plenum Press: New York, NY, USA; London, UK, 1971; Volume 6, pp. 177–191.
104. Herzenberg, C.L.; Riley, D.L. Analysis of returned lunar samples by techniques based on Mössbauer spectrometry. *Phys. Earth Planet. Inter.* **1971**, *4*, 204–214. [CrossRef]
105. Herzenberg, C.L.; Riley, D.L. Mössbauer instrumental analysis of Apollo 12 lunar rock and soil samples. In *Proceedings of the Second Lunar Science Conference, Houston, TX, USA, 11–14 January 1971*; Levinson, A.A., Ed.; Massachusetts Institute of Technology Press: Cambridge, UK, 1971; Volume 3, (Suppl. 2), pp. 2103–2123.
106. Huffman, G.P.; Dunmyre, G.R.; Fisher, R.M.; Wasilewski, P.J.; Nagata, T. Mössbauer and supplementary studies of Apollo 11 lunar samples. In *Proceedings of the Sixth Symposium on Mössbauer Effect Methodology, New York, NY, USA, 25 January 1970*; Gruverman, I.J., Ed.; Plenum Press: New York, NY, USA; London, UK, 1971; Volume 6, pp. 209–224.
107. Huffman, G.P.; Schwerer, F.C.; Fisher, R.M. Iron distribution and metallic-ferrous ratios for Apollo lunar samples: Mössbauer and magnetic analyses. In *Proceedings of the Fifth Lunar Science Conference, Houston, TX, USA, 18-22 March 1974*; Gose, W.A., Ed.; Pergamon Press: New York, NY, USA, 1974; Volume 3, (Suppl. 5), pp. 2779–2794.
108. Gay, P.; Bancroft, G.M.; Bown, M.G. Diffraction and Mössbauer studies of minerals from lunar soils and rocks. *Science* **1970**, *167*, 626–628. [CrossRef] [PubMed]
109. Muir, A.H., Jr.; Housley, R.M.; Grant, R.W.; Abdel-Gawad, M.; Blander, M. Mössbauer spectroscopy of Moon samples. *Science* **1970**, *167*, 688–690. [CrossRef] [PubMed]

110. Gay, P.; Bancroft, G.M.; Bown, M.G. Diffraction and Mössbauer studies of minerals from lunar soils and rocks. In *Proceedings of the Apollo 11 Lunar Science Conference, Houston, TX, USA, 5–8 January 1970*; Levinson, A.A., Ed.; Pergamon Press: New York, NY, USA, 1970; Volume 1, (Suppl. 1), pp. 481–497.
111. Greenwood, N.N.; How, A.T. Mössbauer studies of Apollo 11 lunar samples. In *Proceedings of the Apollo 11 Lunar Science Conference, Houston, TX, USA, 5–8 January 1970*; Levinson, A.A., Ed.; Pergamon Press: New York, NY, USA, 1970; Volume 3, (Suppl. 1), pp. 2163–2169.
112. Muir, A.H., Jr.; Housley, R.M.; Grant, R.W.; Abdel-Gawad, M.; Blander, M. Mössbauer investigation of Apollo 11 lunar samples. In *Proceedings of the Sixth Symposium on Mössbauer Effect Methodology, New York, NY, USA, 25 January 1970*; Gruverman, I.J., Ed.; Plenum Press: New York, NY, USA; London, UK, 1971; Volume 6, pp. 163–176.
113. Hafner, S.S.; Janik, B.; Virgo, D. State and location of iron in Apollo 11 samples. In *Proceedings of the Sixth Symposium on Mössbauer Effect Methodology, New York, NY, USA, 25 January 1970*; Gruverman, I.J., Ed.; Plenum Press: New York, NY, USA; London, UK, 1971; Volume 6, pp. 193–207.
114. Hafner, S.S.; Virgo, D.; Warburton, D. Oxidation state of iron in plagioclase from lunar basalts. *Earth Planet. Sci. Lett.* **1971**, *12*, 159–166. [CrossRef]
115. Gibb, T.C.; Greatrex, R.; Greenwood, N.N.; Battey, M.H. Mössbauer studies of Apollo 14 lunar samples. In *Proceedings of the Third Lunar Science Conference, Houston, TX, USA, 10–13 January 1972*; Levinson, A.A., Ed.; Massachusetts Institute of Technology Press: Cambridge, UK, 1972; Volume 3, (Suppl. 3), pp. 2479–2493.
116. Virgo, D.; Hafner, S.S. Temperature-dependent Mg, Fe distribution in a lunar olivine. *Earth Planet. Sci. Lett.* **1972**, *14*, 305–312. [CrossRef]
117. Huffman, G.P.; Dunmyre, G.R. Superparamagnetic clusters of Fe^{2+} spins in lunar olivine: Dissolution by high-temperature annealing. In *Proceedings of the Sixth Lunar Science Conference, Houston, TX, USA, 17–12 March 1975*; Merrill, R.B., Ed.; Pergamon Press: New York, NY, USA, 1975; Volume 1, (Suppl. 6), pp. 757–772.
118. Morris, R.V.; Klingelhöfer, G.; Korotev, R.L.; Shelfer, T.D. Mössbauer mineralogy on the moon: The lunar regolith. *Hyperfine Interact.* **1998**, *117*, 405–432. [CrossRef]
119. Wentworth, S.J.; Keller, L.P.; McKay, D.S.; Morris, R.V. Space weathering on the moon: Patina on Apollo 17 samples 75075 and 76015. *Meteorit. Planet. Sci.* **1999**, *34*, 593–603. [CrossRef]
120. Malysheva, T.V. Mössbauer spectroscopy of lunar regolith returned by the automatic station Luna 16. In *Proceedings of the Third Lunar Science Conference, Houston, TX, USA, 10–13 January 1972*; Levinson, A.A., Ed.; Massachusetts Institute of Technology Press: Cambridge, UK, 1972; Volume 1, (Suppl. 3), pp. 105–114.
121. Gibb, T.C.; Greatrex, R.; Greenwood, N.N. Mössbauer studies of Luna 16 and 20 lunar soils. *Phil. Trans. R. Soc. Lond. A* **1977**, *284*, 157–165.
122. Gibb, T.C.; Greatrex, R.; Greenwood, N.N. An assessment of results obtained from Mössbauer spectra of lunar samples. *Phil. Trans. R. Soc. Lond. A* **1977**, *285*, 235–240.
123. Malysheva, T.V. To the problem about the origin of lunar maria and continents (Mössbauer investigations). In *Proceedings of the Soviet-American Conference on Cosmochemistry of the Moon and Planets, Moscow, USSR, 4–8 June 1974*; Pomeroy, J.H., Hubbard, N.J., Eds.; National Aeronautics and Space Administration, Scientific and Technical Information Office: Washington, WA, USA, 1977; Pt. 1, pp. 243–251.
124. Eglinton, G.; Gowar, A.P.; Jull, A.J.T.; Pillinger, C.T.; Agrell, S.O.; Agrell, J.E.; Long, J.V.P.; Bowie, S.H.U.; Simpson, P.R.; Beckinsale, R.D.; et al. The analysis of various size, visually selected and density and magnetically separated fractions of Luna-16 and -20 samples. In *Proceedings of the Soviet-American Conference on Cosmochemistry of the Moon and Planets, Moscow, USSR, 4–8 June 1974*; Pomeroy, J.H., Hubbard, N.J., Eds.; National Aeronautics and Space Administration, Scientific and Technical Information Office: Washington, WA, USA, 1977; Pt. 2, pp. 703–727.
125. Zemčik, T.; Raclavsky, K. Mössbauer spectroscopy of iron in the Luna 20 regolith. In *Proceedings of the Soviet-American Conference on Cosmochemistry of the Moon and Planets, Moscow, USSR, 4–8 June 1974*; Pomeroy, J.H., Hubbard, N.J., Eds.; National Aeronautics and Space Administration, Scientific and Technical Information Office: Washington, WA, USA, 1977; Pt. 2, pp. 729–734.
126. Malysheva, T.V.; Polyakova, N.P.; Mishin, N.E. Mössbauer Spectroscopic Study of Lunar Soil Collected by the Luna 24 Automatic Probe. *Geokhimiia (Moscow)* **1978**, *6*, 835–841. (In Russian)
127. Zemčik, T.; Cimbálniková, A. Variability of silicate glasses from the lunar regolith. *Hyperfine Interact.* **1986**, *29*, 1105–1107. [CrossRef]
128. Khramov, D.A.; Zemčik, T.; Cimbálniková, A. Distribution of Iron in Lunar Olivines from Data of Mössbauer Spectroscopy. *Geokhimiia (Moscow)* **1989**, *8*, 1164–1169. (In Russian)
129. Varnek, V.A.; Mazalov, L.N.; Dikov, Y.P.; Ivanov, A.V. New Data on the Forms of Iron Found in the Luna-16 Regolith, Obtained Using Mössbauer Spectroscopy. *Geokhimiia (Moscow)* **1989**, *8*, 1170–1175. (In Russian)
130. Malysheva, T.V. Study of lunar regolith from the Moon highland region by Mössbauer spectroscopy. In *Soil from the Highland Region of the Moon*; Barsukov, V.L., Surkov, Y.A., Eds.; Publishing House Nauka: Moscow, USSR, 1979; pp. 665–673. (In Russian)
131. Zemčik, T.; Raclavsky, K. Comparison of non-magnetic parts of the Mössbauer spectra of regolith from Luna-16 and Luna-20. In *Soil from the Highland Region of the Moon*; Barsukov, V.L., Surkov, Y.A., Eds.; Publishing House Nauka: Moscow, USSR, 1979; pp. 674–677. (In Russian)

132. Malysheva, T.V. NGR spectroscopy of regolith samples from Mare Crisium. In *Lunar Soil from Mare Crisium*; Barsukov, V.L., Ed.; Publishing House Nauka: Moscow, USSR, 1980; pp. 300–308. (In Russian)
133. Klingelhöfer, G. The miniaturized spectrometer MIMOS II. In *Mössbauer Spectroscopy in Materials Science*; Miglierini, M., Petridis, D., Eds.; Kluwer Academic Publishers: Berlin, Germany, 1999; pp. 413–426.
134. Fleischer, I.; Klingelhöfer, G.; Morris, R.V.; Schröder, C.; Rodionov, D.; De Souza, P.A. In-situ Mössbauer spectroscopy with MIMOS II. *Hyperfine Interact.* **2012**, *207*, 97–105. [CrossRef]
135. Klingelhöfer, G. Extraterrestrial Mössbauer spectroscopy. In *The Rudolf Mössbauer Story*; Kalvius, M., Kienle, P., Eds.; Springer: Berlin/Heidelberg, Germany, 2012; pp. 293–316. ISBN 978-3-642-17951-8.
136. Morris, R.V.; Klingelhöfer, G.; Bernhardt, B.; Schröder, C.; Rodionov, D.S.; de Souza, P.A., Jr.; Yen, A.; Gellert, R.; Evlanov, E.N.; Foh, J.; et al. Mineralogy at gusev crater from the Mössbauer spectrometer on the spirit rover. *Science* **2004**, *305*, 833–836. [CrossRef]
137. Klingelhöfer, G.; Morris, R.V.; Bernhardt, B.; Schröder, C.; Rodionov, D.S.; de Souza, P.A., Jr.; Yen, A.; Gellert, R.; Evlanov, E.N.; Zubkov, B.; et al. Jarosite and hematite at Meridiani Planum from opportunity's Mössbauer spectrometer. *Science* **2004**, *306*, 1740–1745. [CrossRef]
138. Klingelhöfer, G. Mössbauer analysis of the surface of Mars with MIMOS II at Meridiani Planum and Gusev Crater. In *Industrial Applications of the Mössbauer Effect*; Garcia, M., Marco, J.F., Plazaola, F., Eds.; AIP Conference Proceedings, American Institute of Physics: College Park, MD, USA, 2005; Volume 765, pp. 369–379.
139. Klingelhöfer, G.; De Grave, E.; Morris, R.V.; Van Alboom, A.; De Resende, V.G.; De Souza, P.A., Jr.; Rodionov, D.; Schröder, C.; Ming, D.W.; Yen, A. Mössbauer spectroscopy on mars: Goethite in the Columbia Hills at Gusev crater. *Hyperfine Interact.* **2005**, *166*, 549–554. [CrossRef]
140. Klingelhöfer, G.; Morris, R.V.; De Souza, P.A., Jr.; Rodionov, D.; Schröder, C. Two earth years of Mössbauer studies of the surface of Mars with MIMOS II. *Hyperfine Interact.* **2006**, *170*, 169–177. [CrossRef]
141. Morris, R.V.; Klingelhöfer, G.; Schröder, C.; Rodionov, D.S.; Yen, A.; Ming, D.W.; De Souza, P.A., Jr.; Wdowiak, T.; Fleischer, I.; Gellert, R.; et al. Mössbauer mineralogy of rock, soil, and dust at Meridiani Planum, Mars: Opportunity's journey across sulfate-rich outcrop, basaltic sand and dust, and hematite lag deposits. *J. Geophys. Res.* **2006**, *111*, E12S15. [CrossRef]
142. Schröder, C.; Klingelhöfer, G.; Morris, R.V.; Rodionov, D.S.; Fleischer, I.; Blumers, M. Extraterrestrial Mössbauer spectroscopy: More than 3 years of Mars exploration and developments for future missions. *Hyperfine Interact.* **2008**, *182*, 149–156. [CrossRef]
143. Morris, R.V.; Klingelhöfer, G.; Schröder, C.; Fleischer, I.; Ming, D.W.; Yen, A.S.; Gellert, R.; Arvidson, R.E.; Rodionov, D.S.; Crumpler, L.S.; et al. Iron mineralogy and aqueous alteration from Husband Hill through Home Plate at Gusev Crater, Mars: Results from the Mössbauer instrument on the Spirit Mars Exploration Rover. *J. Geophys. Res.* **2008**, *113*, E12S42. [CrossRef]
144. Morris, R.V.; Schröder, C.; Klingelhöfer, G.; Agresti, D.G. Mössbauer spectroscopy at Gusev Crater and Meridiani Planum. Iron mineralogy, oxidation state, and alteration on Mars. In *Remote Compositional Analysis: Techniques for Understanding Spectroscopy, Mineralogy, and Geochemistry of Planetary Surfaces*; Bishop, J.L., Bell, J.F., III, Moersch, J.E., Eds.; Cambridge University Press: Cambridge, UK, 2019; pp. 538–554.
145. Agresti, D.G.; Fleischer, I.; Klingelhöfer, G.; Morris, R.V. On simfitting MER Mössbauer data to characterize Martian hematite. *J. Phys. Conf. Ser.* **2010**, *217*, 012063. [CrossRef]
146. Fleischer, I.; Agresti, D.G.; Klingelhöfer, G.; Morris, R.V. Distinct hematite populations from simultaneous fitting of Mössbauer spectra from Meridiani Planum, Mars. *J. Geophys. Res.* **2010**, *115*, E00F06. [CrossRef]
147. Schröder, C.; Rodionov, D.S.; McCoy, T.J.; Jolliff, B.L.; Gellert, R.; Nittler, L.R.; Farrand, W.H.; Johnson, J.R.; Ruff, S.W.; Ashley, J.W.; et al. Meteorites on mars observed with the Mars exploration rovers. *J. Geophys. Res.* **2008**, *113*, E06S22. [CrossRef]
148. Fleischer, I.; Brückner, J.; Schröder, C.; Farrand, W.; Tréguier, E.; Morris, R.V.; Klingelhöfer, G.; Herkenhoff, K.; Mittlefehldt, D.; Ashley, J.; et al. Mineralogy and chemistry of cobbles at Meridiani Planum, mars, investigated by the mars exploration rover opportunity. *J. Geophys. Res.* **2010**, *115*, E00F05. [CrossRef]
149. Zipfel, J.; Schröder, C.; Jolliff, B.L.; Gellert, R.; Herkenhoff, K.E.; Rieder, R.; Anderson, R.; Bell, J.F., III; Brückner, J.; Crisp, J.A.; et al. Bounce rock—A shergottite-like basalt encountered at Meridiani Planum, Mars. *Meteorit. Planet. Sci.* **2011**, *46*, 1–20. [CrossRef]
150. Agresti, D.G. Temperature dependence of the quadrupole splitting of olivine and pyroxene from the Plains of Gusev crater on Mars. *Hyperfine Interact.* **2012**, *208*, 117–121. [CrossRef]
151. Van Cromphaut, C.; De Resende, V.G.; De Grave, E.; Vandenberghe, R.E. Mössbauer study of Meridiani Planum, the first iron-nickel meteorite found on the surface of Mars by the MER opportunity. *Meteorit. Planet. Sci.* **2007**, *42*, 2119–2123. [CrossRef]